

LATERAL LOAD DISTRIBUTION FOR STEEL BEAMS SUPPORTING AN FRP PANEL

by

HARRISON WALKER POOLE

B.S., Kansas State University, 2009

A THESIS

submitted in partial fulfillment of the requirements for the degree

MASTER OF SCIENCE

Department of Civil Engineering
College of Engineering

KANSAS STATE UNIVERSITY
Manhattan, Kansas

2011

Approved by:

Major Professor
Dr. Hani Melhem

Copyright

HARRISON POOLE

2011

Abstract

Fiber Reinforced Polymer (FRP) is a relatively new material used in the field of civil engineering. FRP is composed of fibers, usually carbon or glass, bonded together using a polymer adhesive and formed into the desired structural shape. Recently, FRP deck panels have been viewed as an attractive alternative to concrete decks when replacing deteriorated bridges. The main advantages of an FRP deck are its weight (roughly 75% lighter than concrete), its high strength-to-weight ratio, and its resistance to deterioration. In bridge design, AASHTO provides load distributions to be used when determining how much load a longitudinal beam supporting a bridge deck should be designed to hold. Depending on the deck material along with other variables, a different design distribution will be used. Since FRP is a relatively new material used for bridge design, there are no provisions in the AASHTO code that provides a load distribution when designing beams supporting an FRP deck. FRP deck panels, measuring 6 ft x 8.5', were loaded and analyzed at KSU over the past 4 years. The research conducted provides insight towards a conservative load distribution to assist engineers in future bridge designs with FRP decks.

Two separate test periods produced data for this thesis. For the first test period, throughout the year of 2007, a continuous FRP panel was set up at the Civil Infrastructure Systems Laboratory at Kansas State University. This continuous panel measured 8.5 ft by 6 ft x 6 in. thick and was supported by 4 Grade A572 HP 10 x 42 steel beams. The beam spacing's, along the 8.5 ft direction, were 2.5 ft-3.5 ft-2.5 ft. Strain gauges were mounted at mid-span of each beam to monitor the amount of load each beam was taking under a certain load. Linear variable distribution transformers (LVDT) were mounted at mid-span of each beam to measure deflection. Loads were placed at the center of the panel, with reference to the 6 ft direction and at several locations along the 8.5 ft direction. Strain and deflection readings were taken in order to determine the amount of load each beam resisted for each load location.

The second period of testing started in the fall of 2010 and extended into January of 2011. This consisted of a simple-span/cantilever test set-up. The test set-up consisted of, in the 8.5 ft direction, a simply supported span of 6 ft with a 2.5 ft cantilever on one side. As done previously both beams had strain gauges along with LVDTs mounted at mid-span. There were also strain gauges were installed spaced at 1.5ft increments along one beam in order to analyze

the beam behavior under certain loads. Loads were once again applied in the center of the 6 ft direction and strain and deflection readings were taken at several load locations along the 8.5 ft direction. The data was analyzed after all testing was completed. The readings from the strain gauges mounted in 1.5 ft increments along the steel beam on one side of the simple span test set-up were used to produce moment curves for the steel beam at various load locations. These moment curves were analyzed to determine how much of the panel was effectively acting on the beam when loads were placed at various distances away from the beam. Using these “effective lengths,” along with the strain taken from the mid-span of each beam, the loads each beam was resisting for different load locations were determined for both the continuously supported panel and the simply supported/cantilever panel data. Using these loads, conservative design factors were determined for FRP panels. These factors are $S/5.05$ for the simply supported panel and $S/4.4$ for the continuous panel, where “S” is the support beam spacing. Deflections measurements were used to validate the results. Percent errors, based on experimental and theoretical deflections, were found to be in the range of 10 percent to 40 percent depending on the load locations for the results in this thesis.

Table of Contents

List of Figures	viii
List of Tables	xi
Acknowledgements.....	xiii
CHAPTER 1 - Introduction and Literature Review	1
1.1 Introduction.....	1
1.2 Literature Review	2
1.2.1 Kumar, Chandrashekhara, and Nanni	2
1.2.2 Temeles	3
1.2.3 Allampalli & Kunn	5
1.2.4 Bakis et al.....	6
1.2.5 Hayes et al.....	7
1.2.6 Kalny	7
1.2.7 Plunkett	10
1.2.8 Schreiner	11
CHAPTER 2 - Material Properties, Testing Program, and Data Analysis	12
2.1 Material Properties.....	12
2.1.1 FRP Panel.....	13
2.1.2 Steel Beams and Rigid Frame	14
2.2 Testing Configuration	15
2.2.1 Continuous Panel	15
2.2.1.1 Continuous Panel Instrumentation	18
2.2.2 Simple/Cantilever Panel.....	20
2.2.2.1 Simple Span/Cantilever Panel Instrumentation	22
2.3 Testing Procedure	23
2.3.1 Simple Span/Cantilever	23
2.3.2 Continuous Panel	23
2.4 Data Analysis	24
CHAPTER 3 - Load Distribution on Steel Beams.....	25

3.1 Determining Moments	25
3.2 Analyzing Moments.....	26
3.3 Determining Beam Loads	30
CHAPTER 4 - Simple Span/Cantilever Testing	32
4.1 Distribution Lengths and Determining Loads	32
4.2 Simple Span Load Distribution.....	34
4.3 Cantilever Analysis.....	37
4.4 LVDT Results – Simple Span/Cantilever	39
CHAPTER 5 - Continuous Panel Testing.....	42
5.1 Load Distribution on Beams	42
5.2 Continuous Panel Analysis	42
CHAPTER 6 - Panel Strain Analysis.....	49
6.1 Tongue Edge – Center of Beam 2.....	49
6.2 Tongue Edge – MS 2-3.....	51
CHAPTER 7 - Conclusions	52
CHAPTER 8 - Bibliography.....	55
Appendix A - Test Set-Up	56
A- 1 Continuous Panel	57
A-2 Simple Span/Cantilever Set-Up.....	58
A-3 Cross Sections and Details	59
Appendix B - Moment Curves/Distribution Lengths.....	62
B-1 Moments	63
B-2 Lengths of Uniform Load	65
Appendix C - Simple Span/Cantilever Test Results	66
C-1 Loading Scenario: CL BM 1.....	67
C-2 Loading Scenario: 1.25' OC BM1	70
C-3 Loading Scenario: Center of SS.....	73
C-4 Loading Scenario: OPP BM	76
C-5 Loading Scenario: CNTLVR.....	79
C-6 Load Ratio Charts	82
C-7 Load Ratio Summary	83

Appendix D - Continuous Panel Test Results.....	84
D-1 Loading Scenario: CL BM1	85
D-2 Loading Scenario: MS 1-2.....	88
D-3 Loading Scenario: CL BM2	91
D-4 Loading Scenario: MS 2-3.....	94
D-5 Loading Scenario: CL BM 3	97
D-6 Load Ratios – Cont. Test	100
D-7 Load Distribution Summary	104

List of Figures

Figure 2-1 Tongue and Groove Connection (Left) & Tongue Edge (Right)	12
Figure 2-2 Face Lay-up Schedule	13
Figure 2-3 Continuous Panel Test Configuration	16
Figure 2-4 Panel Connection Detail.....	17
Figure 2-5 (a) Actuator Used to Load Panel (b) Foot with Rubber Pad	18
Figure 2-6 Picture of (a) Metal C Shape (b) LVDT (c) Optim Megadac 200	19
Figure 2-7 Continuous Panel Instrumentation	20
Figure 2-8 Simple Span/Cantilever Test Configuration	21
Figure 2-9 Simple Span/Cantilever Instrumentation	22
Figure 3-1 Beam 1 Moment Curve at Load Magnitude of 15 kips.....	27
Figure 3-2 Shear, Moment, Deflection Diagram for Uniform Load Partially Distributed (AISC, 2008)	28
Figure 3-3 Beam 1 Analyzed Moment Curves at Load Magnitude of 15 kips (Figure B-1 contain moments curves at different load magnitudes)	28
Figure 3-4 Moment Calculation.....	30
Figure 4-1 Load Ratio Graphs for a Load Magnitude of (a) 10 kips, (b) 15 kips, and.....	35
Figure 4-2 Experimental vs. Theoretical Deflections – CL BM1 – Simple Span	41
Figure 5-1 Loading Scenario - Beam 1 - Load Magnitude: 20 kips.....	43
Figure 5-2 Load Ratio for (a) Beam 1 and (b) Beam 4 for Load magnitude of 20 kips.....	43
Figure 5-3 Loading Scenarios - Load Magnitude - 20 kips.....//...../...46	46
Figure 5-4 Load Ratios for (a) Beam 2 and (b) Beam 3 for Load Magnitude of 20 kips.....	46
Figure 5-5 Deflections - CL BM1 - Cont. Test.....	48
Figure 6-1 Panel Strain for Load at Tongue Edge above BM 2 at a Load Magnitude of 22 kips	49
Figure 6-2 Panel Strain for Load at Tongue Edge of MS 2-3 at a Load Magnitude of 22 kips ...	51
Figure A-1 Continuous Panel Test Set-Up	57
Figure A-2 Cross Section of Continuous Panel Test - View Toward East.....	57
Figure A-3 Simple Span/Cantilever Test Set-Up.....	58
Figure A-4 Cross Section of Simple Span/Cantilever Test - View Toward East	58
Figure A-5 Typ. Cross Section - View Toward North.....	59

Figure A-6 Cross Section - Simple Span/Cantilever Test - View Toward North.....	59
Figure A-7 Connection Detail - FRP Deck to Steel Beam Connection.....	60
Figure A-8 Strain Gauge Locations	60
Figure A-9 Example of Current AASHTO Load Distribution Factors.....	61
Figure A-10 AASHTO Truck Wheel Dimensions.....	61
Figure B-1 Moment Curves for Load Magnitudes of (a) 10 kips, (b) 15 kips, and (c) 20 kips....	64
Figure B-2 Length of Uniform Load.....	65
Figure C-1 Load Location - CL BM1.....	67
Figure C-2 CL BM1 Test Picture.....	67
Figure C-3 Beam Reactions - CL BM1.....	68
Figure C-4 Deflection - CL BM1.....	69
Figure C-5 Load Location - 1.25' OC BM1.....	70
Figure C-6 1.25' OC BM1 Test Picture.....	70
Figure C-7 Beam Reactions - 1.25' OC BM1.....	71
Figure C-8 Deflections - 1.25' OC BM1.....	72
Figure C-9 Load Locations - Center of SS.....	73
Figure C-10 Center of SS Test Picture.....	73
Figure C-11 Beam Reactions - Center of SS.....	74
Figure C-12 Deflections - Center of SS.....	76
Figure C-13 Load Location - OPP BM.....	77
Figure C-14 OPP BM Test Picture.....	77
Figure C-15 Beam Reactions OPP BM.....	78
Figure C-16 Deflections -OPP BM.....	79
Figure C-17 Load Locations - CNTLVR.....	80
Figure C-18 CNTLVR Test Picture.....	80
Figure C-19 Beam Reactions - CNTLVR.....	81
Figure C-20 Deflections - CNTLVR.....	82
Figure C-21 Load Ratio Charts for Load Magnitudes of (a) 10 kips, (b) 15 kips, and (c) 20 kips- Simple Span.....	// 84
Figure D-1 Load Locations - CL BM1 - Cont. Test.....	85
Figure D-2 Reactions - CL BM1.....	86

Figure D-3 Deflections - CL BM1.....	87
Figure D-4 Load Location 0 MS 1-2.....	88
Figure D-5 Beam Reactions - MS 1-2.....	89
Figure D-6 Deflections - MS 1-2.....	90
Figure D-7 Load Locations - CL BM2 - Cont. Test.....	91
Figure D-8 Beam Reactions - CL BM2.....	92
Figure D-9 Deflections - CL BM2.....	93
Figure D-10 Load Locations - MS 2-3.....	94
Figure D-11 Beam Reactions - MS 2-3.....	95
Figure D-12 Deflections - MS 2-3.....	96
Figure D-13 Load Location - CL BM3.....	97
Figure D-14 Beam Reactions - CL BM3.....	98
Figure D-15 Deflections - CL BM3.....	99
Figure D-16 Load Ratio Chart BM 1 for Load Magnitudes of (a) 10 kips, (b) 15 kips, and (c) 20 kips - Cont. Test.....	100
Figure D-17 Load Ratio Chart BM 2 for Load Magnitudes of (a) 10 kips, (b) 15 kips, and (c) 20 kips - Cont. Test.....	103
Figure D-18 Load Ratio Chart BM 3 for Load Magnitudes of (a) 10 kips, (b) 15 kips, and (c) 20 kips - Cont. Test.....	104
Figure D-19 Load Ratio Chart BM4 for Load Magnitudes of (a) 10 kips, (b) 15 kips, and (c) 20 kips - Cont. Test.....	105

List of Tables

Table 4-1 Simple Span Analysis.....	33
Table 4-2 Simple Span Load Distribution	37
Table 4-3 Cantilever Ratios	38
Table 4-4 Experimental vs. Theoretical Deflections – CL BM1 – Simple Span.....	41
Table 5-1 Load Distribution Summary for Beam 1	45
Table 5-2 Load Distribution Summary for Beam 2	47
Table 5-3 Experimental vs. Theoretical Deflections - CL BM1 - Cont. Test.....	48
Table B-1 Moment Curve Data (kip*ft)	63
Table B-2 Load Distribution Lengths	65
Table C-1 Reactions - CL BM1.....	68
Table C-2 Experimental/Theoretical Deflections - CL BM1.....	69
Table C-3 Reactions -1.25' OC BM 1	71
Table C-4 Experimental/Theoretical Deflections - 1.25' OC BM1.....	72
Table C-5 Reactions - Center of SS.....	74
Table C-6 Experimental/Theoretical Deflections - Center of SS.....	75
Table C-7 Reactions -OPP BM.....	77
Table C-8 Experimental/Theoretical Deflections - OPP BM.....	78
Table C-9 Reactions - CNTLVR.....	80
Table C-10 Experimental/Theoretical Deflections - CNTLVR.....	81
Table C-11 Load Ratio Analysis - Simple Span.....	83
Table D-1 Reactions - CL BM1.....	86
Table D-2 Experimental/Theoretical Deflections - CL BM1.....	87
Table D-3 Reactions - MS 1-2.....	89
Table D-4 Experimental/Theoretical Deflections - MS 1-2.....	90
Table D-5 Reactions - CL BM2.....	92
Table D-6 Experimental/Theoretical Deflections - CL BM2.....	93
Table D- 7 Reactions - MS 2-3	95
Table D-8 Experimental/Theoretical Deflections - MS 23.....	96
Table D-9 Reactions - CL BM3.....	98

Table D-10 Experimental/Theoretical Deflections...../.....	99
Table D-11 Load Distribution Summary - BM 1 - Cont. Test.....	104
Table D-12 Load Distribution Summary - BM 2 - Cont. Test.....	105
Table D-13 Load Distribution Summary - BM 3 - Cont. Test.....	106
Table D-14 Load Distribution Summary - BM 4 - Cont. Test.....	107

Acknowledgements

The author would like to recognize the following people for their support and helpfulness during the research detailed in this thesis:

Dr. Hani Melhem, for serving as my advisor and his constant guidance and help during the data analysis. His deep background in structural engineering as well as mathematics was extremely useful for analyzing the beam behavior as well as the panel behavior in this thesis. Dr. Robert Peterman, for providing knowledge about the instrumentation and tools used for during testing as well as serving on my committee. Dr. Asad Esmaily, for serving on my committee. Mr. Dave Meggers, from the Kansas Department of Transportation, for his continual guidance during testing and his background knowledge on the subject of FRP. Dr. Moni El-Aasar for his input on the research from a design perspective as well as his knowledge on FRP- bridge components.

Thanks to the Kansas State University Transportation Center for financial support during my graduate studies.

In conclusion, I would like to thank Mr. Kory Rankin and other structure Kansas State graduate students for their help with testing and analysis of my research. My experience would have been much more difficult without their help.

CHAPTER 1 - Introduction and Literature Review

1.1 Introduction

FRP is a composite material consisting of fibers made out of materials such as carbon or glass, bonded together using an epoxy-polymer. Although FRP has been used for over half a century in Aerospace Engineering applications, its use is generally new in other engineering disciplines.

The most common form of FRP in Civil Engineering is found in pultruded shapes that can be used as structural materials. More recently FRP honeycomb decks have been used to replace existing deteriorated bridge decks. These new FRP decks have several advantages such as a high strength to weight ratio, great weather resistance, and minimal construction time.

The high strength-to-weight ratio allows bridges to increase their load capacity since the FRP will allow for additional live loads due to a reduction in dead loads. FRP is extremely resilient against weather and will not deteriorate nearly as quick as other materials such as steel in high sulfate environments. The time required to replace an existing bridge deck with an FRP deck is very small, taking as little as a day, compared to the weeks it could take to replace an existing bridge deck with a new concrete deck. Consequently, although FRP costs substantially more than concrete, the reduced labor costs and time requirements more than compensate for the additional material costs, translating into overall cost savings in bridge construction. States that have implemented FRP include: Kansas, Missouri, West Virginia, New York, Colorado, Ohio, Maryland, and Pennsylvania.

Due to the fact that it is not commonly used in construction, there are no design standards or codes for designing bridge elements with FRP decks. Consequently, most designs using FRP that have been implemented up to this point have used experimental data along with computer modeling. The American Association of State Highway and Transportation Officials (AASHTO) provides distribution factors for beams supporting bridge decks made from other materials. These distribution factors are dependent on the spacing of the beams supporting the bridge decks. There are also different factors for different bridge constructions. For example, a bridge with a timber deck supported by steel beams will have a different factor than a bridge with a concrete deck supported on steel beams. For ASD, these factors are in terms of the beam spacing "S" divided by a certain variable dependent upon the situation. After substituting the

spacing, the resulting factor represents the load on the bridge deck for which that particular beam needs to be designed for. For example, if there is a 10 kip wheel load on a bridge with a longitudinal beam spacing of 4 ft and the AASHTO design factor for this particular bridge is $S/8$, then that beam needs to be designed to support $4/8$ or 0.5 of the wheel load, which equals 5 kips. AASHTO provides these design factors for most common materials, however due to the limited use of FRP, there are no stipulations for FRP in the specifications.

The main objective of the research detailed in this thesis is to determine a conservative lateral load distribution factor for FRP that would assist design engineers. Data was collected from two different testing periods, including the year of 2007, and also the fall of 2010 extending into January of 2011. The original testing in 2007 consisted of a panel continuously supported while the more recent tests were performed on a panel with a simple span/cantilever set-up. For the original testing, strain gauges were placed at mid-span of the supporting beams to determine the reactions along with LVDTs to measure beam deflections. The instrumentation was the same in the simple span/cantilever testing, however strain gauges were added along one beam in order to determine the behavior of the beam during various loading circumstances. After the reactions were determined from all the data, distribution factors were established for the FRP panel supported on steel beams by modeling different loading scenarios.

Strain gauges were also placed at 6 in. spacing along the panel in three rows. These provided some insight into the behavior of the panel during loading. This data was not completely necessary for determining distribution factors, however, it is briefly discussed in Chapter 6. It can be found on the (Data CD) for further analysis.

1.2 Literature Review

1.2.1 Kumar, et al

Kumar, et al (Kumar, et al., March 2001) completed research on an FRP panel used in the design of a bridge on the Missouri Rolla University Campus. The bridge design consisted of a deck made out of hollow 3 in. square FRP pultruded tube shapes bonded together to form I-shapes. Each I shape consisted of 7 layers of these square tubes alternately laid longitudinally and transversely. The tubes were connected together using an epoxy adhesive. The flanges were approximately 8 tubes across while the webs had a width of 4 tubes. Only one of the I shape

members were fabricated and used for experimental purposes. Experimental tests included a design load test, a fatigue test, and an ultimate load test. The design load test proved that the structure was capable of taking the AASHTO required design load measuring deflection along with visual observations. It was found that the deflection was more than adequate for the maximum design load. The fatigue testing included 2 million cycles where the structure was continuously unloaded to 500 pounds and reloaded to 11,000 pounds. Every 400,000 cycles, the test was paused and a static load was applied to check for any loss of stiffness in the member. All results concluded that the member did not lose any stiffness due to fatigue. The ultimate load test proved the structure to be able to withstand several times the required design load. The failure observed was not violent and it was concluded that in the case of an actual bridge failure, occupants would have sufficient time to evacuate the structure before collapse.

1.2.2 Temeles

Temeles (Temeles, 2001) developed a “testing facility” to analyze the performance of two FRP decks. The testing facility consisted of a bay cut out of the concrete road leading up to a weigh station on Interstate 81 in Virginia. A FRP panel would be laid in the bay in order to monitor the strains and deflections over an extended period of time as trucks passed over. Upon fabrication of the first panel, some design deficiencies were found and corrected for the fabrication of the second deck. The panels consisted of 10 square FRP hollow-core members placed side by side and sandwiched on top and bottom by two 3/8 in. FRP plates. Each tube was 15ft – 3 in. long with a hollow square cross section. The hollow squares had 6 in. in sides and were 3/8 in. thick. The deficiencies found included not enough clear space for a bolt to connect the panel to supporting beams therefore resulting in some delaminating of the tubes from the bottom plate in certain areas. Because of these deficiencies, it was decided that Deck 1 would not be placed in the test facility to avoid any possible failure while a truck was passing over it. However, four stiffness tests were conducted on Deck 1 in addition to ultimate load tests performed in a separate testing facility. The second deck was subject to four stiffness tests before being placed in the testing facility and then four more stiffness tests along with two ultimate strength tests. It was possible to complete two ultimate load tests since the panel spanned two- 6.5 ft bays. The panel was supported by simply-supported beams in the laboratory

set-up and by beams bearing directly on a reinforced concrete slab the entire length of the beams for the “testing facility.” For the tests, there were strain gauges located inside the structure itself along with a strain gauge and a “Wire Pot” (used for measuring deflection) at 3 locations spaced transversely in each bay. (6 readings total)

In Deck 1 testing, (tested only in the laboratory, not in the field), the loads and corresponding deflections show the panel to act linear-elastically for the required AASHTO design loads during all four stiffness tests. The first ultimate load test went up to a maximum of 102 kips, however the panel did not fail since the test had to be stopped because the load cell had reached its maximum capacity. From load-deflection plots, it was determined that the panel failed to exhibit elastic behavior after a load of 60 kips, therefore this bay was not tested again with a larger load cell. The second ultimate strength test for Deck 1 resulted in a maximum load of 107 kips before a punching-shear failure. The load-deflection plot showed the panel to behave linear-elastically up to a load of 70 kips, thereafter; ductile behavior was observed in a non-linear portion of the plot.

Deck 2 performed similarly to Deck 1 in all four stiffness tests. In some locations, the deflections were slightly less than those observed from Deck 1. It was concluded that these differences were probably due to the differences in fabrication. It was also observed that in one bay, the deflection under a load varied by 1.8% from the deflection under the same load in the adjacent bay. Theoretically, these deflections would be the same. Another discrepancy was found when comparing the strain to the deflections. In the West bay, the strain in a location was found to be larger by $100 \mu\epsilon$ than the strain in the East bay under the same loading conditions. During the same period, the deflection in the same location of the west bay was found to be smaller than that of the deflection in the East bay. The cause of these discrepancies in the results was concluded to be uncertain. The field tests proved that the maximum strains produced did not approach the strains recorded from the ultimate load tests of deck 1, in fact the strains were less than half the strains recorded in the ultimate load test. A fraction of the trucks were diverted using a cone so that the panel would experience the maximum amount of strain to ensure a critical load was recorded in the tests. A visual inspection was completed for the panel twice during service and once after the panel was removed from the testing facility. Upon the first two inspections, minor longitudinal cracking had been observed on the top face of the panel over some of the supports as well as on the bottom face of the panel in the middle of supports. By the

time the panel was removed, the cracks in all areas had expanded. It was also unexpectedly observed that the stiffness in the deck increased and became less flexible in the post-field stiffness tests compared to the pre-fields stiffness tests. The reasons for this were uncertain. The flexibility of the panel was also observed to be higher in the field than it was in either the pre or post field stiffness tests. This was concluded to be due to the support conditions of the panel. The supports were free to deflect in the laboratory tests, as opposed to resting on a concrete slab in the field tests, therefore causing more deformation in the panel itself. The ultimate strength tests proved failure loads of 132 kips and 85 kips. The failure caused by the 132 kip load was concluded to be due to a combination of punching shear along with de-bonding in between the tube walls. The second failure at a load of 85 kips was due to a failure in the tube wall where a significant size crack had formed during the field testing.

1.2.3 Allampalli and Kunn

Alampalli and Kunn (Alampalli and Kunn, 2001) worked with the New York State Department of Transportation (NYSDOT) to analyze a new FRP bridge deck installed on the Bentley Creek Bridge in Chermung County, New York. The deterioration of the original concrete deck had required NYSDOT to reduce its load rating of the bridge. During the deck replacement, the sub structure was repaired by replacing rusting rivets with steel bolts, fish-plating areas of section loss, along with cleaning and painting all the steel members. After the new FRP deck was installed, the bridge was instrumented with a total of 18 strain gauges, 6 were placed on a supporting steel beam and the remaining 12 were placed in desired locations of the FRP deck. The six that were placed on the steel beam were all placed in the same area along the beam: 2 were on the top flange, 2 on the web, and 2 were on the bottom flange of the beam. The main objectives of this bridge analysis were to determine: 1) if composite action was present between the steel beams and the FRP deck, 2) if the FRP joints, which were glued together using an epoxy adhesive, were transferring load, and 3) verify the load rating of the deck.

The 6 strain gauges located on the beam were analyzed in order to determine if composite action was happening or not. The result proved that no composite action between the FRP panel and supporting steel beams was present. This was concluded since the strains for the flanges (top and bottom) closely matched each other and the strains at the middle of the web

were approximately zero. Strain gauges were located on either side of a joint connecting two FRP panels. Through data analysis of different loading conditions, it was determined that 60 percent to 75 percent of the flexural load was being transferred between panels. Through the data analysis, the load rating for the deck matched closely what the manufacturers had originally stated. The rating was controlled by the shear capacity of the deck.

1.2.4 Bakis et al.

Bakis et al. (Bakis, et al., May 2002) provided a good introduction into FRP. Subjects discussed in the journal ranged from the fabrication of FRP materials to the different usages of FRP in the world today. The article is authored by various professionals with field experience using FRP. The article's introduction explained the fabrication process of panels and pultruded shapes that are common in FRP members.

In a lot of FRP panels, the core, or web, is actually made out of pultruded shapes sandwiched together by FRP plates. These pultruded shapes are usually hollow-core square FRP. The other main type of FRP deck is the honeycomb core sandwiched between two FRP plates. These can either be fabricated using pultrusion in a mold for the whole panel or the honeycomb structure is hand-laid in the panel.

It has been observed that most failures in these decks occur by punching shear or large scale delamination of the web from the flanges. When judging the feasibility on whether to use FRP or a more conventional material such as concrete, the cost is much greater for FRP. On average, concrete is around \$30 per square foot while FRP is usually around \$65 per square foot. The advantages of the FRP deck are a quick construction time along with an increased live load capacity, which in some circumstances, can bypass the replacement of an old bridge substructure. It is briefly discussed that the deflection criteria for FRP decks is inconclusive since there are so many different panel designs. These various panel designs provide difficult to determine how much any one design is going to deflect with out a computer model or physical experimentation.

1.2.5 Hayes et al.

Hayes, et al. (Hayes, et al., 2000) ran experimental tests on an FRP deck and determined the feasibility of using the design. The design consisted of 12 -102 mm x 102 mm x 6.35 mm square tubes sandwiched together between two 9.35 mm thick plates. The deck spanned a length of 4.27 m. Four W10 x 40 steel beams spaced 1.22 m apart supported the deck creating 3 separate spans. The objectives of the tests included determining: flexural strength and stiffness of the deck under simulated wheel loading, fatigue behavior under cyclic loading and residual strength after, and failure modes from fatigue and static loading.

The first test was completed by loading the middle bay to the AASHTO wheel design load. It was determined that the panel had more than enough flexural strength and it behaved linearly elastic throughout the test. The deflection value turned up to have a ratio of $L/247$ which was not conservative enough for AASTO standards.

The second test loaded one of the outside bays to failure. For the most part, the panel proved to behave linear-elastically up to failure. The maximum load occurred at 347 kN, which is roughly four times the maximum AASHTO wheel design load. The fatigue test was performed in the opposite outside bay and consisted of 3,000,000 loadings with static tests performed incrementally throughout. The static tests proved the panel to keep its flexural stiffness.

After the fatigue testing was complete, the panel was loaded up to failure. The failure load for this bay was 369 kN, just a little bit higher than the opposite bay. It was concluded that both bays stopped behaving linear-elastically around 311 kN. Both failures were due to shear punching in the panel. Upon the panel autopsy, it was conclude that the core failed in shear. It was also concluded that the panel had more than enough flexural and shear strength and the controlling factor in design would be the serviceability of the panel.

1.2.6 Kalny

Kalny (Kalny, 2003) completed a thesis based on the structural performance of FRP honeycomb sandwich panels in 2003. His testing, completed in 2002, included the effect of the width-to-depth ratio on panel stiffness, determining stiffness experimentally and analytically,

identification of failure criteria, exterior corner wraps' effect on ultimate bearing capacity, size effect on ultimate capacity, and the evaluation of fatigue performance.

In order to determine the effect of width to depth ratio on stiffness, 5 sandwich panels were tested for flexural strength. Each panel had the same depth with a varying width. The panels were labeled A6, A 12, A 18, A24, and A30. The number designation relates directly to the width of the panel. For example A 12 had a 12 in. width with a 5.9 in. depth while the A24 panel had a 24 in. width with a 5.9 in. depth. The depth was 5.9 in. for every test conducted. It was found that the stiffness remained relatively consistent for all the panels tested until they deflected 1.2 in. Since the span, the panels were tested with, was roughly 104 in. long, a deflection of 1.2 in. corresponds to the span over deflection ratio of 80. It was also noticed that the panels behaved linearly-elastically up to this point. After this point (span-to-deflection ratio less than or equal to 80), the panels began behaving non-linearly-elastically.

When comparing the non-linear portion for each of the panels, no definite similarities or common behaviors could be established. It was also found that no correlation existed between the width-to-depth ratios and the ultimate strength of each panel. All the panels did however fail conservatively above the design load and it was determined that deflection would be a controlling variable in the panel design.

After the panels had failed in testing, they were repaired through re-bonding the laminates to the core and adding 3 layers of FRP wrap around the corners of the panel. However, the A12 panel was not repaired but was instead cut apart for coupon testing. When loaded to failure again, the panels' results differed. Some panels (A6, A18 and A24) had a great increase in their ultimate load. It is important to note that design flaws were noticed in the A24 panel at time of fabrication. The A18 panel lost roughly 14 kips of load capacity between the original test and the test using the repaired panel. As it was observed in the first round of tests, the panels failed through delamination of the top and bottom laminate sheets from the honeycomb core. It is also important to note that the wraps acted as a clamping mechanism, which in most cases, provided extra capacity for the panel. Another observation was the panel's ability to retain load after delamination had occurred. A loud "popping" noise had occurred for the A18 panel and the load fell from 75 kips to 68 kips.

Three different 32 ft long FRP beams were also analyzed for the thesis. One beam was loaded at Clarkson University to a total load of 75 kips at which it failed through horizontal

shear. (delamination within the beam) The other beam tested was a “damaged beam” that had delaminated over a 10 ft section in route to Clarkson University. The beam was an identical design to the beam that actually was tested at Clarkson. After the discovery of this damage, the beam was shipped to KSU for testing. The damaged side was placed on the bottom so that it would be in tension and a 4 point bending test was performed. The panel proved to still be able to withstand a 40 kip load at mid-span which is more than adequate for the 28 kip AASHTO design load. After failure, the beam was shipped back to the manufacturing company, Kansas Structural Composites Inc. (KSCI) and repaired. The repair consisted of removing all unbounded laminates in the area of failure and replacing with 3 new layers. After all the laminates were replaced on the beam, an additional 2.5 in. long wrap was added on each of the four corners. After the beam was set up for the same four-point flexure test, it was loaded to failure which occurred at 125 kips. The failure mechanism was the same as the damaged beam, through delamination of the core and laminate layers. It was concluded this mechanism is probably due to the weak strength of the resin transferring the load between these two components. Since there are no fibers in that resin, it lacks the capacity that the rest of the components have with fibers.

For the fatigue tests, 3 specimens were cut out of an FRP panel measuring 8 in. deep, 20 in. wide, and 14 ft long. The first specimen was loaded to failure in order to get a good idea of appropriate load limits for the remaining specimens. The second specimen was repetitively loaded from a minimum load of 500 lb. and a maximum load of 5,400 lb for roughly 11 million cycles. Static tests were conducted incrementally through the cycles which found there was negligible loss in stiffness. The creep observed at these increments was also negligible. The third fatigue specimen was loaded from a minimum load of 500 lb. to a maximum load of 10,775 lb for roughly 11 million cycles as well. The results were closely similar to those of the second fatigue specimen.

The author was able to produce two analytical equations that produced the shear and flexural stiffness of a certain FRP member within 20% of the experimental value. The first method included summing the product of Young’s modulus and the transverse moment of inertias of the base FRP material as well as the shear modulus and transverse areas of the base FRP material. The equation formed is as follows:

$$\mathbf{EI} = \sum_{i=1}^n E x I x = E \text{base} \sum_{i=1}^n I \text{transf}, i \quad \text{[Equation 1-1]}$$

$$\mathbf{GA} = \sum_{i=1}^n G i A i = G \text{base} \sum_{i=1}^n A \text{transf}, i \quad \text{[Equation 1-2]}$$

This method proved to yield theoretical results within 20% of those found in the experiments of this thesis. The other equation the author formulated involves shear and flexure deflection equations:

$$\mathbf{GA} = \frac{3PL}{4(11\delta(L/2) - 16\delta(L/2))} \quad \text{[Equation 1-3]}$$

$$\mathbf{EI} = \frac{PL^3}{128(2\delta(L/4) - \delta(L/4))} \quad \text{[Equation 1-4]}$$

These equations were extremely close to the experimental values.

1.2.7 Plunkett

Plunkett (Plunkett, 1997) discusses the characteristics of FRP, provides some insight to FRP design, and provides some testing analysis in his report to the Transportation Research Board in 1997. The report provides some insight into the concept of fabricating an FRP bridge system that would include all the necessary components to build a bridge. (i.e. supports, bridge deck, overlay, etc..) These components would be fabricated by Kansas Structural Composites inc. (KSCI) and ideally be able to all fit on one truck for transportation. They are planned to be deployable to a location in proximity of 500 miles within 24 hours and could be constructed within 24 hours, 4 to 8 hours if the panels need to be installed on existing bridge beams/girders. The paper's discussion of experimentation in FRP panels discussed KSU's testing of FRP panels along with the installation of the No Name Creek Bridge in Russell, KS using panels fabricated from KSCI. The panels were not loaded to failure; however, by using ASTM equations, the shear modulus, modulus of rigidity, and the stiffness of the panel could be determined. The experimental results were found to come close to the calculated results. One discrepancy was

found when the experimental shear stiffness was found much higher than calculated to be. The experimental data led to the conclusions that the two decks behaved very similar to each other.

1.2.8 Schreiner

(Schreiner, 2005) Schreiner completed experimental tests comparing the lateral load distribution for a bridge in Crawford County, Kansas, first while it had a concrete deck then after an FRP deck had been replaced. The bridge decks in both cases were supported by 14 steel girders spaced at equal distances. Instrumentation consisted of strain gauges mounted at mid-span for each beam. In order to come up with the distribution, Hooke's law is used to compute the stress in each beam at mid-span when various wheel loads were placed on the beams. The distribution for a single beam would then be determined by dividing the stress in that particular beam by the sum of the stresses in all the beams. The results showed that the concrete and FRP decks behaved very similarly. No other analysis was completed with the data.

CHAPTER 2 - Material Properties, Testing Program, and Data Analysis

This section provides a description of the properties of the panels used in testing, the set up of the laboratory where the panels were tested, the procedure followed during laboratory tests, and insight into how the data was analyzed.

2.1 Material Properties

This thesis includes data from two separate testing periods. The first period occurred throughout the year of 2007 while the second occurred from September, 2010 to January, 2011. Two panels were used during these testing periods which were composed of identical material properties and dimensions. The only material difference in the panels was on the exterior longitudinal sides. The panel tested in 2007 contained a tongue and groove edge on opposite sides, whereas the panel tested in 2010/2011 contained a tongue edge and a flat edge instead of the groove edge. The images in Figure 2-1 illustrate examples of a tongue and groove edge from two standpoints. One picture (left) demonstrates the interlocking of two panels, and the other (right) shows the panel's tongue edge in its full length. The left picture is from a previous test that had the tongue edge from one panel locked into the groove edge of another panel. The picture on the right details what the full length of the tongue edge looks like. It was assumed that these differences in the side of the panels tested in the two studies had no effect on the performance of the panel.



Figure 2-1 Tongue and Groove Connection (Left) & Tongue Edge (Right)

2.1.1 FRP Panel

The FRP panels tested were fabricated by Kansas Structural Composites Incorporated (KSCI). The design consisted of a honeycomb core sandwiched together by two outer laminates. The panel's dimension were 6 ft x 8.5 ft. The two outer laminates were each ½ in thick which sandwich an inner honeycomb core that was 5 in thick. Each ½ in. thick face is made up of different layers as shown in Figure 2-2. The top and bottom layers of the laminate are composed of CM3205, a stitched fabric material containing equal quantities of fibers running longitudinally down the face as well as transversely, or orthogonally to the longitudinal direction. The 9 innermost layers are composed of a unidirectional layer of fibers, meaning all the fibers are laid longitudinally down the face. The inside-outer layer of the laminate (between the laminate and the sandwich core) is Chop SM, composed of fibers randomly oriented throughout the layer (Kalny, 2003).

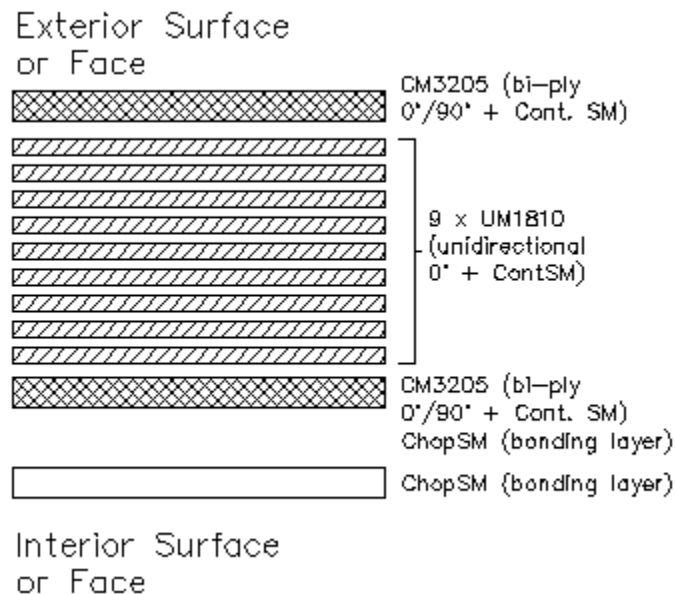


Figure 2-2 Face Lay-up Schedule

As shown in Figure 2-3, the honeycomb core consists of two main components which are called flats and flutes. The flats run longitudinally along the panel and are each roughly 2 in. long and 0.115 in. thick. The flutes are arranged in a sinusoidal pattern running longitudinally

in-between the flats and are also roughly 2 in. long by 0.115 in. thick. These components were fabricated out of ChopSM, which, as stated previously, is composed of randomly oriented fibers.

In order to construct these panels, the top and bottom faces are formed by stacking the resin-soaked plies per Figure 2-2. The honeycomb geometry is then placed on top of the bottom face while the plies are still wet with resin. Dead load is then applied on top of this honeycomb structure for the duration of the curing time. After everything has cured, the top laminate is placed on top of the bare honeycomb section. As shown in Figure 2-2, the ChopSM layer on the bottom (or top if a bottom laminate is in question) is applied between the core structure and the laminate to act as a bonding surface. The total thickness of the panel, after everything was put together, was 6 in. (Two 0.5 in.-thick laminate faces and a 5 in. honeycomb core).

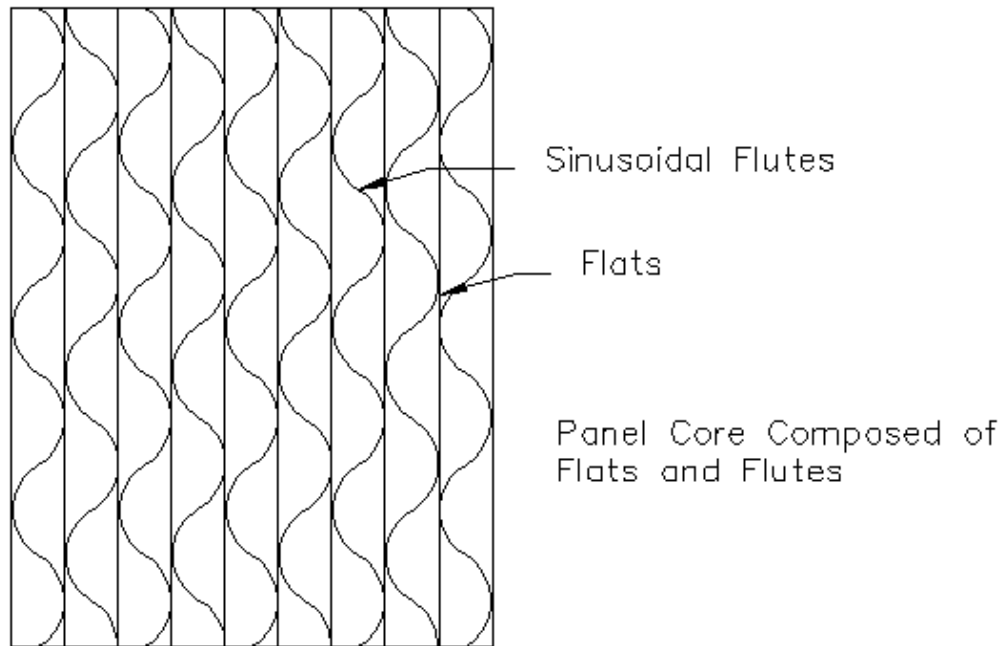


Figure 2-3 Plan of Sandwich Panel Core

2.1.2 Steel Beams and Rigid Frame

The steel beams were HP 10 x 42 shapes grade A572 with a yield strength of 50 ksi. The steel beams also have a 4 in. by 0.5 in. thick plate welded on top of the top flange. This was

placed to more closely simulate a roller support rather than allowing the panel to bear on the entire width of the top flange. The moment of inertia of the built-up shape including the steel beam and the plate on top is 254.84 in.⁴, with its centroid at a distance of 5.56 in. from the bottom of the beam. It was assumed the steel beam behaved linearly-elastic throughout the experimental procedures.

2.2 Testing Configuration

Two different testing configurations are discussed in this thesis. The first configuration describes the test set-up from 2007 when a continuous panel was tested with 4 steel beams supporting it. The second configuration discussed is from the September 2010-January 2011 test where a simple span was set up with a cantilever on one side.

2.2.1 Continuous Panel

The first round of tests, conducted throughout 2007, collected data for a continuous 6 ft x 8.5 ft x 6 in. thick FRP panel. Four steel beams (HP 10 x 42) were used to support the panel forming 3 different spans. The two external spans were 2.5 ft in length each while the internal span was 3.5 ft in length as shown in Figure 2-4. The steel beams supporting the panel were set up on a simple span, 12 ft in length. As shown in the Figure 2-4, there is a 1 in. x 1 in. steel rod placed on the rigid frame in order to better simulate the steel beams being simply supported rather than having the beams bearing on the entire width of the flange (18 in.) of the rigid steel frame. The beams were designated Beam 1 through Beam 4 as shown in Figure 2-4.

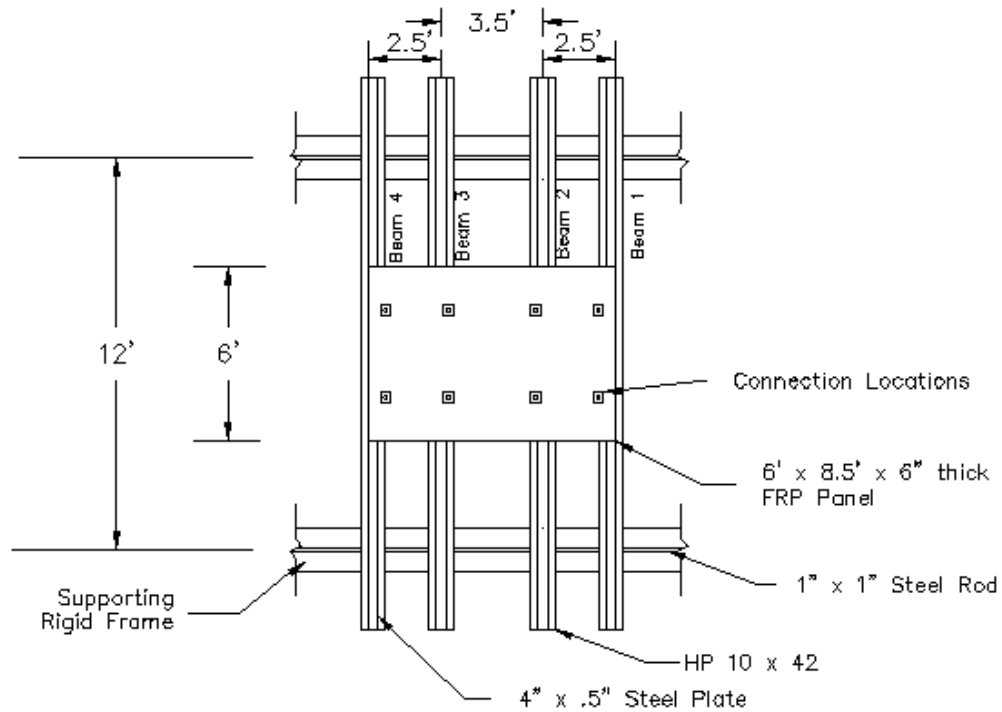


Figure 2-3 Continuous Panel Test Configuration

The panel was connected to each beam using threaded rods along with steel plates as shown in Figure 2-5. This configuration acted as a clamp around the flange of the beam which was then clamped to the panel through tightening the nuts on the threaded rod. The connection locations were 1.5 ft from each longitudinal panel edge. They were on the inner most side of the beam, for example for Beams 1 and 2, the connections were on the side of the beam closest to Beams 2 and 3 respectively; while for Beams 3 and 4, the connections were on the side of the beam closest to Beams 2 and 3, respectively. Loads were placed on the panel in 5 different locations using a hydraulic actuator, which was connected to the rigid frame as shown in Figure 2-6(a). These load locations were directly over Beam 1 (Load Designation “CL BM1”), Beam 2 (Load Designation “CL BM2”), Beam 3 (Load Designation “CL BM3”), in the mid-span between Beams 1 and 2 (Load Designation “MS 1-2”), and in the mid-span between Beams 2 and 3 (Load Designation “MS 2-3”) as shown in Figure 2-4. The actuator was used with a foot connected to the end of the piston rod, as shown in Figure 2-6(b). The foot was a rigid steel plate measuring 20 in. in length by 8 in. in width with the 20 in. side perpendicular to Beams 1 through 4. This represented the standard contact area for an AASHTO double-wheeled tire.

Since Beam 1 was supporting the edge of the panel, not enough room existed to load the panel with 20 in. by 8 in. foot in that location. To resolve this situation, a smaller foot, 10 in. by 6 in., was used in this location, 10 in. x 6 in. with the 10 in. side running parallel to the beams. During loading, a stiff rubber rectangle, matching the dimensions of the foot, was placed between the foot and the panel to prevent damage to the panel. This rubber pad had slots in it to provide room for strain gauge wires to run under the foot during testing. The actuator was powered by an MTS hydraulic pump and servo-valves as seen in Figure 2-6(c).

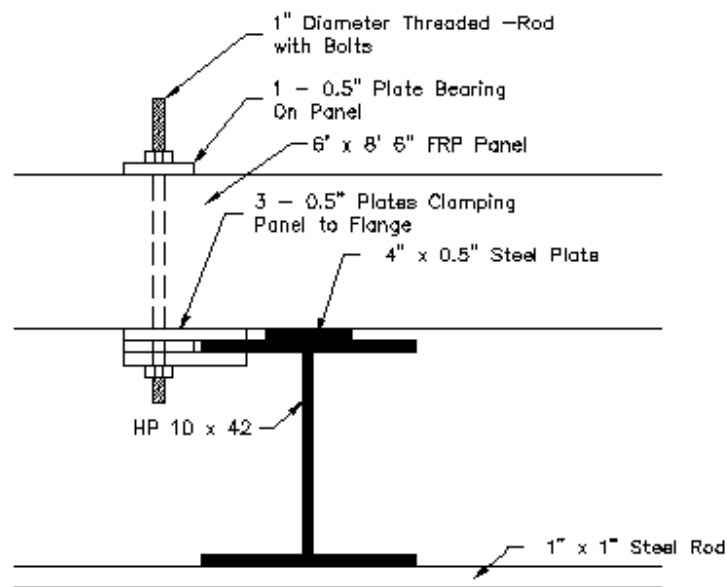
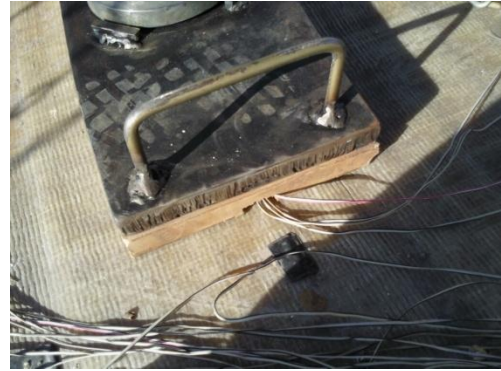


Figure 2-4 Panel Connection Detail



(a)



(b)



(c)

**Figure 2-5 (a) Actuator Used to Load Panel (b) Foot with Rubber Pad
(c) Oil Pump used for Actuator**

2.2.1.1 Continuous Panel Instrumentation

The panel was instrumented with strain gauges and linear variable differential transformers (LVDT). The panel had 3 rows of strain gauges oriented longitudinally on the panel. These strain gauges were spaced every 6 in. starting roughly 3 in. from the 6 ft long edge of the panel. In each of these rows, there were also two strain gauges mounted transversely, one at $\frac{1}{4}$ the 8.5 ft length of the panel and the other at $\frac{3}{4}$ the 8.5 ft length. At the middle of the panel,

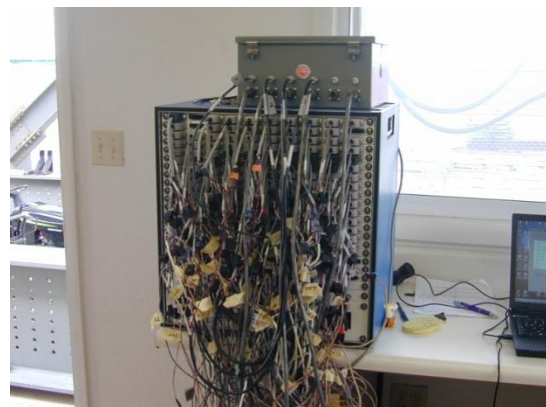
there was an entire row of transverse strain gauges from one outer row of strain gauges to the opposite outer row of strain gauges. A schematic of the panel strain gauge locations can be seen in Figure A-8 in Appendix A. The purpose of these gauges was to provide data about the behavior of the panel when subjected to loads. At mid-span of each steel beam, an LVDT was attached to the bottom flange with a short piece of a steel channel, shown in Figure 2-7(a). A picture of the LVDT can be seen in Figure 2-7(b). At these same locations, 2 strain gauges, located on each side of bottom flange, approximately 1 in. outside the center of the beam, were mounted to measure the longitudinal strain in the steel beam. A load cell with a 50 kip capacity was attached between the actuator and the foot in order to obtain load readings. All strain gauges used were manufactured by Vishay Precision Group. The data acquisition used was a Optim-Megadac 200. All strain gauges, the LVDTs, along with the load cell were plugged into this system through its various channels, as shown in Figure 2-7(c).



(a)



(b)



(c)

Figure 2-6 Picture of (a) Metal C Shape (b) LVDT (c) Optim Megadac 200

. Figure 2-9 shows the locations of loadings along with LVDT and strain gauge row locations.

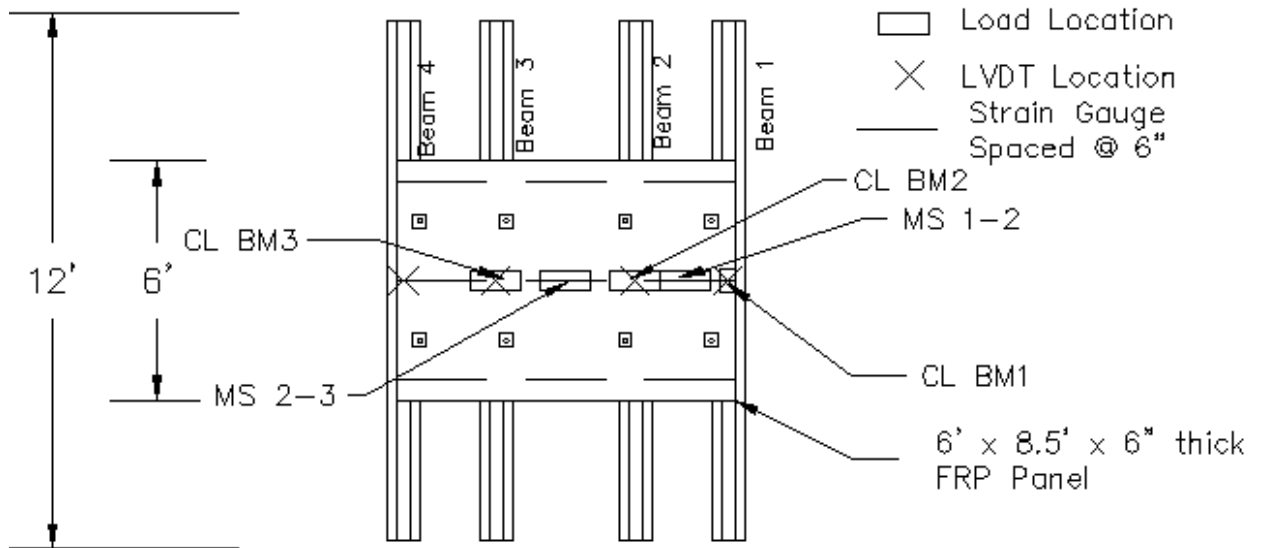


Figure 2-7 Continuous Panel Instrumentation

2.2.2 Simple/Cantilever Panel

Data was collected for the simple/cantilever panel beginning September, 2010 through early January of 2011. The 8.5 ft x 6 ft x 6 in. panel was set up on two steel beams, Beam 1 and Beam 2. Both the beams were HP 10 x 42 shapes just as they were in the previous tests. The beams had a 0.5 in. x 4 in. steel plate welded to the top flange as well. Once again the steel beams were supported by a 1 in. x 1 in. steel rod placed on the rigid frame in order to reduce beam-support bearing area. The panel's simple span was 6 ft in length with one side having an over-hanging cantilever of 2.33 ft with the entire length of the panel equal to 8.5 ft. The cantilever is on the Beam 1 side as shown in Figure 2-10.

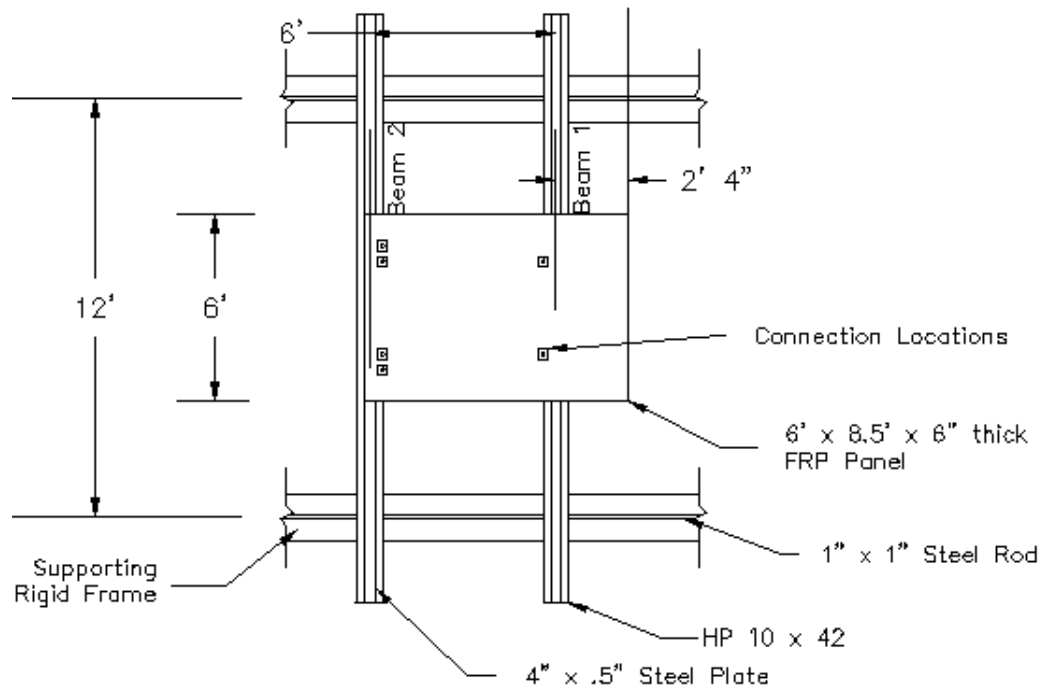


Figure 2-8 Simple Span/Cantilever Test Configuration

Since the 6 ft simple span dimension only takes account for the distances between centerlines of the beams, an extra 2 in. of bearing length exists on Beam 2. The sum of this 2 in., the 6 ft simple span, along with the 2.33 ft cantilever is 8.5 ft which is the entire length of the panel as previously stated. Panel-beam connection locations were located in the same position as they were in the continuous panel test plus two additional connections, 1 ft from the panel edges on Beam 2. These were placed on the beam to add additional anchorage for the negative reaction produced by the cantilever test. Loads were placed at 4 different locations for the simple span test, and one location for the cantilever test, as shown in Figure 2-10. For the simple span test, load was placed directly over the centerline of Beam 1 (load designation “CL BM1”), 1.25 ft off the centerline of Beam 1 on the simple span side (load designation “1.25’ OC”), in the center of the simple span or 3 ft off center of Beam 1 (load designation “C of SS”), and over the opposite beam (load designation “OPP BM”). There was one load placed on the edge of the cantilever (load designation “CNTLVR”).

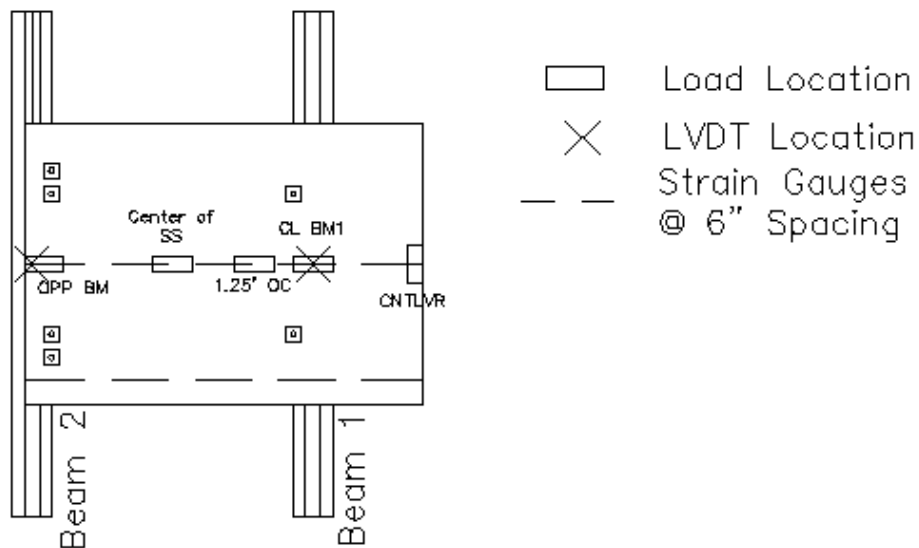


Figure 2-9 Simple Span/Cantilever Instrumentation

In order to apply the load, an actuator was used with a foot connected to the end. The foot was a rigid steel plate measuring 20 in. in length by 8 in. in width. Unlike the continuous panel where a smaller foot was used for loads adjacent to the panel edge, the same 20 in. x 8 in. foot was used for the OPP BM test, shown in Figure 2-11. For the cantilevered test, the foot was placed on the outer edge of the cantilever, rotated 90 degrees so that the centroid of the load was at the maximum possible distance away from Beam 1, providing the largest cantilever action. The locations of the strain gauges and LVDTs can also be seen in Figure 2-10.

2.2.2.1 Simple Span/Cantilever Panel Instrumentation

A panel, that had been previously instrumented, was used for this set of tests. The strain gauges were positioned in the same locations, however only 2 rows were mounted, one row on the edge of the panel and one in the center. It was determined from the previous tests, that the panel behaved symmetrically, therefore, only two rows of strain gauges were necessary in the new tests, one along the center of the panel and the other along one of the edges. The exact locations of strain gauges can be viewed in Appendix A. Before the beginning of testing, the only strain gauges on the supporting beams were the two located at mid-span of each beam just as discussed in Section 2.2.1.1. It was later determined that additional strain gauges would be

added to Beam 1 in order to obtain more data about the beam behavior. These strain gauges were placed in pairs every 1.5 ft along Beam 1. The exact locations of these gauges are detailed in Figure A-6 in Appendix A. This addition was done to determine the moment along the beam which will be discussed further in Chapter 3. All strain gauges used were manufactured by Vishay Precision Group. LVDTs were also connected at the center span of each steel beam. The same LVDT-connection was used as in the continuous panel configuration. The data acquisition used was a Optim-Megadac 200. All strain gauges, the LVDTs, along with the load cell were plugged into this system through channels.

2.3 Testing Procedure

2.3.1 Simple Span/Cantilever

The testing procedure began with the set up and positioning of the actuator. The actuator was hung on a steel I-beam from which it could be slid transversely along the panel (North to South). Once the actuator was slid into the desired loading location, the load cell and foot were attached to it. Since the foot was rigid steel, a dense rubber mat was placed in-between the foot and the panel to prevent damage that the foot might cause to the panel. The dense rubber mat contained grooves which allowed for strain gauges and wires to be located underneath the foot. Load was then gradually applied to the panel by the hydraulic actuator. The load would be slowly increased to the desired level then held static for approximately 1.5 minutes. It was necessary to wait this time at each load since the Optim Megadac 200 system took roughly 11 seconds to scan all the channels. Over a minute and a half, it would be possible to collect roughly 9 data points. Load was then completely removed from the panel and the same procedure was completed again to provide another set of data points to ensure the precision of the data. It was noticed early on in testing that the panel behaved differently under various load magnitudes. After this realization, it was decided to hold loads static at increments of 5 kips up to a total of 20 kips. These four load levels represented the data points used for analysis.

2.3.2 Continuous Panel

The continuous panel test procedure was relatively the same as the Simple Span/Cantilever, to the extent that the foot/actuator assembly would be placed then load would be increased in increments and held static for a few minutes. When analyzing the data from

2007, it was apparent that the loads were increased and held static in smaller increments. For example, the load would be increased to 2.5 kips and held static for a minute or two, then increased another 2.5 kips. In order to analyze this data and compare to the data observed from the simple span/cantilever tests, data points at 5, 10, 15 and 20 kips were the only data analyzed. For the continuous panel, the load was increased to levels above 20 kips in some cases. Most tests reach 25 kips and some went up to 30, however such data was not used in the analysis for this thesis.

2.4 Data Analysis

After the data was collected from the computer connected to the Optim Megadac 200, it was converted to a Microsoft Excel file to be analyzed. All strain gauge along with LVDT readings were zeroed out using the first data point reading when no load was on the panel. This took care of subtracting the panel dead weight when finding the beam reactions from the load induced by the actuator. A dummy gauge was also placed on an additional H10 x 42 steel beam that was not loaded. This strain, although its changes were small during testing, was subtracted from every other strain value analyzed in order to account for temperature changes during that particular test period. When analyzing a strain data points for a specific location at a particular load, the values were checked against each other for precision then, once any floating values were disregarded, the data was averaged for a final strain value.

CHAPTER 3 - Load Distribution on Steel Beams

When analyzing the continuous panel test data, the question was raised of how to effectively analyze the data collected from testing. It was unknown how to calculate the load each beam was resisting when given a strain value from the center span of a steel beam supporting the panel. Consequently, it was decided to analyze the behavior each beam when subject to different loads at various locations. In order to do this, using the simple span/cantilever test set-up, moment curves were produced for an instrumented beam, Beam 1, when subject to various loading conditions. This chapter presents the procedure used to determine these moment curves along with a discussion of the results and conclusion from these tests.

3.1 Determining Moments

The beam-moment analysis was done using the simple span/cantilever test configuration. As discussed in Chapter 2, two strain gauges were mounted every 1.5 ft along Beam 1 for the entire 12 ft span, as shown in Figure A-6 in Appendix A. Since two strain readings were taken at every location, errors could be identified when the 2 strains were dissimilar. Theoretically, the strain in the beam should be symmetrical about mid-span of the beam which allows for even further comparison of the strain readings. With four strains at each location, faulty gauge readings were identified and disregarded, which left the remaining readings to be averaged for a final strain value for that particular location on the beam. For the most part, the strains were within $10\mu\epsilon$ to $20\mu\epsilon$ of each other. Using these strain values, a moment was determined using the following equations:

$$\sigma = E\epsilon = \frac{Mc}{I} \quad \text{[Equation 3-1(a)]}$$

Solving for M:

$$M = \frac{E\epsilon I}{c} \quad \text{[Equation 3-1(b)]}$$

Where σ = stress, E is equal to the modulus of elasticity, ϵ is equal to the strain, M is equal to the moment, c is equal to the distance from neutral axis, and I is equal to the moment of inertia.

The values for “I” and “c” were 254.84.56 in.⁴ and 5.56 in. respectively as discussed in Section 2.1.2. A moment curve was then produced through plotting these moments, which were determined at 1.5 ft increments along Beam 1 resulting in 5 locations from beam end through midspan. For all 5 loading locations, moment curves were produced for 4 different loading magnitudes. For example, the moments were produced for the load of 5 kips in the loading location of CL BM1 and a curve was produced. Next a moment curve was produced for a load of 10 kips at the loading location of CL BM1. This procedure was repeated for the other 3 locations along the simple span of the panel. After brief analysis of the moment curves for 5 kips, it was observed that the panel did not have a uniform behavior which produced erratic curves. It was then decided to ignore such curves. This coincides with the unpredictable panel behavior at low loads as discussed earlier in the Section 2.3.1. A moment curve was also produced for the cantilever test at a magnitude of 15 kips.

3.2 Analyzing Moments

Three line graphs were used for the moment analysis at three different load levels (10, 15, and 20 kips). For example, Figure 3-1 shows the moment graph for a 15 kip load, placed in various positions along the panel centerline.

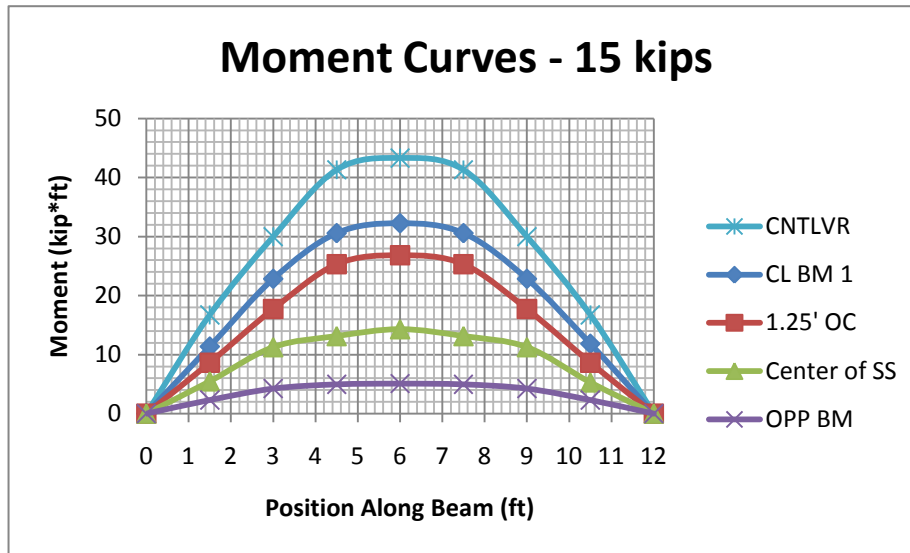


Figure 3-1 Beam 1 Moment Curve at Load Magnitude of 15 kips

After producing the moment curves using strain gauge readings, the next step was to derive a loading scenario that would produce such shapes of these moments. Using Table 3-23 of the AISC Manual (Figure 3-2), the graph representing a uniform load partially distributed over a beam would correspond to the experimental results. (AISC, 2008) For a uniform partially distributed load on a beam, the moment curve is linear up to the point where the load begins, then is parabolic just like any moment curve for a uniform load would be. Looking back to Figure 3-1, for the most part, all 5 moment curves are somewhat linear for a period of length, depending on the load location, and then appear to have a parabolic-type shape in the middle. After this realization, straight lines were drawn on the curves to determine a point where the load from the panel effectively started acting on the beams. This procedure is shown in Figure 3-3 below.

4. SIMPLE BEAM — UNIFORM LOAD PARTIALLY DISTRIBUTED

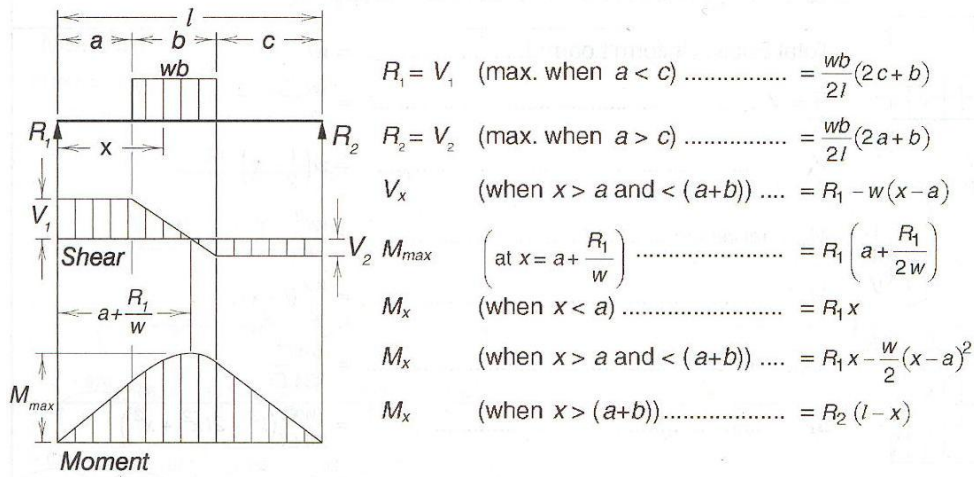


Figure 3-2 Shear, Moment, Deflection Diagram for Uniform Load Partially Distributed (AISC, 2008)

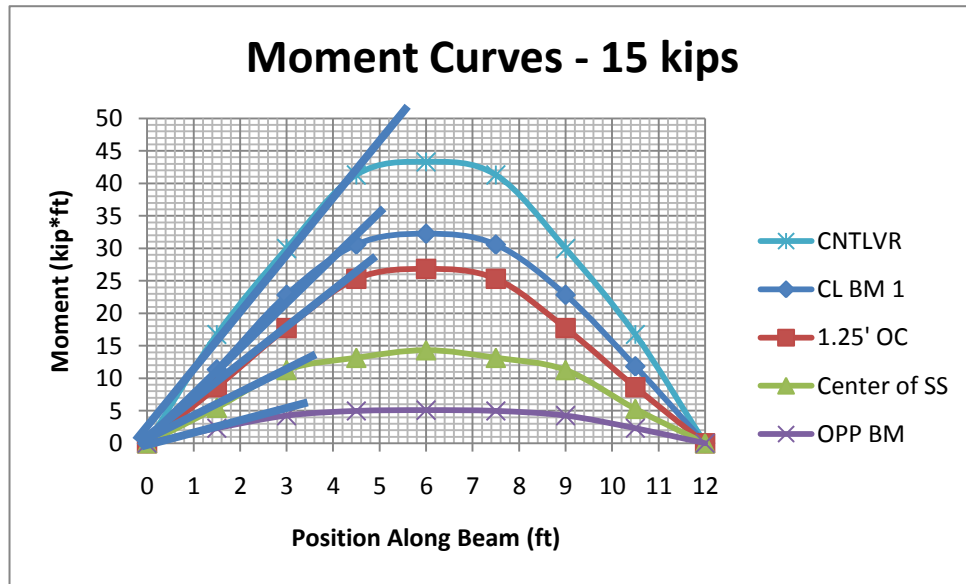


Figure 3-3 Beam 1 Analyzed Moment Curves at Load Magnitude of 15 kips (Figure B-1 contains moments curves at different load magnitudes)

From Figure 3-3, panel load distribution lengths (i.e. the lengths of the assumed uniformly distributed load) were selected. The point where the line appears to deviate from the straight line was identified as the point at which the load started to act on the beam. For example, for CL BM1, the moment curve seems to differ from the straight line drawn at roughly 4 ft into the curve. Since the curve is symmetrical, the curve would differ from a straight line drawn on the other side at 4 ft into the curve as well. Since there are two linear sections of 4 ft, it can be concluded that the panel is not acting on the beam for 8 ft of the beam's 12 ft length. Therefore, the remaining length of 4 ft, in the center section of the beam, is receiving the distributive load from the panel.

Table 3-1 Panel Distribution Length on Steel Beams

10 kips		15 kips		20 kips	
<i>Load Location (ft)</i>	<i>Length (ft)</i>	<i>Load Location (ft)</i>	<i>Length (ft)</i>	<i>Load Location (ft)</i>	<i>Length (ft)</i>
0	4	0	4	0	3
1.25	4.4	1.25	4	1.25	3
3	6	3	6	3	6
6	6	6	6	6	6

As seen in Table 3-1, the distribution length for a 15 kip load 0 ft away from the beam is 4 ft as explained in the previous paragraph. The distance is “0 ft” because the loading position is CL BM1 which is directly over the instrumented beam, Beam 1. Likewise, a load location of 1.25 ft in Table 3-1 corresponds to loading location 1.25’ OC BM1 and a load location of 3 ft corresponds to the loading location Center of SS. The same procedure was followed in finding all of the distribution lengths that are shown in Table 3-1. The moment curves for other load magnitudes are located in Appendix B-1. It can be argued that each moment curve contains a certain degree of curvature even in the locations that were stated as being linear in Figure 3-3. In reality, this is true, as the panel is not acting on the beam as a perfect uniform load starting at a specified location and ending at another. There is likely some change in the magnitude of the distributive load that starts small at the edge of the panel with a peak magnitude at the center. Since it would be quite difficult to compute a load from such an irregular loading pattern, the procedure of finding a uniform partially distributive load is much more manageable. Similar engineering procedures are used commonly such as assuming the effective compressive force in

a flexural concrete member to be 85% of the actual compression depth, using the Whitney Stress Block. With these distribution lengths determined, it was possible to calculate the load each beam was resisting in the corresponding testing scenario.

3.3 Determining Beam Loads

Using the distribution length from the moment curves determined for Beam 1, the actual load that each beam was resisting in a given test could be calculated. Since there weren't strain gauges at 1.5 ft increments on the other beams for each test, the moments had to be determined based on the strain gauges available at the mid-span of the beam. (These are Beam 2 for the simple/cantilevered test configuration, and Beam 2 through Beam 4 for the continuous panel test configuration.) Using these strains, the stress at that location could be calculated just by multiplying by the modulus of elasticity, 29,000 ksi. With the knowledge that the stress is also related to the moment, a moment could be calculated as shown in Equation 3-1. After this moment is computed, determining the magnitude of the uniform load, w , is relatively simple as shown in Figure 3-4. Equation 3-2 shows the final equation used to determine the load resisted by beams in all the tests. When considering a particular test, besides the varying strain from different load circumstances, the " ℓ " factor would be the only variable that changed from beam to beam. The value of " ℓ " is taken from Table 3-1. The total load on the beam is $w\ell$.

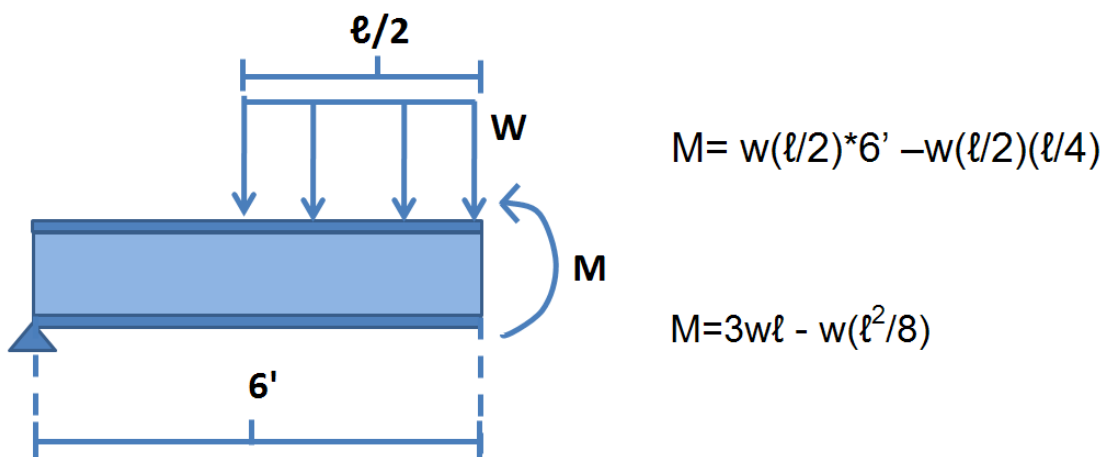


Figure 3-4 Moment Calculation

$$w\ell = \frac{M}{(3 - \frac{\ell}{8})} \quad \text{[Equation 3-2]}$$

Using Equation 3-2 to substitute for “M,” the load resisted by the steel beam becomes:

$$w\ell = \frac{EI}{c(3 - \ell/8)} \quad \text{[Equation 3-3]}$$

CHAPTER 4 - Simple Span/Cantilever Testing

This chapter will analyze the results from the tests conducted in the fall/winter of 2010 into early January, 2011. The test set ups, as discussed in Chapter 1 consisted of a simple span panel with a 2.33 ft cantilever on one side. Although this data was collected roughly 3 years after the previous tests were done in 2007, it is important to analyze it first in order to establish a conservative-base distribution factor that can be compared with the continuous panel analysis. Load resisted by the two steel beams was determined for 4 different loading scenarios shown in Figure 2-11. (CL BM 1, 1.25' OC, Center of SS, and OPP BM) After this, the panel was modeled somewhat as a continuous panel. Using this model, wheel loads were modeled and a load distribution ratio was determined from the analysis. The analysis of the cantilever load scenario served as a validation to support the data. The procedures used to complete these steps are discussed in the following sections.

4.1 Distribution Lengths and Determining Loads

The second part of Equation 3-2 was used to calculate the load resisted by each beam. This procedure is illustrated as follows. For example, when a load of 15 kips was directly over Beam 1, or loading "CL BM 1," the average strains at the center span of Beam 1 and Beam 2 were 291 $\mu\epsilon$ and 22 $\mu\epsilon$ respectively (Data CD). Using Table 3-1, the distribution lengths for Beam 1 and Beam 2 with a 15 kip load were 4 ft and 6 ft respectively. The 4 ft distribution length was used because the load was acting 0 ft away from (i.e. directly on top of) Beam 1, and the 6 ft was used given that the load was acting 6 ft away from Beam 2. Substituting these values into Equation 3-3, a load that each beam was resisting is found. This same procedure was used to calculate the beam loads for the rest of the loading cases in this test set-up. The cantilever wasn't used for this particular analysis, however, the results will be discussed in Section 4.4.

The results from this procedure are given in Table 4-1 below. Initial assessment of the results reveals inaccuracies between the stated loads for each test and the total load that was applied on the panel. For instance, when the 15 kip load was applied over Beam 1, the sum of the loads on the two support beams is equal to 13.4 kips. This difference is attributed to experimental error as well as panel behavior. The procedure for finding the beam reactions uses

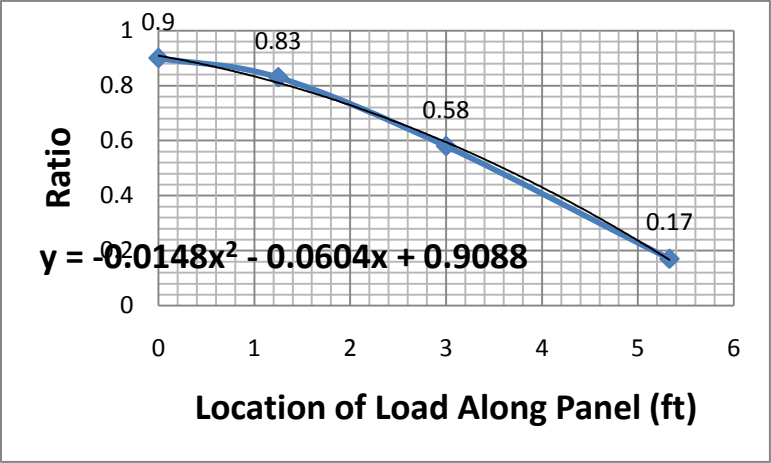
the distribution lengths found in Chapter 3. As discussed previously in Chapter 3, using a uniform load with a particular length is an approximate method to find the beam reactions and does contain some experimental and modeling errors.

Table 4-1 Simple Span Analysis

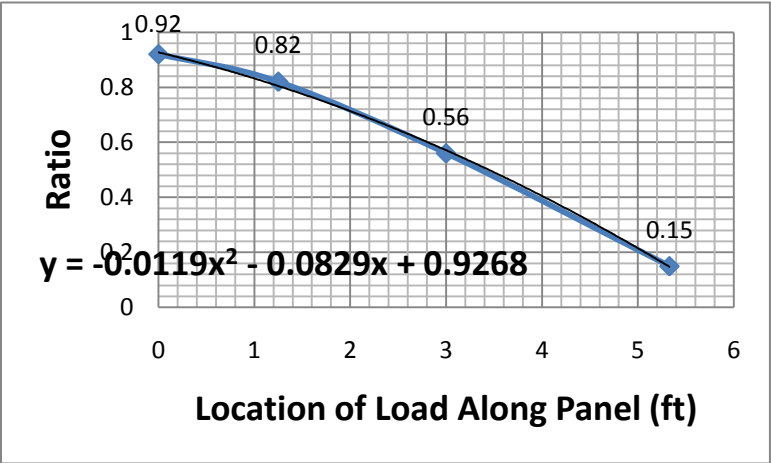
CL BM 1				1.25' OC SS				Center of Simple Span				OPP Beam SS							
Load	Reactions			Sum	Load	Reactions			Sum	Load	Reactions			Sum	Load	Reactions			Sum
	Beam 1	Beam 2	Beam 2			Beam 1	Beam 2	Beam 2			Beam 1	Beam 2	Beam 2			Beam 1	Beam 2	Beam 2	
0.0	0.00	0.00	0.00	0.0	0.0	0.00	0.00	0.00	0.0	0.0	0.00	0.00	0.00	0.0	0.0	0.00	0.00	0.00	0.0
5.3	4.01	0.60	0.77	4.6	5.4	2.58	0.77	3.4	3.4	5.2	2.55	1.71	4.3	4.1	5.2	0.77	3.32	4.1	4.1
10.3	8.08	0.94	1.27	9.0	10.5	6.03	1.27	7.3	7.3	10.4	5.99	4.25	10.2	9.6	10.4	1.61	8.02	9.6	9.6
15.6	12.29	1.07	2.28	13.4	15.6	10.61	2.28	12.9	12.9	15.6	8.41	6.70	15.1	14.9	15.6	2.21	12.66	14.9	14.9
20.8	17.28	1.34	3.21	18.6	20.7	15.13	3.21	18.3	18.3	20.1	11.29	9.21	20.5	20.0	20.6	2.68	17.36	20.0	20.0
Fraction of Load Taken By Each Member				Fraction of Load Taken By Each Member	Fraction of Load Taken By Each Member				Fraction of Load Taken By Each Member	Fraction of Load Taken By Each Member									
Load	Beam 1	Beam 2	Sum	Load	Beam 1	Beam 2	Sum	Load	Beam 1	Beam 2	Sum	Load	Beam 1	Beam 2	Sum	Load	Beam 1	Beam 2	Sum
0	0.00	0.00	0.00	0	0.00	0.00	0.00	0	0.00	0.00	0.00	0	0.00	0.00	0.00	0	0.00	0.00	0.00
5	0.87	0.13	1.00	5	0.77	0.23	1.00	5	0.60	0.40	1.00	5	0.60	0.40	1.00	5	0.19	0.81	1.00
10	0.90	0.10	1.00	10	0.83	0.17	1.00	10	0.58	0.42	1.00	10	0.58	0.42	1.00	10	0.17	0.83	1.00
15	0.92	0.08	1.00	15	0.82	0.18	1.00	15	0.56	0.44	1.00	15	0.56	0.44	1.00	15	0.15	0.85	1.00
20	0.93	0.07	1.00	20	0.82	0.18	1.00	20	0.55	0.45	1.00	20	0.55	0.45	1.00	20	0.13	0.87	1.00
Modified Load (kips)				Modified Load (kips)	Modified Load (kips)				Modified Load (kips)	Modified Load (kips)									
Load	Beam 1	Beam 2	Sum	Load	Beam 1	Beam 2	Sum	Load	Beam 1	Beam 2	Sum	Load	Beam 1	Beam 2	Sum	Load	Beam 1	Beam 2	Sum
0	0.0	0.0	0.0	0	0.0	0.0	0.0	0	0.0	0.0	0.0	0	0.0	0.0	0.0	0	0.0	0.0	0.0
5	4.3	0.7	5.0	5	3.9	1.1	5.0	5	3.0	2.0	5.0	5	3.0	2.0	5.0	5	0.9	4.1	5.0
10	9.0	1.0	10.0	10	8.3	1.7	10.0	10	5.8	4.2	10.0	10	5.8	4.2	10.0	10	1.7	8.3	10.0
15	13.8	1.2	15.0	15	12.3	2.7	15.0	15	8.3	6.7	15.0	15	8.3	6.7	15.0	15	2.2	12.8	15.0
20	18.6	1.4	20.0	20	16.5	3.5	20.0	20	11.0	9.0	20.0	20	11.0	9.0	20.0	20	2.7	17.3	20.0

4.2 Simple Span Load Distribution

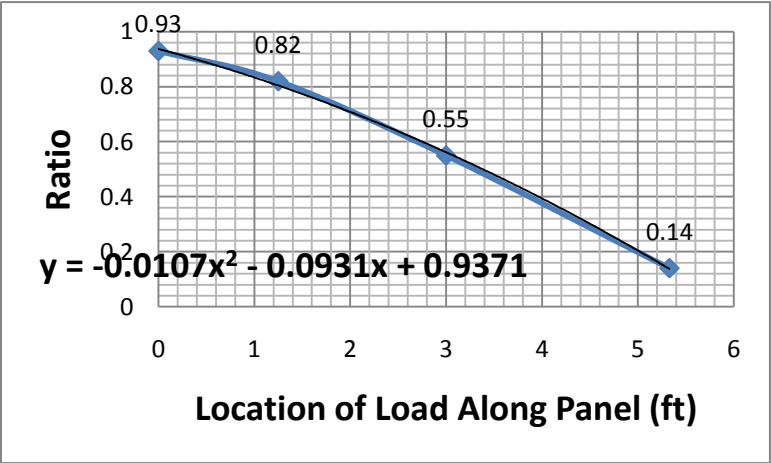
The load resisted by each beam, or termed “beam reactions”, were determined for all four simple span load scenarios that were tested (CL BM1, 1.25’ OC BM1, Center of SS, and OPP BM), which were then used to produce a load distribution factor that could be compared with other bridge deck materials in the AASHTO code. In order to produce these ratios, line graphs were made for each load level analyzed (10, 15, and 20 kips) comparing the load ratios. These are shown in the center section of Table 4-1, and the distance from Beam 1 where the load was applied. Beam 1 was modeled as the “design beam.” This means that the load ratio charts (as will be shown later in Figure 4-1) are based on how far the load is acting from Beam 1 (x-axis value). The graphs model how much load would be transferred to Beam 1 when a single load is placed on the panel at a certain location. For example, when a 15 kip load is placed 5.33 ft away from Beam 1, then the load ratio would be 0.15. Another way to look at this is that 15% of that 15 kip load placed on the panel 5.33ft away was resisted by Beam 1. Likewise, if a 15 kip load was placed 1.25 ft away on the panel, then the resulting load ratio would be 0.82. The x-values of the four data points on the graph consist of 0 ft, 1.25 ft, 3 ft, and 5.33 ft which are the locations away from the design beam where the load is applied. (Note that the load distance corresponding to the OPP BM loading position was 5.33 ft away from the design beam rather than being the entire 6 ft span since the centroid of the loading foot was not directly over the center line of Beam 2 as shown in Figure 2-9.) In order to estimate the load ratio associated with any distance between these four data points, a 2nd-degree polynomial was generated as a best fit curve through these points. It is important to note that these equations are only valid for distances from 0 ft to 6 ft. Theoretically, the ratio in the center of the simple span should be 0.500 (each beam takes half the load) however the highest collected ratio was taken. This was done to keep a consistent procedure for analyzing data. It was also observed that if the data point was reduced to 0.55, it would produce a less conservative line of best fit curve.



(a)



(b)



(c)

Figure 4-1 Load Ratio Graphs for a Load Magnitude of (a) 10 kips, (b) 15 kips, and (c) 20 kips - Simple Span Analysis

In order to get a load distribution ratio from the data shown in Figure 4-1, different loading scenarios would have to be analyzed and the most critical case would be selected. The critical case refers to the maximum ratio of the amount of load the design beam is taking to the amount of loading being applied on the panel. As discussed earlier in this thesis, the standard AASHTO truck has a wheel spacing of 6 ft and truck spacing of 4 ft. Therefore to get the most realistic value, two loads would have to be analyzed per scenario. Since the plotted ratios on the line graphs in Figure 4-1 are not all in perfect 6 ft increments, the equations for the polynomial lines of best fit will be used. For example, to analyze the scenario where one wheel (20 kips) was placed at CL BM1, or 0 ft away from the design beam, then the ratio would be equal to the sums of plugging 0 and 6 into the equation shown in Figure 4-1(c), $y = -0.0107x^2 - 0.0931x + 0.9371$. The “6 ft” value was used in the equation to model the other truck’s wheel at a distance of 6 ft away. The schematic for the standard AASHTO truck is shown in Figure A-20 in Appendix A-3. In order to analyze a case where a 20 kip wheel load was 1 ft away from the design beam, the values of “1” and “5” were used in the equation shown in Figure 4-2. The values of 1 and 5 were used to simulate the wheel load 1 ft away on one side of the beam and another wheel load 5 ft away on the opposite side of the beam making a total distance of 6 ft between the wheel loads. Although it is conservative to model the data from the simple span as a continuous span, it was necessary to use a conservative value initially that could be later compared to the continuous test data. Just as the values of “1” and “5” were added together for a loading scenario, so were the values of “2” and “4” as well as “3” and “3.” The results of these calculations are shown in Table 4-2.

The AASHTO code has different design factors for two different types of bridges, one for bridges with single lanes of traffic and the other for bridges with multiple lanes of traffic. For the case of a bridge bearing multiple lanes of traffic, it was necessary to apply extra wheel loads to the distribution factor. These wheel loads would theoretically be placed at distances of 4 ft from the outside wheel load to model another truck. Due to the size of the panel and the testing facilities, the results of this thesis are applicable for design factors considering one traffic lane only.

Table 4-1 Simple Span Load Distribution

Design Case for Interior Beam Spacing = 6'			
10 kips		20 kips	
Equation for Magnitude of Load with Relevance to Distance from Design Beam: <i>Magnitude = $-0.0148x^2 - 0.0604x + 0.9088$</i>		Equation for Magnitude of Load with Relevance to Distance from Design Beam: <i>Magnitude = $-0.0107x^2 - 0.0931x + 0.9371$</i>	
Wheel Load Locations (ft)	Load Magnitude	Wheel Load Locations (ft)	Load Magnitude
0	0.92	0	0.93
1	1.07	1	1.04
2	1.16	2	1.10
3	1.19	3	1.12
Critical Design:	1.19	Critical Design:	1.12
Design Equation: S/ 5.05		Design Equation: S/ 5.34	
15 kips		Critical Design Value for Interior Beam (6' Spacing)	
Equation for Magnitude of Load with Relevance to Distance from Design Beam: <i>Magnitude = $-0.0119x^2 - 0.0829x + 0.9268$</i>		S/ 5.05	
Wheel Load Locations (ft)	Load Magnitude		
0	0.93		
1	1.05		
2	1.12		
3	1.14		
Critical Design:	1.14		
Design Equation: S/ 5.25			

From Table 4-2, the most critical load distribution ratio was found to be S/5.05 or S/5. This was formulated from the scenario where two 10 kip loads were modeled to be 3 ft on either side of the beam producing a ratio of 1.19. This means that the design beam, which had the two 10 kip loads on either side, would be designed for 1.19*10 kips for a total of 11.9 kips. The “S” ratio may be derived from the load ratio of 1.19 since the beam spacing is 6 ft, S/5.05 is found by setting $6/x = 1.19$ and solving for x.

4.3 Cantilever Analysis

It was originally thought that the cantilever analysis would provide data for a design ratio to be used when considering an exterior beam. Upon further research and discussion with practicing engineers, it was found that simple statics calculations are used to determine the

design load for an exterior beam with a cantilever. Since the data collected from the cantilever would not be used to produce a load distribution ratio, it was used primarily to validate test results. The reactions of the two beams were based on the measured strains at mid-span of each beam - when a load was placed on the cantilever. These reactions were then compared to values derived from static calculations. The beam reactions along with ratios are shown in Table 4-3. Since the sum of the beam reactions does not add up to the total load put on the beam, these normalized load ratios provide an estimate of the portion of the load one beam is taking compared to the other beam. The beam distribution length used for Beam 1, on the cantilever side, is based on the moment curve labeled “CNTLVR” for the 15 kip graph in Figure 3-3. The procedure followed is the same as the one that was used to produce the graphs of Figure 4-1.

Table 4-2 Cantilever Ratios

Reactions (kips)				Ratios of Load Taken By Each Member			
Load	Beam 1	Beam 2	Sum	Load	Beam 1	Beam 2	Sum
0.0	0.00	0.00	0.00	0.0	0.00	0.00	0.00
1.1	0.83	-0.40	0.43	1.1	1.94	-0.94	1.00
2.1	1.45	-0.54	0.91	2.1	1.59	-0.59	1.00
3.1	2.48	-0.67	1.81	3.1	1.37	-0.37	1.00
4.1	3.43	-0.94	2.49	4.1	1.38	-0.38	1.00
5.3	4.55	-1.34	3.21	5.3	1.42	-0.42	1.00
6.2	5.47	-1.81	3.66	6.2	1.49	-0.49	1.00
7.2	6.47	-2.34	4.13	7.2	1.57	-0.57	1.00
8.3	7.62	-2.75	4.88	8.3	1.56	-0.56	1.00
9.3	8.81	-3.08	5.72	9.3	1.54	-0.54	1.00
10.3	9.99	-3.75	6.24	10.3	1.60	-0.60	1.00
11.4	11.17	-3.82	7.35	11.4	1.52	-0.52	1.00
12.4	12.26	-4.35	7.91	12.4	1.55	-0.55	1.00
13.4	13.50	-4.89	8.61	13.4	1.57	-0.57	1.00
14.4	14.69	-5.22	9.46	14.4	1.55	-0.55	1.00
				Max:	1.60	-0.60	
				Min:	1.37	-0.37	

From Table 4-3, the Load Ratios are listed for a load ranging from 1 to 14.5 kips. From a simple static calculation, the load ratio for Beam 1 should be 1.33P while the load ratio for Beam 2 should be -0.33P. From the Table, it can be concluded that these ratios are consistently within

the range of (1.37 to 1.60) upward for Beam 1 and (-0.37 to -0.60) downward for Beam 2 respectively. Although these ratios do not match exactly, they are close enough for testing purposes. Errors can be associated with the approximate method of determining the beam reactions.

4.4 LVDT Results – Simple Span/Cantilever

LVDT readings were used to validate the beam reactions. The AISC tables used to determine the beam reactions were also used to determine theoretical deflections for the beams. Since no equation is given in the AISC manual to determine the deflection of a beam with a partial-uniform-distributed-load in the center of the beam, an equation had to be derived to determine the deflections. Deflection equations are tabulated for a partial-uniform-distributed-load at the end of the beam, and it was decided that the combination of this equation and the equation of a uniform-distributed-load across the entire length of a beam would provide the desired deflections. Using the difference of the distribution lengths developed in Chapter 3 and the entire length of the span, the lengths of the partial-distributed-loads on each end of the beam were found. Using these lengths, the deflection for each partial-uniform-distributed-load at the end of the beam was found. By subtracting this deflection from the deflection of a uniform-distributed-load across the entire beam, the deflection of a partial-uniform-distributed-load in the center of the beam was found. The following equations help better describe the process of determining the theoretical beam deflections.

For uniform-distributed-load across entire beam, the midspan deflection is:

$$\Delta_1 = \frac{5wL^4}{384EI} \quad \text{[Equation 4-1]}$$

where L = length of entire span and w = magnitude of distributive load

For partially-uniform-distributed-load at end of beam,

$$\Delta_2 = \frac{wa^2(L-x)}{24EIL}(4xL - 2x^2 - a^2) \quad \text{[Equation 4-2(a)]}$$

where a = length of distributive load, x = location of desired deflection
Substituting “x=L/2” to find the deflection at mid-span,

$$\Delta_2' = \frac{wa^2}{48EI(L^2 - a^2)} \quad \text{[Equation 4-2(b)]}$$

By superposition, the total theoretical deflection at mid-span,

$$\Delta_{\text{Theoretical}} = \Delta_1 - 2\Delta_2' \quad \text{[Equation 4-2]}$$

The value of “L” is to be taken as 12 ft and the “a” value in Equation 4-2 is equal to: *12 ft – the distributive length (determined in Chapter 3)* since there is a load on each side of the beam. The value for “w” is the same in both Equation 4-1 and Equation 4-2, for the purpose of subtracting out the deflection due to load on the sides of the beam. “E” was taken as 29,000 ksi and “I” was taken as 254.84 in.⁴ These theoretical deflections were then graphed against the experimental deflections to evaluate the adequacy of the method of determining beam reactions developed in Chapter 3. Figure 4-2 and Table 4-4

Table 4-3 show the results of the 1.25' OC loading scenario. As it can be seen, the experimental and theoretical deflections for CL BM1 were very similar. The Beam 1 deflections do start to stray away from each other after a load of 10 kips is reached. This may be due to the change in load distribution lengths. Even though the percent error is around 30% for the higher loads, the difference in deflection at a load magnitude of 20 kips, is only 0.079 in. The deflection graphs and tables for the rest of the loading scenarios can be found in Appendix C. For the most part, when reviewing the deflection results from the other loading scenarios, the percent error does not go above 30% and usually stays under 20%. When it does exceed 30%, it is high, around 80%, which is due to the miniscule amount of deflection, such as 0.002 in. Even such relatively small values may produce high % error readings. With this in mind, the high percent errors in these circumstances is acceptable.

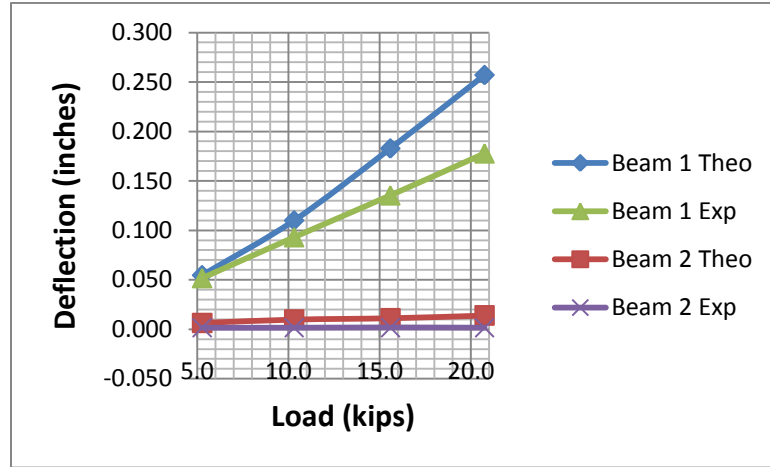


Figure 4-2 Experimental vs. Theoretical Deflections – CL BM1 – Simple Span

Table 4-3 Experimental vs. Theoretical Deflections – CL BM1 – Simple Span

Deflections - Theoretical vs. Experimental						
Load	Theoretical		Experimental		% Error	
	Beam 1	Beam 2	Beam 1	Beam 2	Beam 1	Beam 2
5.3	0.055	0.006	0.052	0.002	5.38%	74.36%
10.3	0.110	0.010	0.093	0.002	15.38%	83.52%
15.6	0.183	0.011	0.135	0.002	25.93%	84.89%
20.8	0.257	0.014	0.178	0.002	30.81%	88.46%

CHAPTER 5 - Continuous Panel Testing

This chapter will outline the procedure used for data analysis, as well as the corresponding results of the 2007 continuous panel tests.

Load resisted by the four steel beams was determined for 5 different loading scenarios. (CL BM1, MS 1-2, CL BM2, MS 2-3, and CL BM3) Just as was done in Chapter 4, the panel load ratios were determined, then different loading scenarios were produced. From these loading scenarios, load distribution factors were found. The process of determining these factors will be discussed in this chapter.

5.1 Load Distribution on Beams

Beam reactions were determined for the data collected from the continuous panel testing using the same distribution lengths that were determined in Chapter 3. Even though these distribution lengths were obtained through testing on a simple span rather than a continuous panel, it was decided that they would be adequate for this analysis. Just as in the simple span analysis, the strain reading used to determine the beam reactions was collected at the mid-span of the beam. The same equations were also used to determine the beam reactions in the continuous analysis as were used in the simple span analysis.

5.2 Continuous Panel Analysis

A similar method was used to determine the load distribution ratios for the continuous panel as the method used for the simple span. The main difference between the continuous analysis and the simple span analysis is that the polynomial line of best fit equations were not used to determine the load ratios. Since loads were placed at the mid-spans of every span along with on top of every beam along the panel, it proved to provide enough data points to combine for load ratios. For this reason, interpolation using the best fit curves was not necessary. The analyzed loading scenarios used only loads at distances that had been tested and had resulting corresponding data. Figure 5- analyzes different loading scenarios for Beam 1.

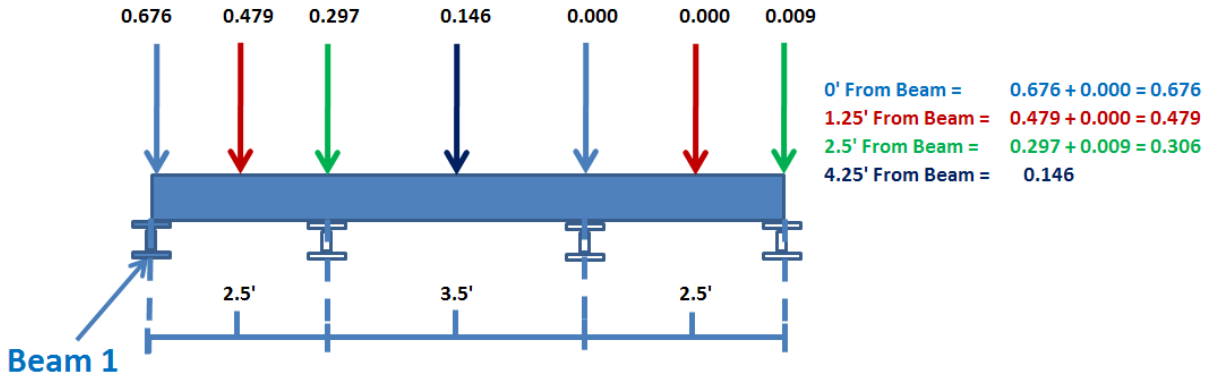
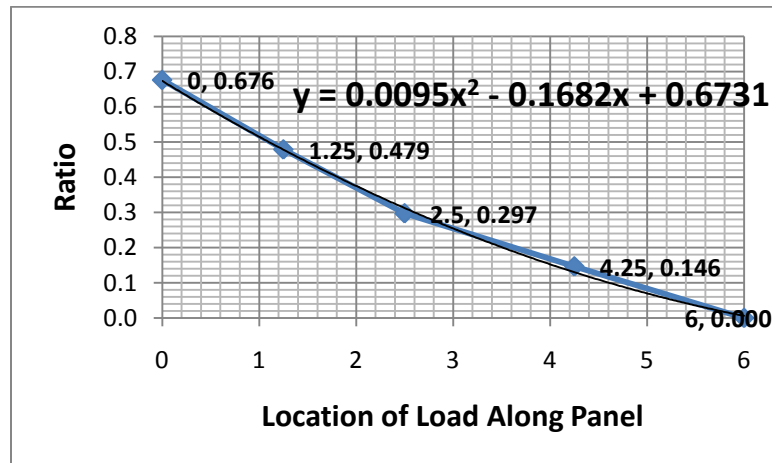
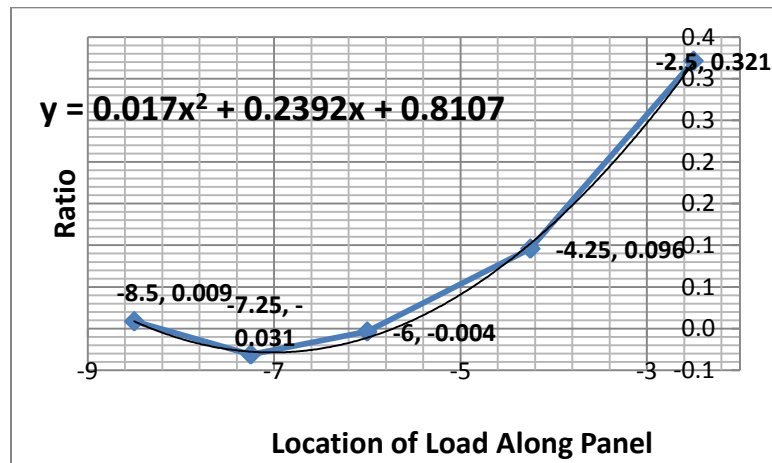


Figure 5-1 Loading Scenarios - Beam 1 – Load Magnitude: 20 kips



(a)



(b)

Figure 5-2 Load Ratio for (a)Beam 1 and (b)Beam 4 for Load Magnitude of 20 kips

The first line graph in Figure 5- represents the load ratios obtained for Beam 1 when the load is placed along the panel at various locations. This curve compares the load resisted by Beam 1 to the total load placed on the panel. For example, for the first graph which is plotted for Beam 1, when the load is placed 0 ft away, the y-coordinate of line graph is at 0.676 which means Beam 1 is taking 67.6% of the load at this location. Shown above in Figure 5-1, the different loading scenarios are analyzed for Beam 1. These scenarios include modeled wheel loads that are 0 ft, 1.25 ft, 2.5 ft and 4.25 ft away from the design beam, or in this case, Beam 1.

The second line graph in Figure 5-2 represents load ratios for Beam 4 corresponding to various loading locations along the panel. This line graph is the same as the first line graph except for the range of the x-axis values. Since Beam 4 is located 8.5 ft from Beam 1 (Beam 1 is treated as the starting point of the x-axis), all the x values are negative. For example, the coordinate point on the graph representing the load ratio when a load is placed over Beam 3 is (-2.5, 0.321) since Beam 3 is located 2.5 ft from Beam 4 and the load ratio is 0.321. This means that Beam 4 is taking 32.1% of the total load when a load is placed over Beam 3. Likewise, a coordinate point on this graph with an x-value of “-8.5” would correspond to a load ratio for Beam 4 when the load is directly over Beam 1. This same coordinate system is applied for line graphs representing load ratios for Beam 2 and Beam 3 in Appendix C.

In order to model a truck on the panel, a wheel load is 0 ft away, or directly over Beam 1, and a load 6 ft away are added together (modeling the 6 ft truck wheel spacing). Since there were no load scenarios for load in the mid-span of Beams 3 and 4 or directly over Beam 4, the beam reactions from Beam 4 were used for these ratios. For example, when considering the design of Beam 1, it would be necessary to analyze the effects of the combination of a load 2.5 ft away along with 8.5 ft (modeling the truck axle with 6 ft spacing). In this case, the load ratios from Beam 4 would have to be taken into account. Since there were not tests with load 8.5 ft away from Beam 1, the reaction of Beam 4 when a load was directly over Beam 1 would be taken into account. This is easier to visualize when looking at Figure 5-1. The ratio for Beam 1 when the load is directly over Beam 4 is 0.009. Referencing this value of 0.009 back to the chart in Figure 5-2 titled “20 kips BM 4,” the load ratios including the effect of the second wheel of the truck axle become:

Table 5-1 shows the Distribution Summary for Beam 1. This includes the load ratios for all loading scenarios along with the corresponding S ratio. The average critical design value was S/4.6 for Beam 1.

Table 5-1 Load Distribution Summary for Beam 1

Simulated Wheel Load	10 kips		15 kips		20 kips	
Location of First Wheel Along Panel (ft)	Load Ratio	S Ratio	Load Ratio	S Ratio	Load Ratio	S Ratio
0	0.63	S/4.7	0.66	S/4.5	0.68	S/4.4
1.25	0.48	S/6.3	0.48	S/6.2	0.48	S/6.3
2.5	0.33	S/9.1	0.31	S/9.6	0.31	S/9.8
4.25	0.19	S/16.1	0.16	S/18.6	0.15	S/20.5
Critical Design Value:	0.63	S/4.7	0.66	S/4.5	0.68	S/4.4
Controlling Critical Design Value:	S/4.4		Average Critical Design Value:		S/4.6	

It is possible to see unequal values for beam spacing on some bridges. This is not uncommon in some older bridges. After inquiring with local engineers, the researchers at KSU determined using the average of the beam spacing's would be adequate for this analysis. Therefore, when computing the S ratio, the spacing value used was 3 ft (average of 2.5 ft and 3.5 ft). The same procedure was used for the analysis of Beam 2 which can be seen in Figure 5-3 through Figure 5-5 seen below. The line graphs in Figure 5-2 start at -2.5 ft on the horizontal axis and go up to 3.5 ft. Referring to Figure 2-9, the axis starts negative because anything on the Beam 1 side of Beam 2 is considered to be negative, therefore the point at -2.5 ft is when the load is located over Beam 1. Just as data from the load ratios for Beam 4 was used in the analysis of Beam 1, data from Beam 3 must be used for the analysis of Beam 2. When modeling a wheel load directly over Beam 2, the load ratio for a load directly over Beam 2 must be added to a load ratio for a load 6 ft away (modeling the other wheel on the axle). Since there was no load placed 6 ft away from Beam 2, a load ratio for Beam 3 from a load placed over Beam 1 was used. For Figure 5-1 and Figure 5-3, the ratio for the load directly in the center of the panel (4.25 ft for Figure 5-1 and 1.75 ft for Figure 5-3) contains only one load ratio. There was no data that could be modeled as a load 6 ft away and subsequently it was decided that load would stand alone.

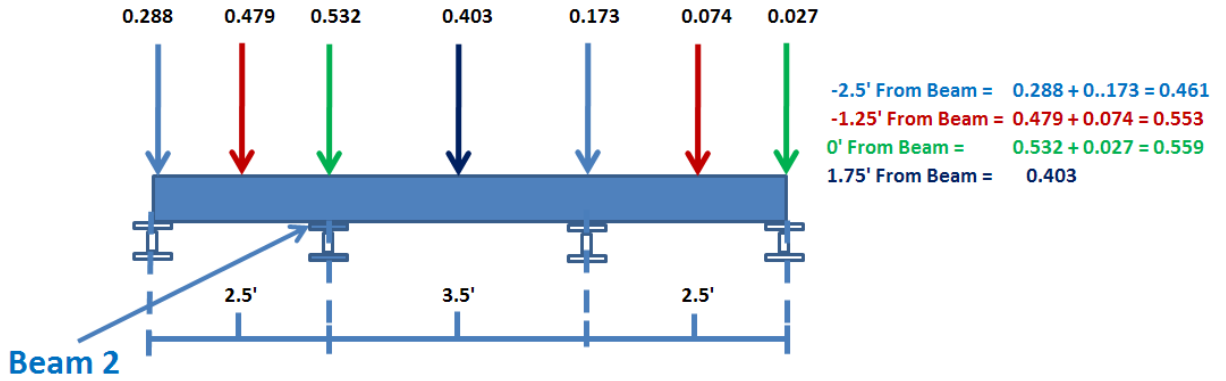
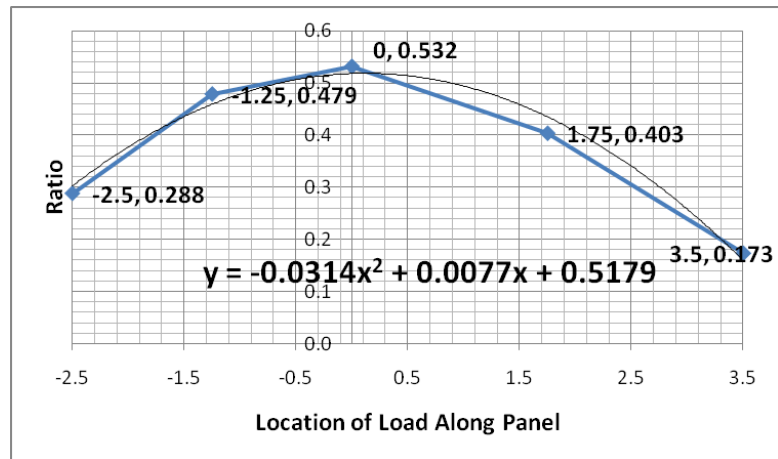
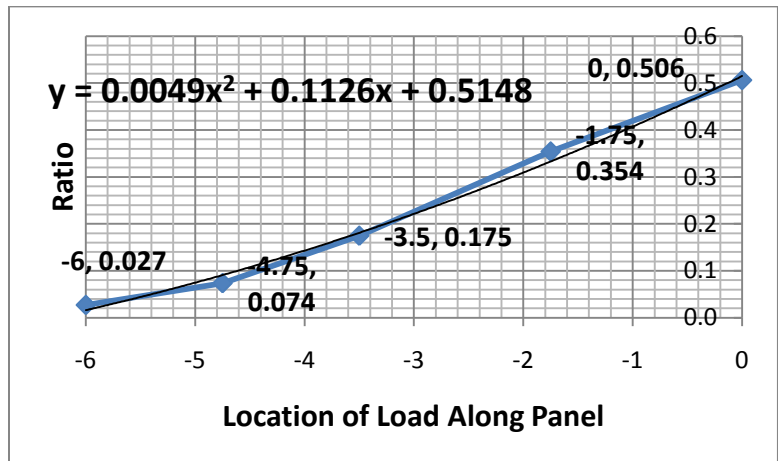


Figure 5-3 Loading Scenarios – Load Magnitude: 20 kips



(a)



(b)

Figure 5-4 Load Ratios for (a) Beam 2 and (b) Beam 3 for Load Magnitude of 20 kips

Table 5-2 Load Distribution Summary for Beam 2

Simulated Wheel Load	10 kips		15 kips		20 kips	
Location of First Wheel Along Panel (ft)	Load Ratio	S Ratio	Load Ratio	S Ratio	Load Ratio	S Ratio
-2.5	0.49	S/6.2	0.47	S/6.4	0.46	S/6.5
-1.25	0.55	S/5.5	0.55	S/5.5	0.55	S/5.4
0	0.45	S/6.6	0.56	S/5.4	0.56	S/5.4
1.75	0.35	S/8.6	0.38	S/7.8	0.40	S/7.4
Critical Design Value:	0.55	S/5.5	0.56	S/5.4	0.56	S/5.4
Controlling Critical Design Value:	S/5.4		Average Critical Design Value:		S/5.4	

5.3 LVDT Results – Continuous Panel

The same approach and equations were used to determine the deflections for the continuous panel tests as were used for the simple span and detailed in Section 4.4. Just as was done in the simple span analysis, the theoretical deflections were graphed and tabulated against the experimental deflections. An example of this can be seen in Figure 5-3 and Table 5-3 for the loading scenario, CL BM1. The theoretical and experimental deflections are not as close as they were for the simple span, reaching 45% error (0.154 in.) in some circumstances as seen below for Beam 1 at a load of 20 kips. The deflection tables and charts for other loading scenarios are located in Appendix C. The percentage of errors generally stayed under 40% and dropped as low as 20% and less for the MS 2-3 loading scenario. For the deflections of beams that had load directly over them, the % error ranged from 35-40%. For the beams adjacent to the beams with load directly over them, the percent error was usually around 20%. However, if the adjacent beam was greater than 3 ft away, the percent error increased to around 40%. The maximum percent error where the deflection values are small, in such cases as Beam 3 and Beam 4 below, can be ignored. Error can also be attributed to the beam reactions not being exact as well as some error in the LVDT's reading the deflection.

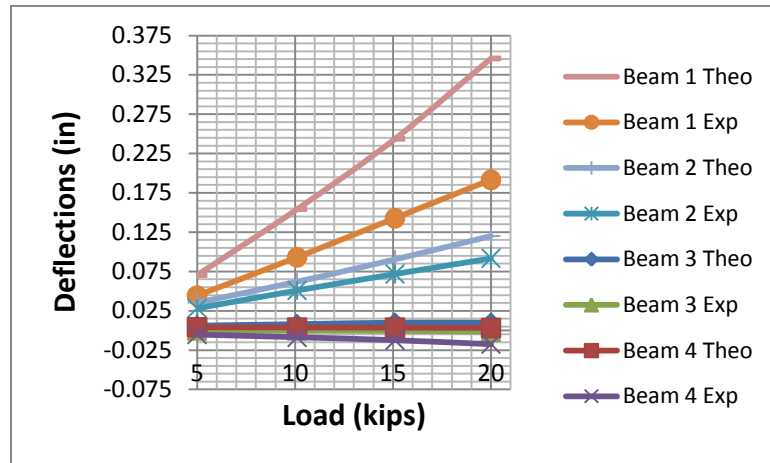


Figure 5-5 Deflections - CL BM1 - Cont. Test

Table 5-3 Experimental vs. Theoretical Deflections - CL BM1 - Cont. Test

Deflections - Theoretical vs. Experimental					
Theoretical			Experimental		
Load	Beam 1	Beam 2	Load	Beam 1	Beam 2
5.0	0.071	0.035	5.0	0.044	0.028
10.1	0.154	0.062	10.1	0.093	0.051
15.1	0.244	0.090	15.1	0.143	0.072
20.0	0.346	0.120	20.0	0.192	0.092
Load	Beam 3	Beam 4	Load	Beam 3	Beam 4
5.0	0.006	0.004	5.0	0.000	-0.005
10.1	0.008	0.004	10.1	0.000	-0.009
15.1	0.010	0.003	15.1	0.000	-0.012
20.0	0.010	0.003	20.0	-0.002	-0.017
% Error					
Load	Beam 1	Beam 2			
5.0	37.19%	20.31%			
10.1	39.71%	17.61%			
15.1	41.43%	20.37%			
20.0	44.63%	23.48%			
Load	Beam 3	Beam 4			
5.0	100.00%	227.92%			
10.1	100.00%	324.65%			
15.1	104.66%	451.97%			
20.0	115.99%	649.15%			

CHAPTER 6 - Panel Strain Analysis

Due to time constrictions and the fact that panel strains were not pertinent to the objectives of this thesis, the panel strain was not analyzed in depth and needs further analysis. The two panel strain graphs that are included in this thesis were generated from tests conducted in 2007. In these two tests, the load was placed on the tongue edge of the panel. Besides the location of the load, the test set up was the same as detailed in Appendix A for the continuous panel test. Each graph title contains the load location. For example, a graph titled “Panel Strain – Tongue Edge – Center of Beam 2,” signifies the load was placed along the center-line of Beam 2 longitudinally and was placed on the tongue edge of the panel transversely. Positive strains recorded signify tension while negative strains signify compression. Both strain graphs are for the top surface strain of the panel. Panel strain data exists for all the tests completed in 2007 and is available for each test on the (Data CD). The two representative graphs provide data for the two different loading locations specified.

6.1 Tongue Edge – Center of Beam 2

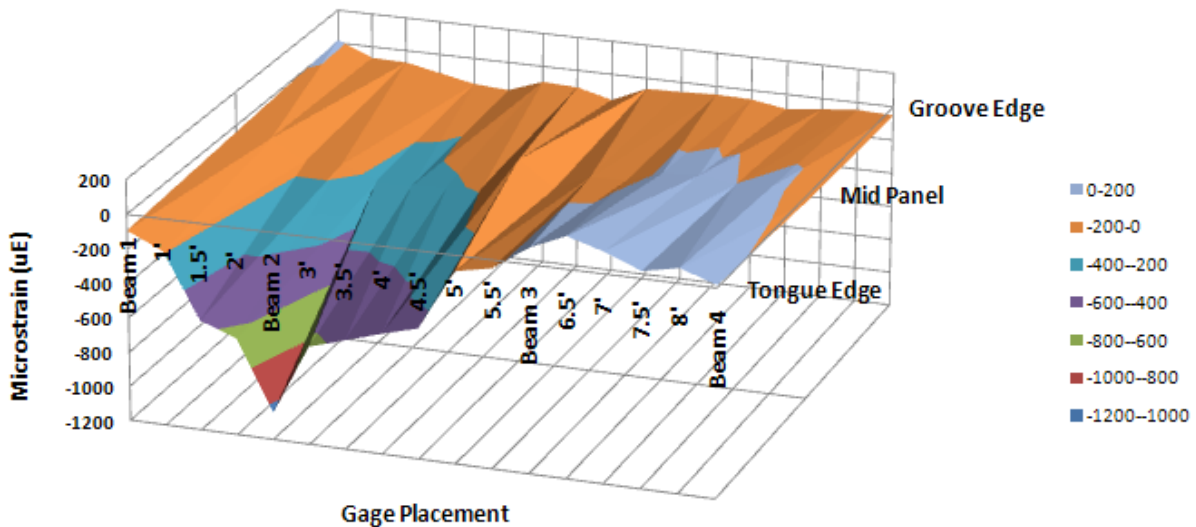


Figure 6-1 Panel Strain for Load at Tongue Edge above BM 2 at a Load Magnitude of 22 kips

When the load was placed directly over Beam 2 on the tongue edge, there was a significant amount of strain present in the panel, even though it was supported by a beam at that location (Figure 6-1). The strain reached a maximum compression value of approximately 1000 $\mu\epsilon$ at the point of loading. The strain decreased almost to zero traveling longitudinally along the tongue edge towards Beam 1. The strain in the opposite direction, towards Beam 3, also gradually reached zero at the Beam 3 support. From these observations, it is evident that the panel had compressive strain on the top surface until it reaches an adjacent support, after which it changed to tension. Consequently, the effective span length was confirmed to be the distance between Beam supports since the strain reading had an inflection point at those locations. It is important to note that the strain gauges were placed 6 in. on center in each longitudinal row, therefore, it is likely that the inflection point was not directly at the beam support, but was within 6 in. on either side of the beam. The longitudinal strains seemed to somewhat converge to zero traveling transversely across the panel toward the groove edge. Comparison of the strains provided in this graph in both directions indicates that they appear to vary in a linear fashion, however some outlying data points are present making it impossible to confirm this with the strain gauges provided.

6.2 Tongue Edge – MS 2-3

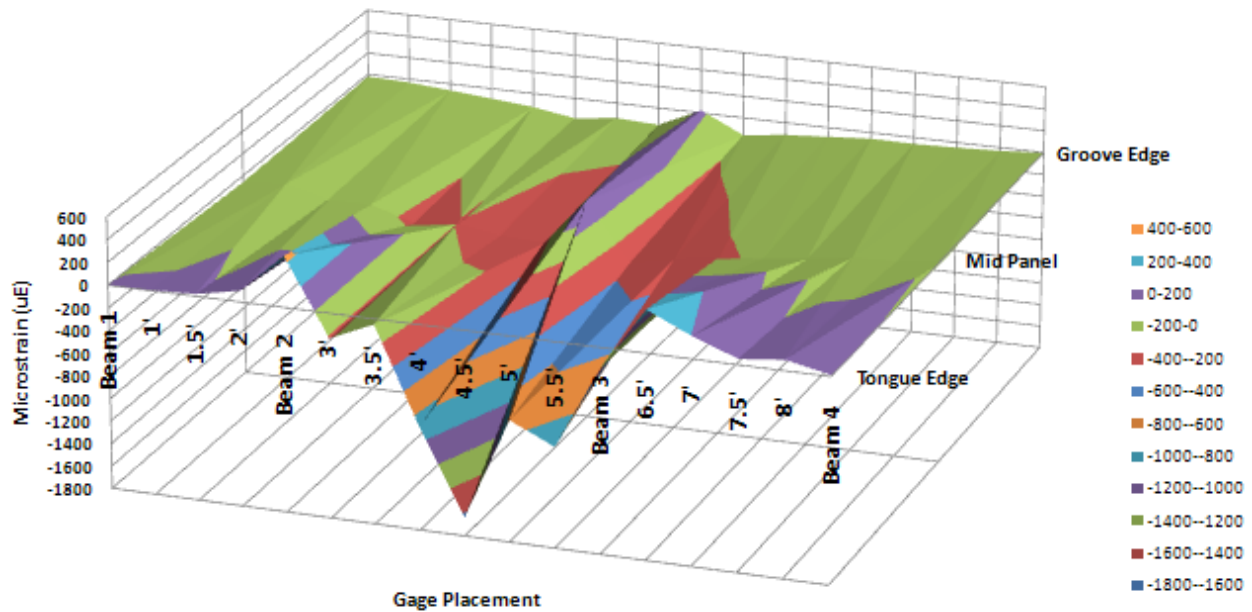


Figure 6-2 Panel Strain for Load at Tongue Edge of MS 2-3 at a Load Magnitude of 22 kips

Panel strain data was collected for the second graph considering a load at mid-span along the panel in between Beam 2 and Beam 3 (Figure 6-2). The maximum compressive strain occurred at the point of loading with a magnitude of approximately 1700 $\mu\epsilon$. This higher strain reading can be attributed to the lack of support under the load, therefore allowing a greater deflection at that point. Similar to the previous graph, the strain, in general, varies linearly until it reaches zero at the adjacent supports. On either side of the supports, tensile strain is present from the negative moment induced due to the panel having a continuous support condition. These results confirm that the effective span length is the distance between adjacent supports as was found in the previous test. This is because the panel appears to be directly resisting the load throughout the whole span since it is in compression in this area and switches to tension in the adjacent span. The change occurs at the beam supports. The strain slowly converges to zero transversely across the panel as well.

CHAPTER 7 - Conclusions

Two FRP panels were tested using two different support configurations. The continuous panel test was completed throughout the year of 2007 while the simple span and cantilever tests were completed November, 2010 through January, 2011. Load increments of 5 kips from 0 to 20 kips were analyzed in this thesis. From strain results, load ratios for beams were developed and a distribution ratio for each tests setup was determined. Additional testing was completed on the simple span in order to determine the moment curve for a beam with different loading scenarios. These moment curves provided the researchers with insight that would determine an effective load distribution length of the panel bearing on the supporting beam. The following sections will discuss the conclusions drawn from the experimental research completed for this thesis.

- The experiments conducted to determine the moment curves of the exterior beam for the various loading scenario proved that the effective load distribution length is shorter than the panel bearing length (<6 ft) when the position of the load is near or on top of the beam, and that it increases until it reaches the entire length of the panel (6 ft) at a loading distance of 3 ft or more away from the beam.
- The load distribution lengths determined from the moment curves were used to determine the beam reactions using the strain reading at the center line of the beam. In order to validate these beam reactions, LVDTs were used to measure deflection at mid-span of each beam supporting the FRP panel. These deflections were compared against “theoretical deflections” which were determined from substituting the beam reactions into beam deflection equations as described in Section 4.4. For the simple span/cantilever analysis, the percentage of error for the deflections was generally under 30%. At times when the two values differed, the theoretical deflection frequently had a larger value than the experimental deflection at loads of 10 kips and higher. This can be attributed to the load distribution lengths values being too large for these loads and creating a higher beam reaction which in turn would create a larger theoretical deflection.

- The load distribution factor determined in the simple span analysis was “ $S/5$ ” where S is the longitudinal beam spacing. Although this ratio may be too conservative, this value was established for the purpose of providing a benchmark for comparing the results from the continuous panel. The AASHTO Specification load distributions range from $S/4$ to $S/6$ for a timber deck, and $S/6$ to $S/8$ for a concrete deck, depending on the support materials and conditions. Based on the simple span analysis described in this chapter, the FRP deck performed more like a timber deck rather than a concrete deck.
- Although the cantilever tests validated the results to a certain degree, the reactions do not entirely concur with expected results using a simple statics calculation. While the load ratios for the beam on the side of the cantilever should have been 1.33, they averaged around 1.45 in the experiment. The ratios for the beam on the opposite side of the cantilever, theoretically, should have been -0.33, however they averaged around -0.45. Although these ratios are off by around 0.12, they do show that the variations of the experimental beam reactions are consistent and in the range where they should be.
- The deflections of the continuous panel test were very similar to the simple span deflections. The percent errors for the continuous test were, in general, 40% and lower. The theoretical deflections were usually larger than the experimental deflections, just as it was observed in the simple span analysis. In both cases, this can be attributed to large load distribution lengths. The higher percent error is due to the load distribution lengths being determined for a simple span test and not for a continuous panel test. It is important to recognize that the theoretical deflections are consistently above the experimental beams for all the beams in all the loading scenarios. Consequently, the load ratios determined for the analysis should be valid. Even though the beam reactions were somewhat large, they were consistently larger than they should have been for all the beams analyzed based on the deflection analysis.

- For the continuous panel load distribution factor determination, the final controlling values for the exterior and interior beams are $S/4.6$ and $S/5.4$ respectively. As expected, the panel behaved symmetrically; wheel load distribution factors for opposite exterior beams and opposite interior beams closely resembled each other. Unlike the results from the simple span testing, the critical wheel load distribution occurred, for the most part, when the load was directly over the design beam rather than when the load was in the center of the spans. This is due to the close spacing of supporting beams and might not be the case if the beams were spaced at larger intervals greater than the 6 ft wheel spacing. These results confirm the previously stated values of $S/5$ when modeling a simple span as continuous in Chapter 4.
- The brief analysis of the panel strain shows that the spans, in between supports, resisted the load for the entire length of the span. This conclusion was made since when a load is applied in the middle of a span, the top panel surface has compressive strain for the entire length of the span and tensile strain in the adjacent span. This validates the method of using the entire span distance as the effective beam spacing when determining the load distribution factors. Since the strain gauges were spaced at 6 in. on center, the location of the strain inflection points were only accurate to within 6 in. and the exact location remains unknown. Further research should be done in this area using strain gauges placed at closer intervals.

CHAPTER 8 - Bibliography

- Alampalli, S., & Kunn, J. (2001). *Load Testing of an FRP Bridge Deck Located on a Truss Bridge*. New York State Department of Transportation, Transportation Research and Development Bureau, Albany, New York.
- American Association of State Highway and Transportation Officials (AASHTO, 2010). (2010). *Standard Specifications for Highway Bridges* (17th ed.). Washington D.C.
- American Institute of Steel Construction Inc.: *Steel Construction Manual* (13th Edition ed.). (2008).
- Bakis, C. E., Bank, L. C., Brown, V. L., Cosenza, E., Davalos, J. F., & Lesko, J. J., (2002). Fiber-Reinforced Polymer Composites for Construction-State-of-the-Art Review. *Journal of Composites for Construction* , 6 (2).
- Data CD. (n.d.).
- Hayes, M. D., Ohanehi, D., Lesko, J. J., Cousine, T. E., & Wichter, D. (2000). Performance of Tube and Plate Fiberglass Bridge Deck. *Journal of Composites for Construction* , 4 (2).
- Kalny, O. (2003). *Structural Performance of Fiber-Reinforced Polymer Honeycomb Sandwich Panels for Bridge Applications*. Master's Thesis, Kansas State University, Civil Engineering.
- Kumar, P., Chandrashekhara, K., & Nanni, A. (March 2001). Structural Performance of an FRP Bridge Deck. *Journal of Composites for Construction* .
- Plunkett, J. (1997). Fiber-Reinforced Polymer Honeycomb Short Span Bridge For Rapid Installation. Idea Project Final Report. Transportation Research Board.
- Schreiner, J. (2005). *Lateral Distribution in Kansas DOT Steel Girder Bridge With FRP Deck*. Kansas Department of Transportation.
- Temeles, A. B. (2001). *Field and Laboratory Tests of a Proposed Bridge Deck Panel Fabricated from Pultruded Fiber Reinforced Polymer Components*. Master's Thesis, Virginia Polytechnic Institute and State University, Civil Engineering, Blacksburg, Virginia.

Appendix A - Test Set-Up

A- 1 Continuous Panel

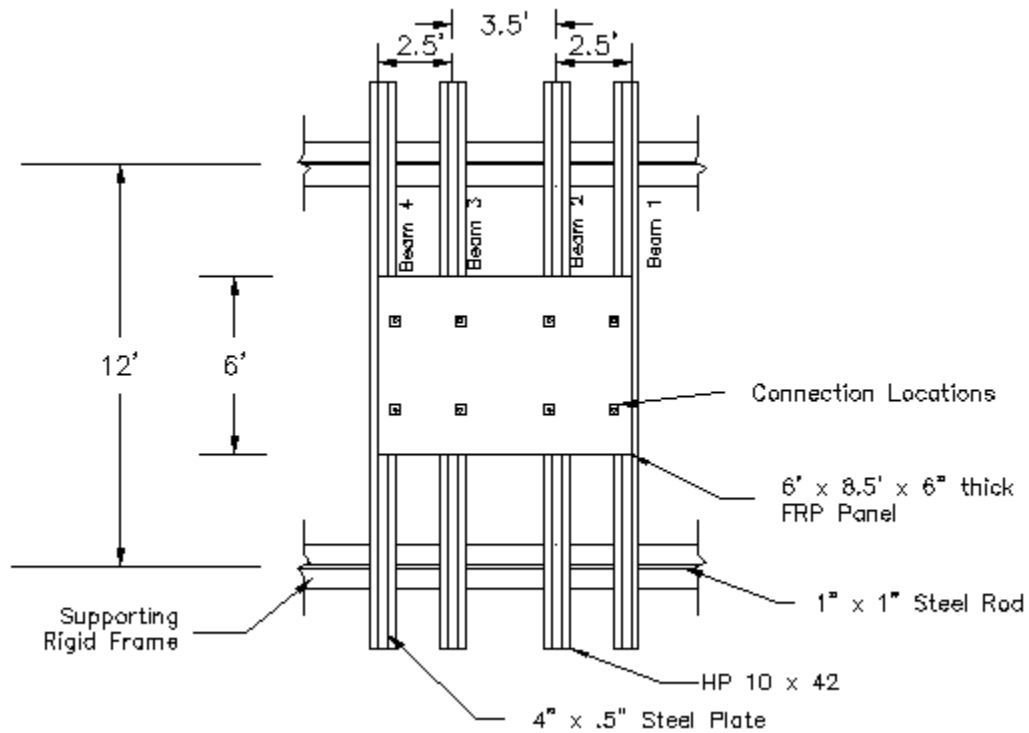


Figure A-1 Continuous Panel Test Set-Up

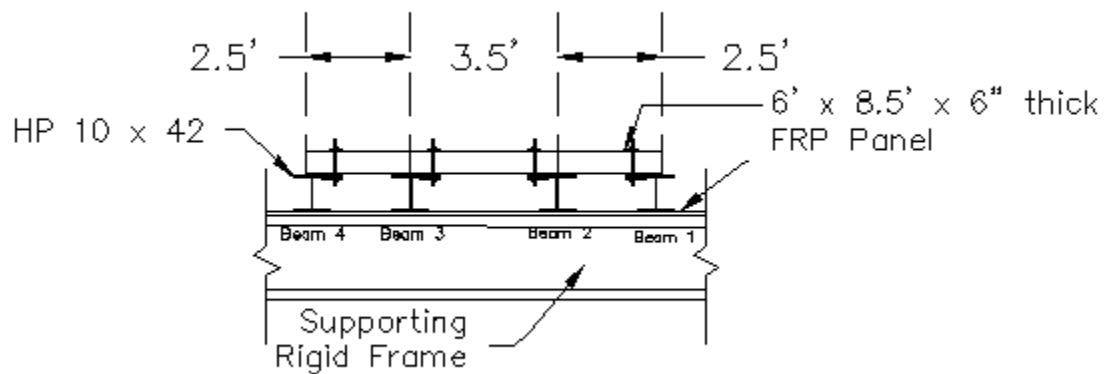


Figure A-2 Cross Section of Continuous Panel Test - View Toward East

A-2 Simple Span/Cantilever Set-Up

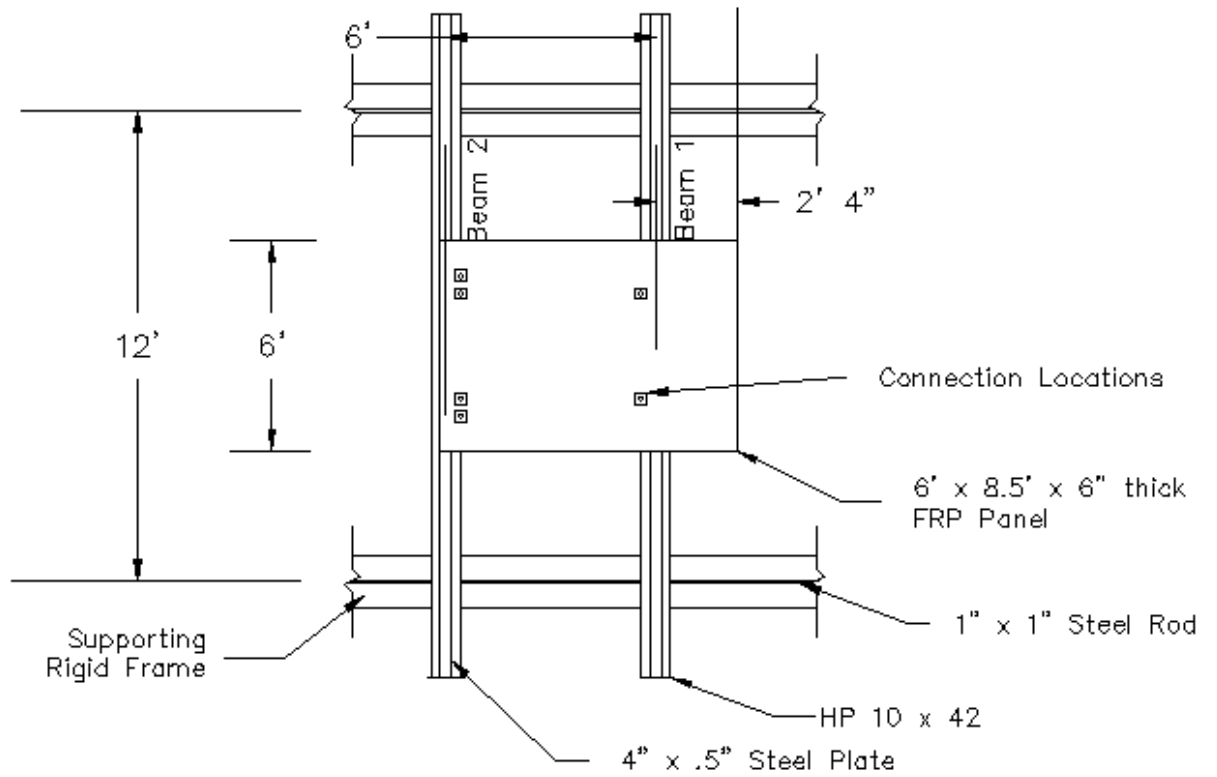


Figure A-3 Simple Span/Cantilever Test Set-Up

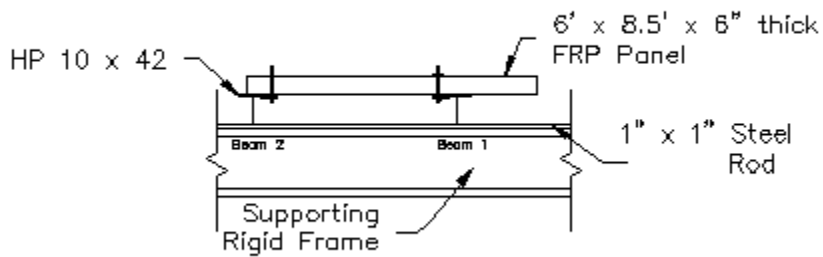


Figure A-4 Cross Section of Simple Span/Cantilever Test - View Toward East

A-3 Cross Sections and Details

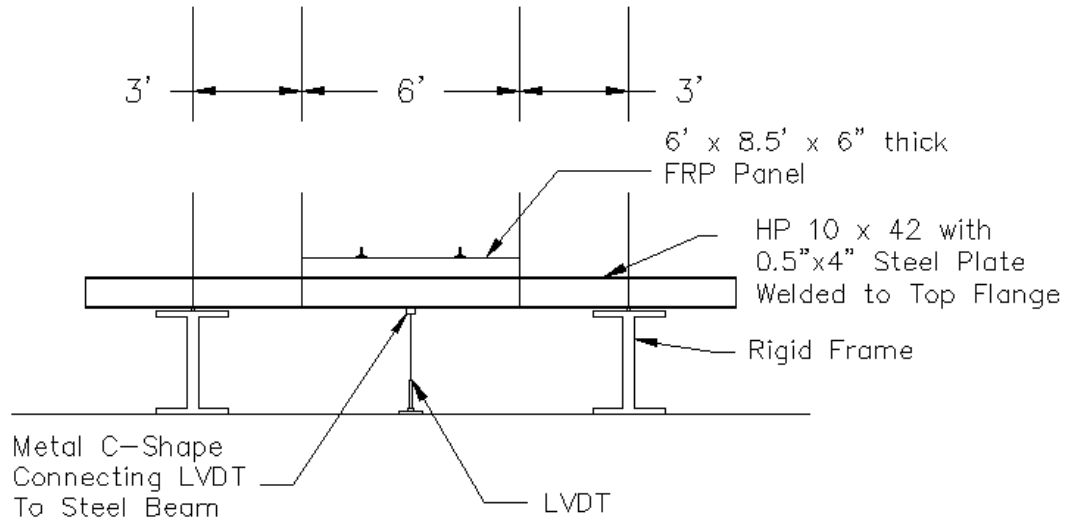


Figure A-5 Typ. Cross Section - View Toward North

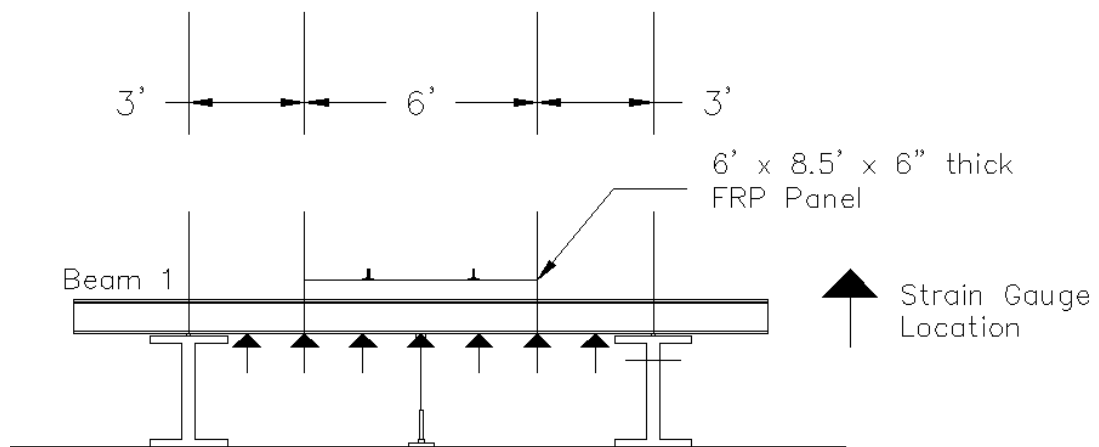


Figure A-6 Cross Section - Simple Span/Cantilever Test - View Toward North

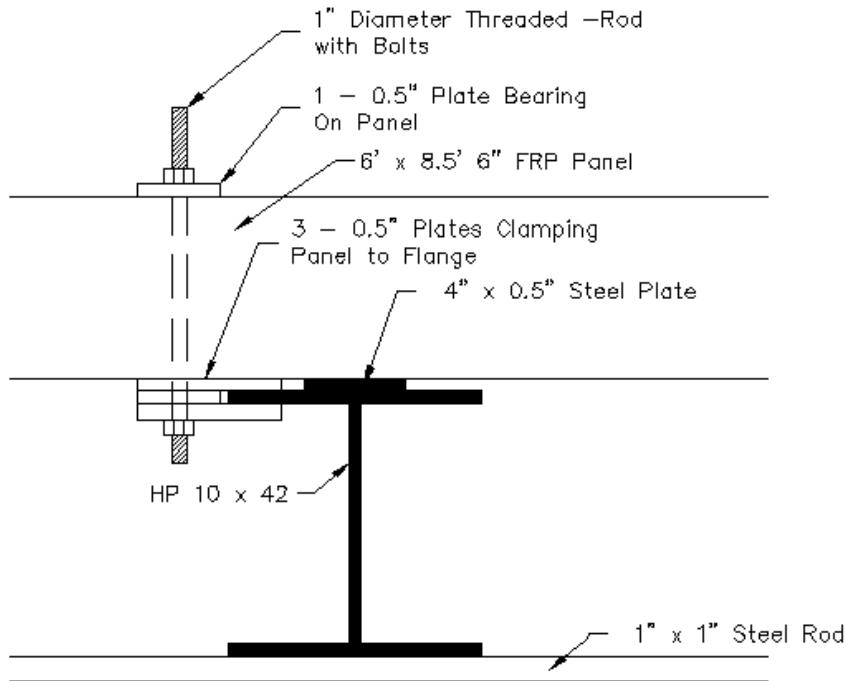


Figure A-7 Connection Detail - FRP Deck to Steel Beam Connection

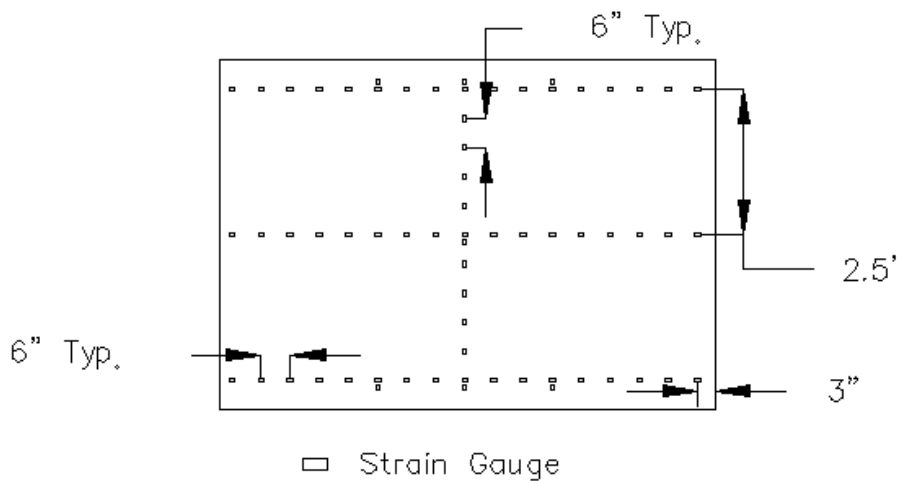


Figure A-8 Strain Gauge Locations

TABLE 3.23.1 Distribution of Wheel Loads in Longitudinal Beams

Kind of Floor	Bridge Designed for One Traffic Lane	Bridge Designed for Two or More Traffic Lanes
Timber: ^a		
Plank ^b	S/4.0	S/3.75
Nail laminated ^c 4" thick or multiple layer ^d floors over 5" thick	S/4.5	S/4.0
Nail laminated ^c 6" or more thick	S/5.0 If S exceeds 5' use footnote f.	S/4.25 If S exceeds 6.5' use footnote f.
Glued Laminated ^e Panels on Glued Laminated Stringers		
4" thick	S/4.5	S/4.0
6" or more thick	S/6.0 If S exceeds 6' use footnote f.	S/5.0 If S exceeds 7.5' use footnote f.
On Steel Stringers		
4" thick	S/4.5	S/4.0
6" or more thick	S/5.25 If S exceeds 5.5' use footnote f.	S/4.5 If S exceeds 7' use footnote f.
Concrete:		
On Steel I-Beam Stringers ^g and Prestressed Concrete Girders	S/7.0 If S exceeds 10' use footnote f.	S/5.5 If S exceeds 14' use footnote f.

Figure A-9 Example of Current AASHTO Load Distribution Factors

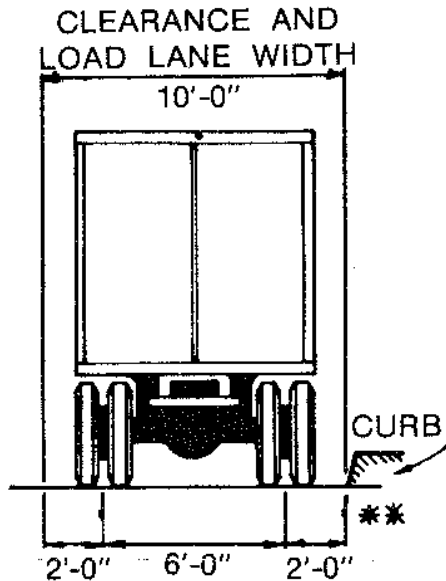


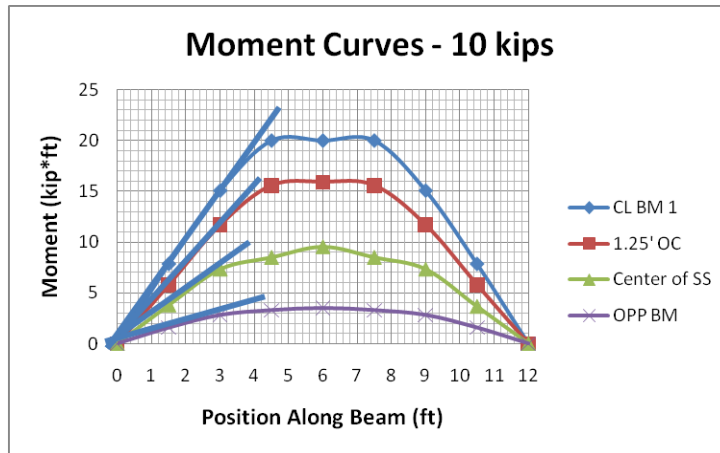
Figure A-10 AASHTO Truck Wheel Dimensions

Appendix B - Moment Curves/Distribution Lengths

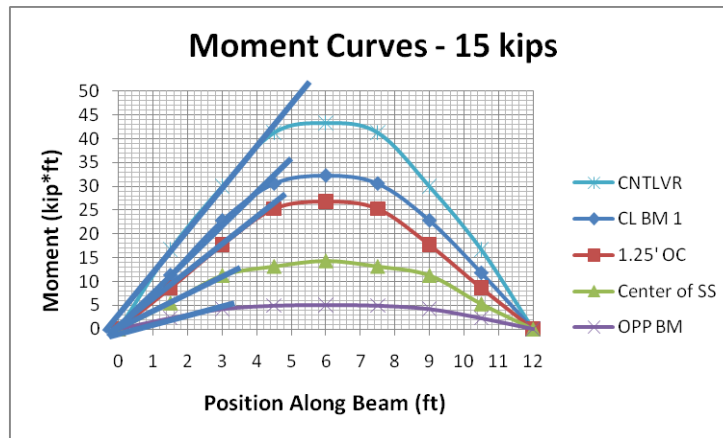
B-1 Moments

Table B-1 Moment Curve Data (kip*ft)

10 kips	CL BM 1	1.25 OC	SS	OPP BM	
0.0	0.0	0.0	0.0	0.0	
1.5	7.8	5.8	3.8	1.6	
3.0	15.1	11.7	7.3	2.8	
4.5	20.0	15.6	8.5	3.3	
6.0	20.0	15.9	9.5	3.5	
7.5	20.0	15.6	8.5	3.3	
9.0	15.1	11.7	7.3	2.8	
10.5	7.8	5.8	3.6	1.6	
12.0	0.0	0.0	0.0	0.0	
15 kips	CL BM 1	1' OC	SS	OPP BM	CNTLVR
0	0.0	0.0	0.0	0.0	0.0
1.5	11.4	8.6	5.5	2.3	16.7
3	22.8	17.7	11.3	4.3	30.0
4.5	30.6	25.3	13.1	5.0	41.3
6	32.3	26.8	14.3	5.1	43.3
7.5	30.6	25.3	13.1	5.0	41.3
9	22.8	17.7	11.3	4.3	30.0
10.5	11.8	8.6	5.3	2.3	16.7
12	0.0	0.0	0.0	0.0	0.0
20 kips	CL BM 1	1' OC	SS	OPP BM	
0.0	0.0	0.0	0.0	0.0	
1.5	14.1	12.0	7.5	2.8	
3.0	30.0	23.5	14.8	5.5	
4.5	41.3	33.9	17.9	6.1	
6.0	45.2	39.6	19.1	6.2	
7.5	41.3	33.9	17.9	6.1	
9.0	30.0	23.5	14.8	5.5	
10.5	14.1	11.2	7.5	2.8	
12.0	0.0	0.0	0.0	0.0	

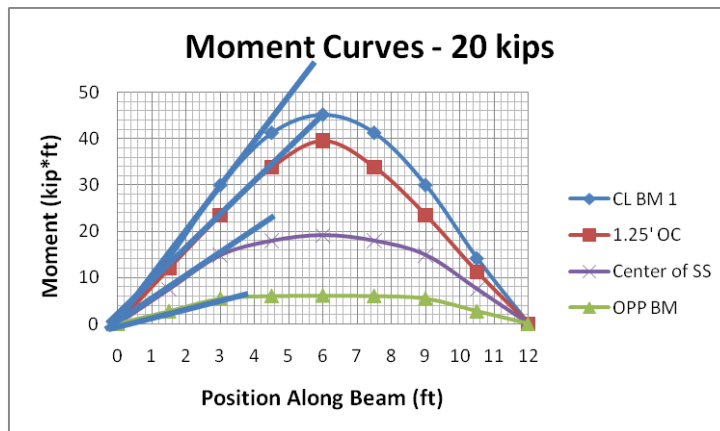


(a)



(b)

(same as Figure 3-3)



(c)

Figure B-1 Moment Curves for Load Magnitudes of (a) 10 kips, (b) 15 kips, and (c) 20 kips

B-2 Lengths of Uniform Load

Table B-2 Load Distribution Lengths¹

10 kips	
Location	Length(ft)
CL BM 1	4
1.25' OC	4.4
Center of SS	6
OPP BM	6
15 kips	
Location	Length(ft)
CL BM 1	4
1.25' OC	4
Center of SS	6
OPP BM	6
CNTLVR	3.6
20 kips	
Location	Length(ft)
CL BM 1	3
1.25' OC	3
Center of SS	6
OPP BM	6

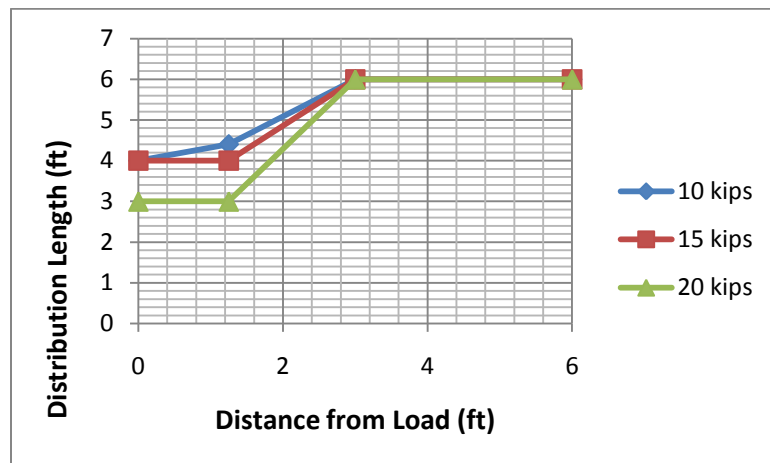


Figure B-2 Lengths of Uniform Load

¹ Note: This Table contains the same information as Table 3-1

Appendix C - Simple Span/Cantilever Test Results

C-1 Loading Scenario: CL BM 1

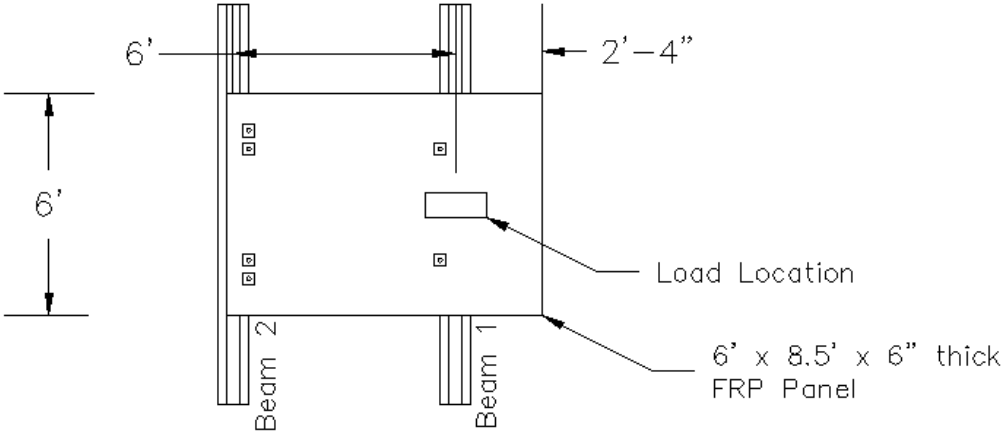


Figure C-1 Load Location – CL BM1



Figure C-2 CL BM1 Test Picture

Table C-1 Reactions – CL BM1

Reactions (kips)				Ratios of Load Taken By Each Member			
Load	Beam 1	Beam 2	Sum	Load	Beam 1	Beam 2	Sum
0.0	0.00	0.00	0.00	0.0	0.00	0.00	0.00
5.3	4.01	0.60	4.61	5.3	0.87	0.13	1.00
10.3	8.08	0.94	9.02	10.3	0.90	0.10	1.00
15.6	12.29	1.07	13.36	15.6	0.92	0.08	1.00
20.8	17.28	1.34	18.62	20.8	0.93	0.07	1.00

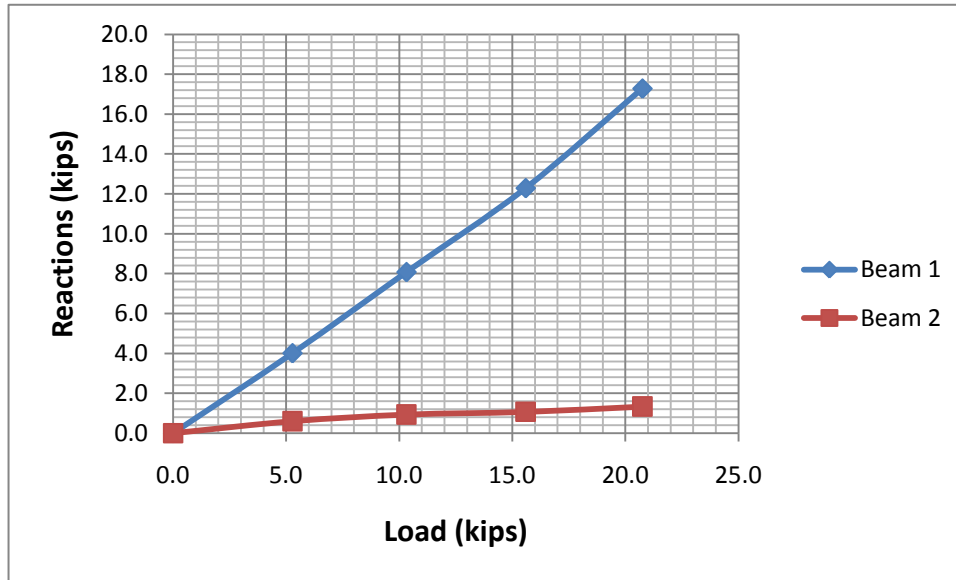


Figure C-3 Beam Reactions - CL BM1

Table C-2 Experimental/Theoretical Deflections – CL BM1

Deflections - Theoretical vs. Experimental						
Load	Theoretical		Experimental		% Error	
	Beam 1	Beam 2	Beam 1	Beam 2	Beam 1	Beam 2
5.3	0.055	0.006	0.052	0.002	5.38%	74.36%
10.3	0.110	0.010	0.093	0.002	15.38%	83.52%
15.6	0.183	0.011	0.135	0.002	25.93%	84.89%
20.8	0.257	0.014	0.178	0.002	30.81%	88.46%

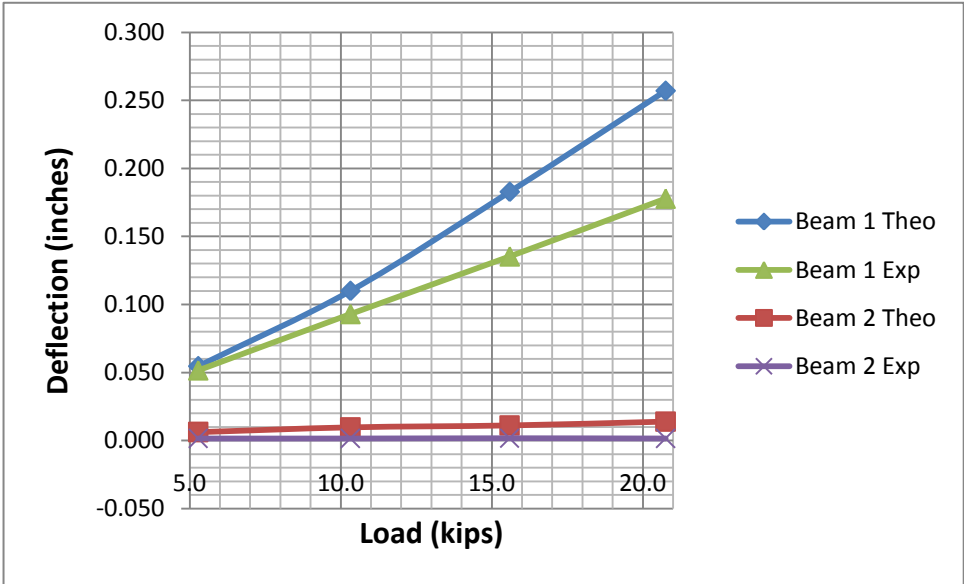


Figure C-4 Deflections - CL BM1

C-2 Loading Scenario: 1.25' OC BM1

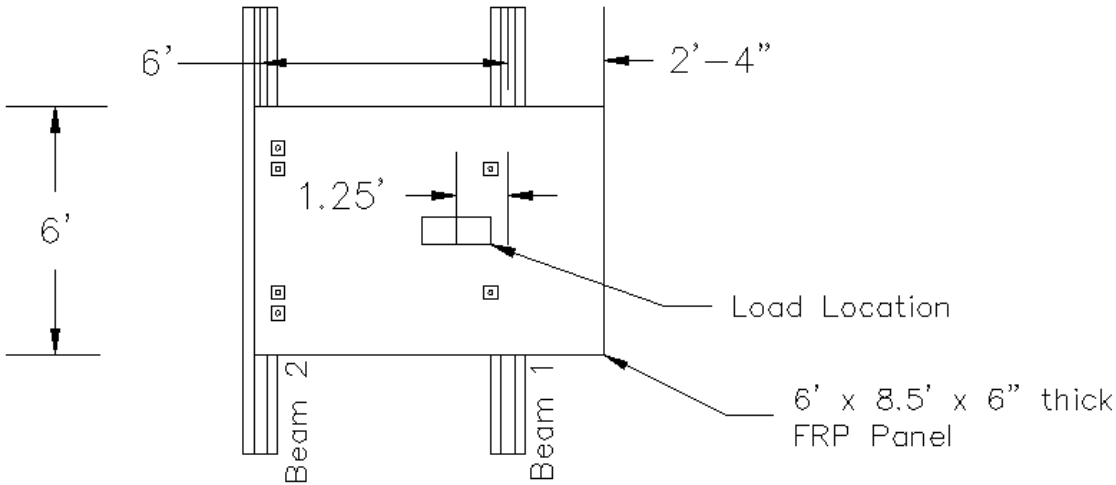


Figure C-5 Load Location – 1.25' OC BM1

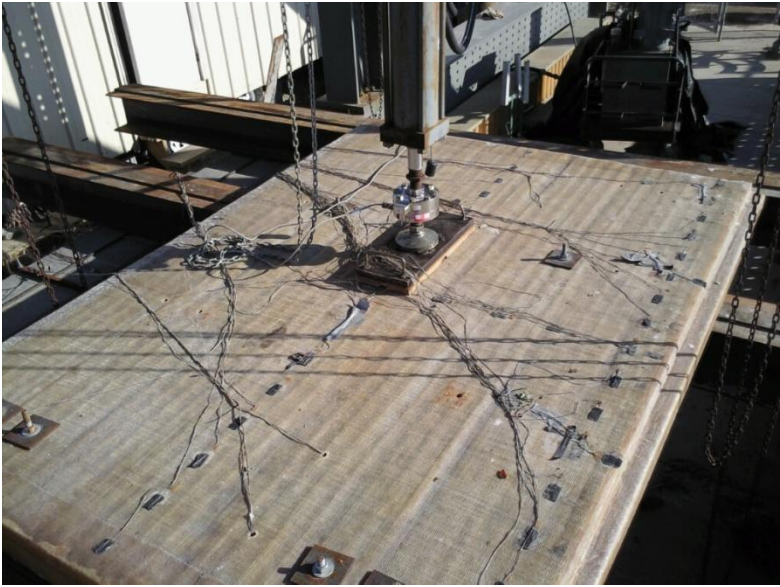


Figure C-6 1.25' OC BM1 Test Picture

Table C-3 Reactions – 1.25' OC BM1

Reactions (kips)				Ratios of Load Taken By Each Member			
Load	Beam 1	Beam 2	Sum	Load	Beam 1	Beam 2	Sum
0	0	0	0	0	0	0	0
5.4	2.58	0.77	3.35	5.4	0.77	0.23	1.00
10.5	6.03	1.27	7.30	10.5	0.83	0.17	1.00
15.6	10.61	2.28	12.89	15.6	0.82	0.18	1.00
20.7	15.13	3.21	18.34	20.7	0.82	0.18	1.00

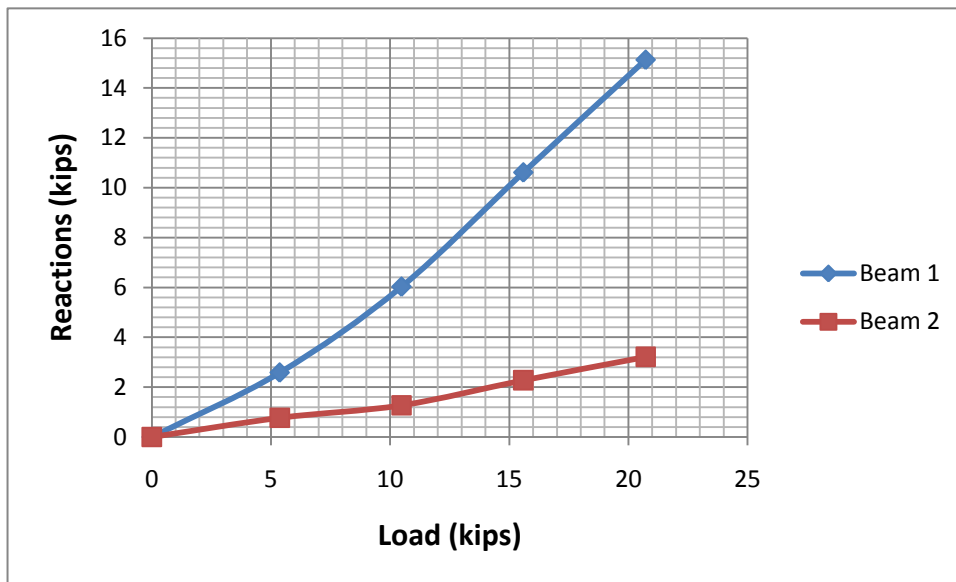


Figure C-7 Beam Reactions - 1.25' OC BM1

Table C-4 Experimental/Theoretical Deflections – 1.25' OC BM1

Deflections - Theoretical vs. Experimental						
Load	Theoretical		Experimental		% Error	
	Beam 1	Beam 2	Beam 1	Beam 2	Beam 1	Beam 2
5.4	0.035	0.008	0.043	0.011	-23.42%	-32.80%
10.5	0.082	0.013	0.076	0.022	6.91%	-65.59%
15.6	0.158	0.024	0.109	0.032	31.02%	-34.60%
20.7	0.225	0.034	0.142	0.042	36.79%	-25.13%

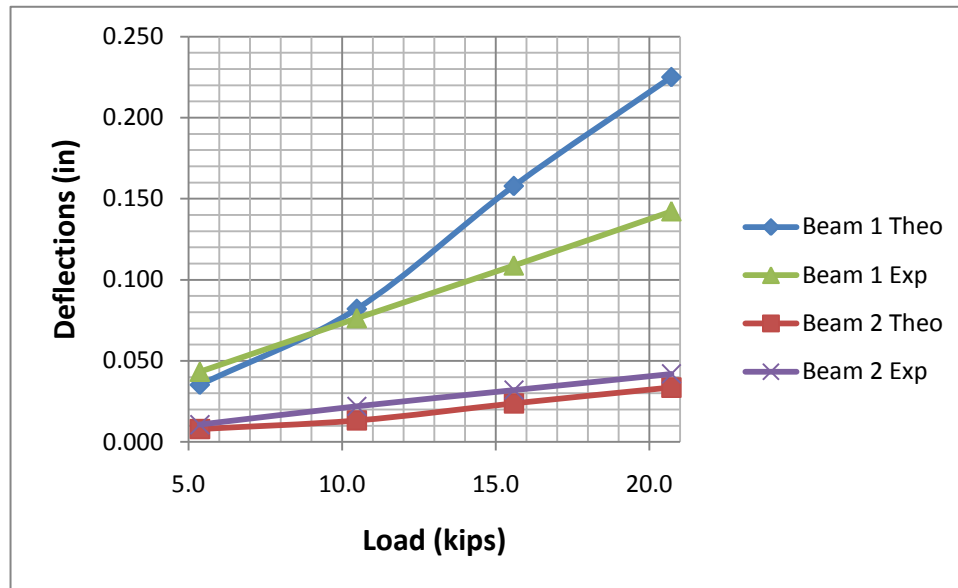


Figure C-8 Deflections - 1.25' OC BM1

C-3 Loading Scenario: Center of SS

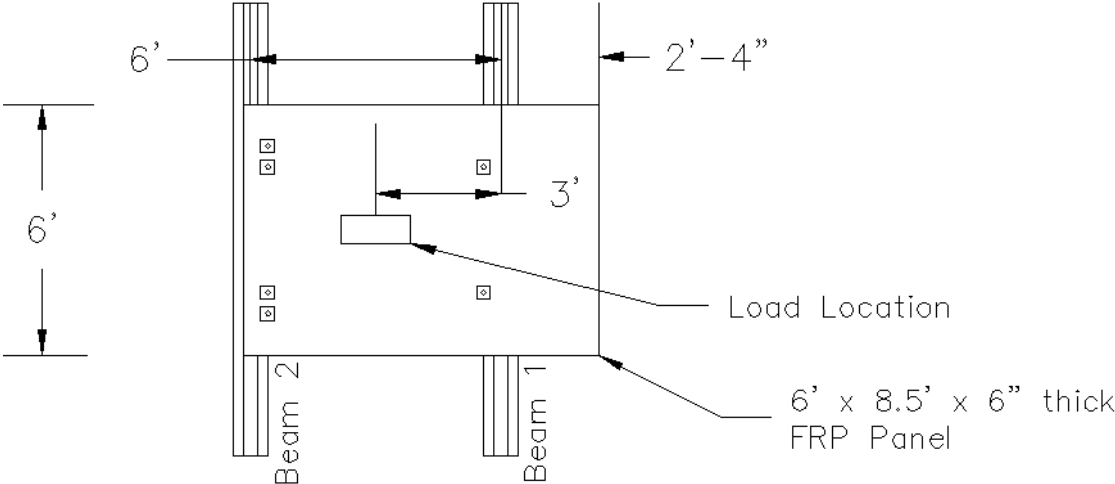


Figure C-9 Load Location – Center of SS



Figure C-10 Center of SS Test Picture

Table C-5 Reactions – Center of SS

Reactions (kips)				Ratio of Load Taken By Each Member			
Load	Beam 1	Beam 2	Sum	Load	Beam 1	Beam 2	Sum
0.0	0.00	0.00	0.00	0.0	0.00	0.00	0.00
5.2	2.55	1.71	4.25	5.2	0.60	0.40	1.00
10.4	5.99	4.25	10.25	10.4	0.58	0.42	1.00
15.6	8.41	6.70	15.10	15.6	0.56	0.44	1.00
20.1	11.29	9.21	20.50	20.1	0.55	0.45	1.00

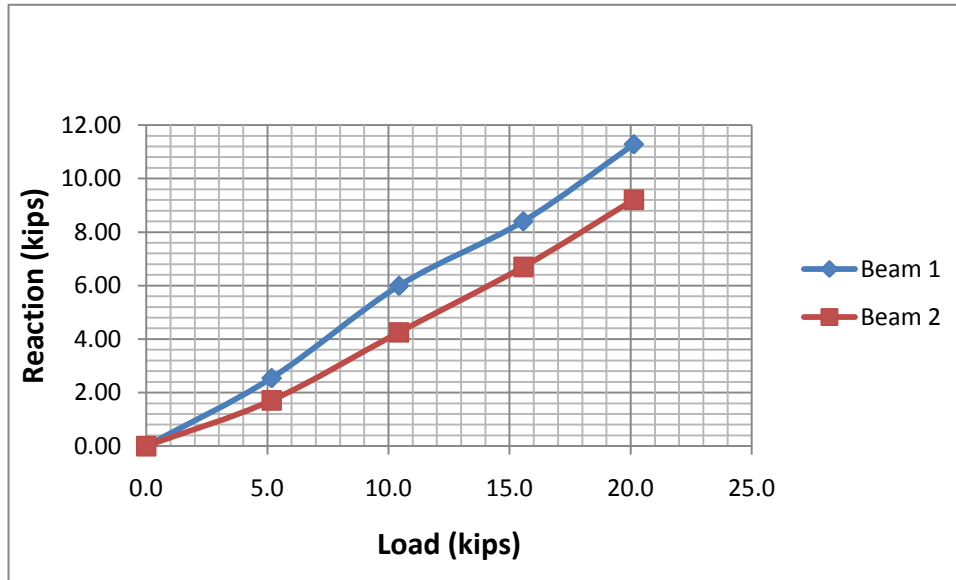


Figure C-11 Beam Reactions – Center of SS

Table C-6 Experimental/Theoretical Deflections – Center of SS

Deflections - Theoretical vs. Experimental						
Load	Theoretical		Experimental		% Error	
	Beam 1	Beam 2	Beam 1	Beam 2	Beam 1	Beam 2
5.2	0.027	0.018	0.026	0.025	2.52%	-40.21%
10.4	0.063	0.044	0.049	0.049	21.68%	-10.35%
15.6	0.088	0.070	0.068	0.072	21.99%	-2.97%
20.1	0.118	0.096	0.084	0.094	28.39%	2.23%

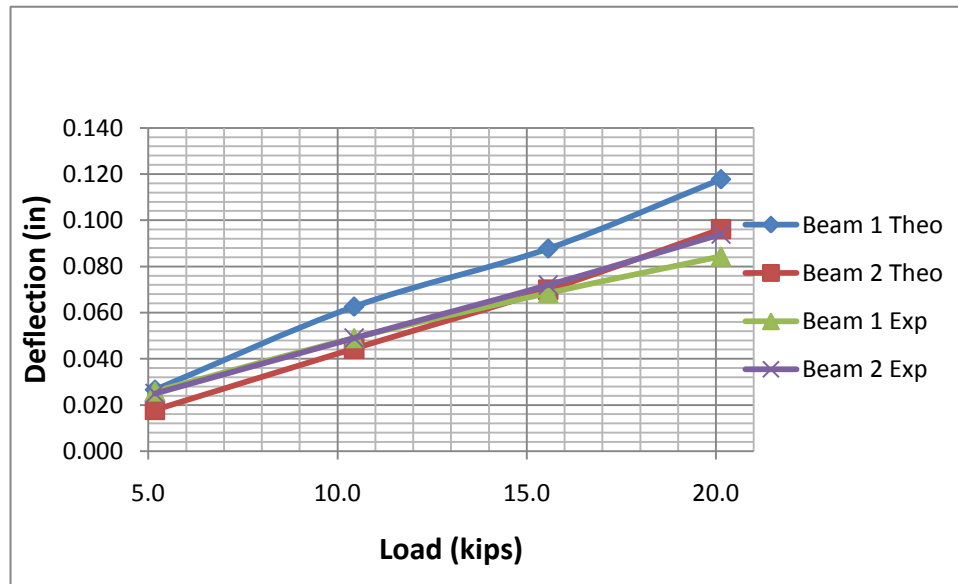


Figure C-12 Deflections - Center of SS

C-4 Loading Scenario: OPP BM

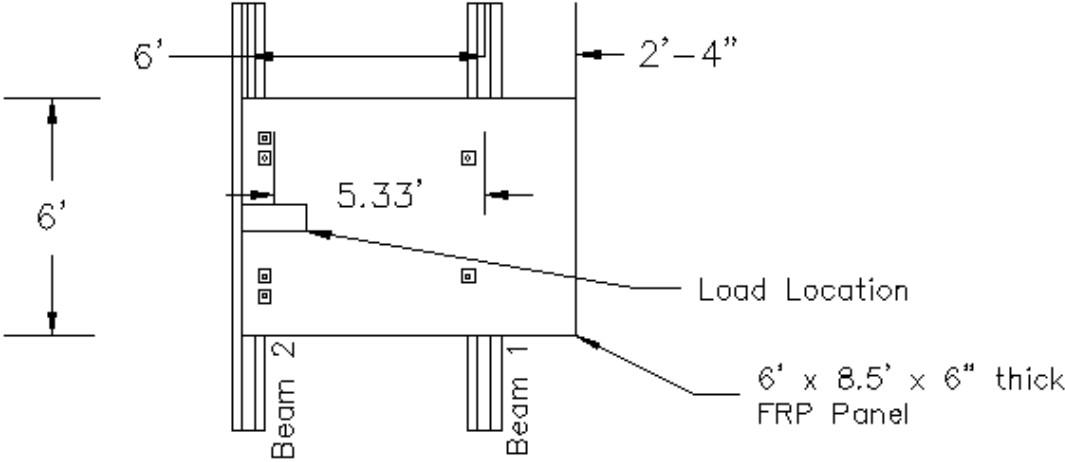


Figure C-13 Load Location – OPP BM



Figure C-14 OPP BM Test Picture

Table C-7 Reactions – OPP BM

Reactions (kips)				Ratio of Load Taken By Each Member			
Load	Beam 1	Beam 2	Sum	Load	Beam 1	Beam 2	Sum
0.0	0.00	0.00	0.00	0.0	0.00	0.00	0.00
5.2	0.77	3.32	4.09	5.2	0.19	0.81	1.00
10.4	1.61	8.02	9.62	10.4	0.17	0.83	1.00
15.6	2.21	12.06	14.27	15.6	0.15	0.85	1.00
20.6	2.68	16.53	19.21	20.6	0.14	0.86	1.00

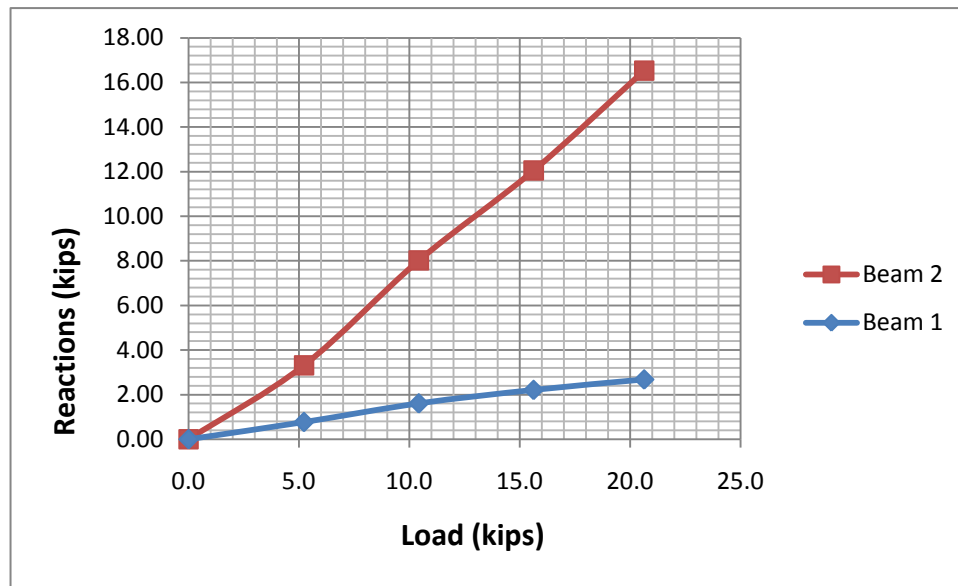


Figure C-15 Beam Reactions OPP BM

Table C-8 Experimental/Theoretical Deflections - OPP BM

Deflections - Theoretical vs. Experimental						
Load	Theoretical		Experimental		% Error	
	Beam 1	Beam 2	Beam 1	Beam 2	Beam 1	Beam 2
5.2	0.008	0.045	0.007	0.041	11.20%	9.14%
10.4	0.017	0.109	0.013	0.084	20.66%	23.02%
15.6	0.023	0.179	0.019	0.128	17.25%	28.63%
20.6	0.028	0.246	0.025	0.170	11.80%	30.89%

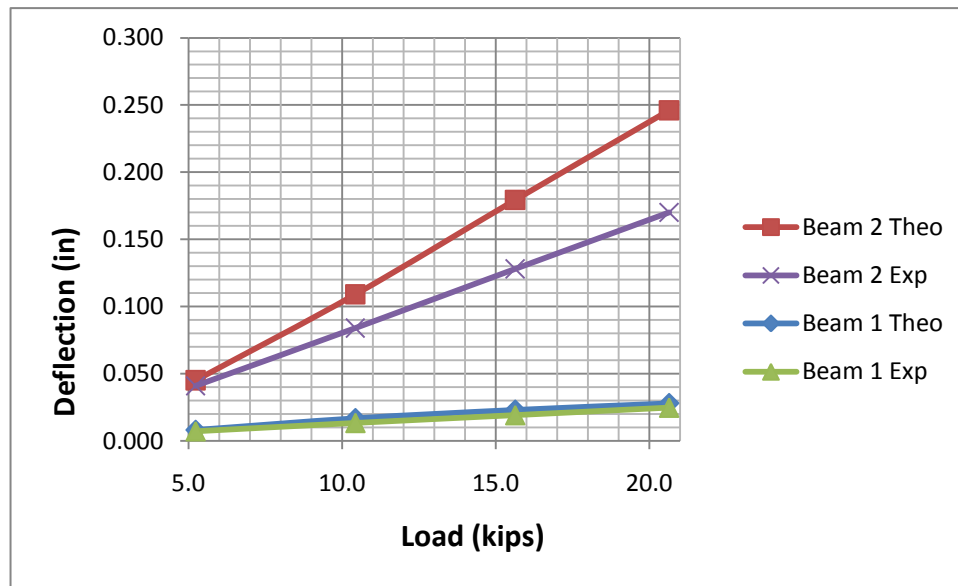


Figure C-16 Deflections - OPP BM

C-5 Loading Scenario: CNTLVR

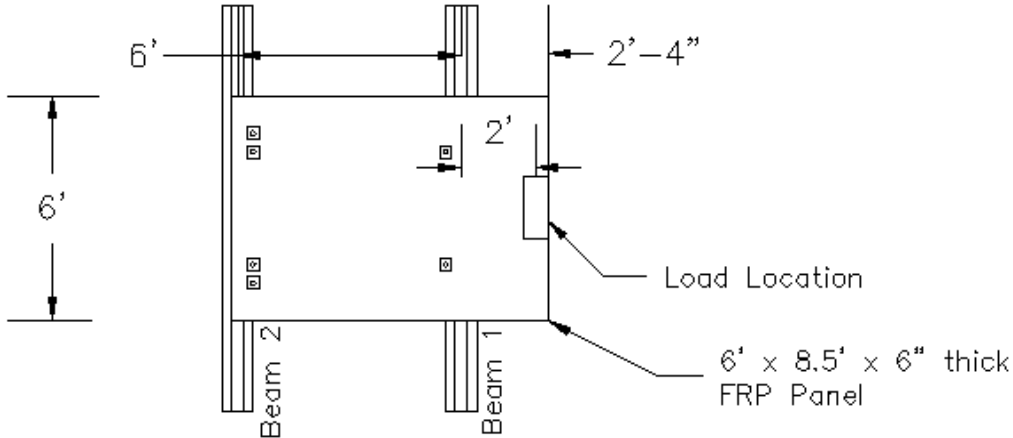


Figure C-17 Load Location – CNTLVR



Figure C-18 CNTLVR Test Picture

Table C-9 Reactions – CNTLVR

Reactions (kips)				Ratios of Load Taken By Each Member			
Load	Beam 1	Beam 2	Sum	Load	Beam 1	Beam 2	Sum
0.0	0.00	0.00	0.00	0.0	0.00	0.00	0.00
1.1	0.83	-0.40	0.43	1.1	1.94	-0.94	1.00
2.1	1.45	-0.54	0.91	2.1	1.59	-0.59	1.00
3.1	2.48	-0.67	1.81	3.1	1.37	-0.37	1.00
4.1	3.43	-0.94	2.49	4.1	1.38	-0.38	1.00
5.3	4.55	-1.34	3.21	5.3	1.42	-0.42	1.00
6.2	5.47	-1.81	3.66	6.2	1.49	-0.49	1.00
7.2	6.47	-2.34	4.13	7.2	1.57	-0.57	1.00
8.3	7.62	-2.75	4.88	8.3	1.56	-0.56	1.00
9.3	8.81	-3.08	5.72	9.3	1.54	-0.54	1.00
10.3	9.99	-3.75	6.24	10.3	1.60	-0.60	1.00
11.4	11.17	-3.82	7.35	11.4	1.52	-0.52	1.00
12.4	12.26	-4.35	7.91	12.4	1.55	-0.55	1.00
13.4	13.50	-4.89	8.61	13.4	1.57	-0.57	1.00
14.4	14.69	-5.22	9.46	14.4	1.55	-0.55	1.00

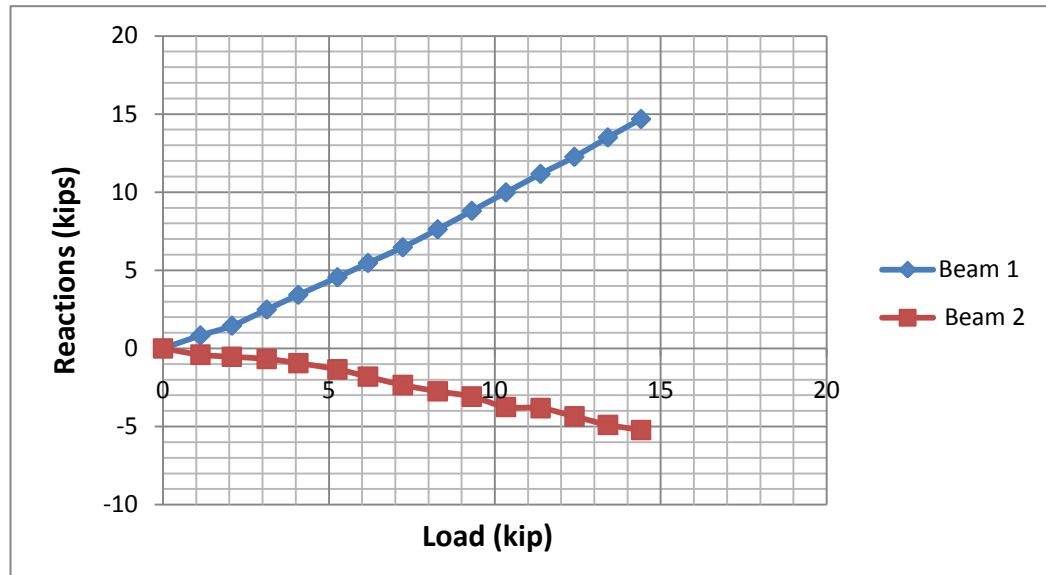


Figure C-19 Beam Reactions – CNTLVR

Table C-10 Experimental/Theoretical Deflections

Deflections - Theoretical vs. Experimental						
Load	Theoretical		Experimental		% Error	
	Beam 1	Beam 2	Beam 1	Beam 2	Beam 1	Beam 2
1.1	0.012	-0.004	0.015	-0.003	-30.02%	27.07%
2.1	0.020	-0.006	0.030	-0.007	-44.14%	-21.54%
3.1	0.035	-0.007	0.044	-0.011	-25.03%	-61.41%
4.1	0.048	-0.010	0.058	-0.017	-19.43%	-73.63%
5.3	0.064	-0.014	0.071	-0.024	-10.81%	-72.59%
6.2	0.077	-0.019	0.082	-0.031	-5.68%	-65.66%
7.2	0.092	-0.024	0.093	-0.040	-1.68%	-61.96%
8.3	0.108	-0.029	0.105	-0.047	2.82%	-65.30%
9.3	0.125	-0.032	0.117	-0.054	6.45%	-66.99%
10.3	0.141	-0.039	0.128	-0.059	9.17%	-49.84%
11.4	0.158	-0.040	0.140	-0.064	11.22%	-60.01%
12.4	0.173	-0.045	0.152	-0.069	12.64%	-50.79%
13.4	0.191	-0.051	0.163	-0.073	14.72%	-43.98%
14.4	0.208	-0.055	0.174	-0.078	16.05%	-43.73%

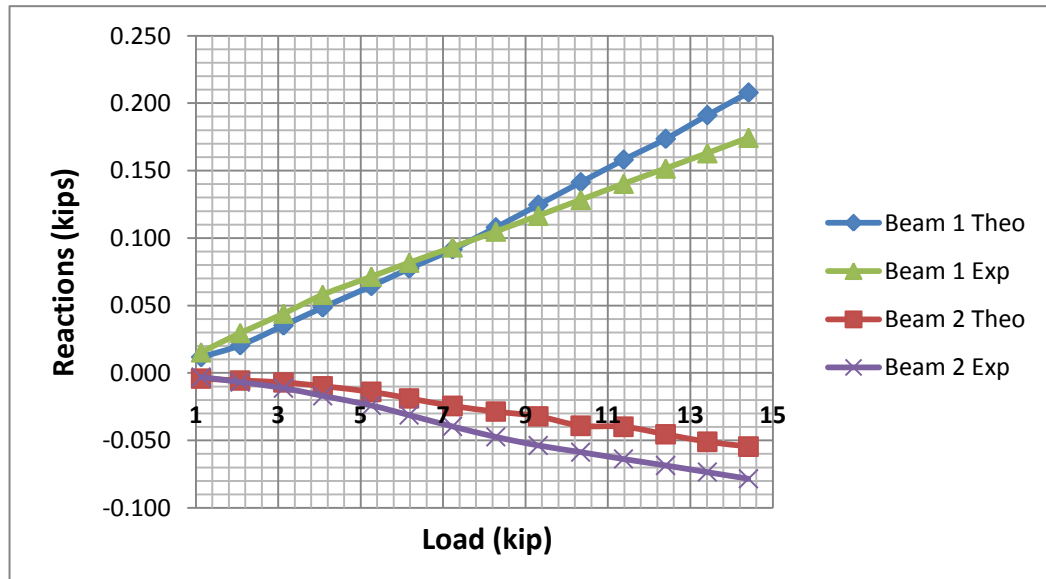
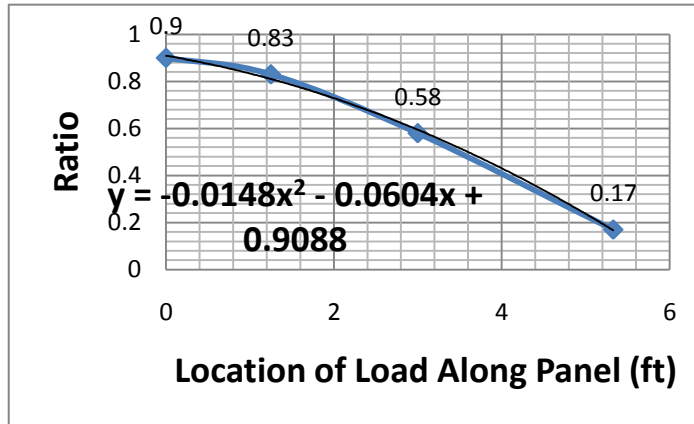
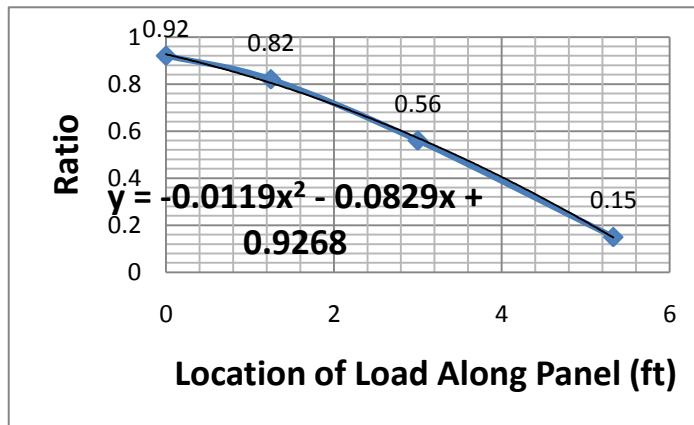


Figure C-20 Deflections – CNTLVR

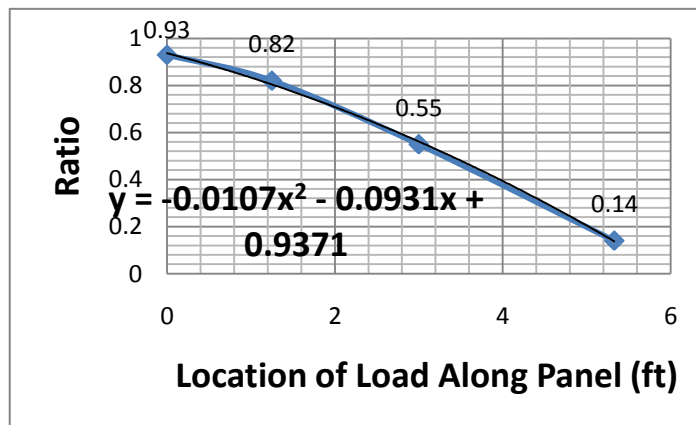
C-6 Load Ratio Charts



(a)



(b)



(c)

Figure C-21 Load Ratio Charts for Load Magnitudes of (a) 10 kips, (b) 15 kips, and (c) 20 kips - Simple Span

C-7 Load Ratio Summary

Table C-11 Load Ratio Analysis – Simple Span

Design Case for Interior Beam Spacing = 6'			
10 KIPS		20 KIPS	
Equation for Magnitude of Load with Relevance to Distance from Design Beam: $Magnitude = -0.0148x^2 - 0.0604x + 0.9088$		Equation for Magnitude of Load with Relevance to Distance from Design Beam: $Magnitude = -0.0107x^2 - 0.0931x + 0.9371$	
Wheel Load Locations (ft)	Load Magnitude	Wheel Load Locations (ft)	Load Magnitude
0	0.92	0	0.93
1	1.07	1	1.04
2	1.16	2	1.10
3	1.19	3	1.12
Critical Design:	1.19	Critical Design:	1.12
Design Equation: S/ 5.05		Design Equation: S/ 5.34	
15 KIPS		Critical Design Value for Interior Beam (6' Spacing)	
Equation for Magnitude of Load with Relevance to Distance from Design Beam: $Magnitude = -0.0119x^2 - 0.0829x + 0.9268$			
Wheel Load Locations (ft)	Load Magnitude		
0	0.93		
1	1.05		
2	1.12		
3	1.14		
Critical Design:	1.14		
Design Equation: S/ 5.25		S/ 5.05	

(same as Table 4-2 in Thesis)

Appendix D - Continuous Panel Test Results

D-1 Loading Scenario: CL BM1

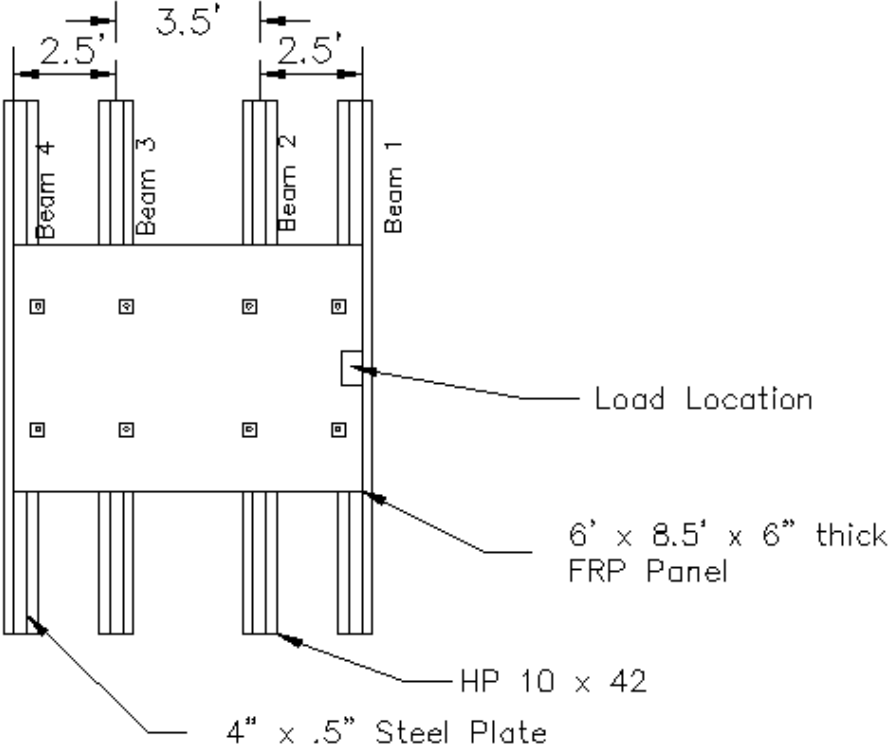


Figure D-1 Load Location – CL BM1 – Cont. Test

Table D-1 Reactions – CL BM1

Reactions (kips)					
Load	Beam 1	Beam 2	Beam 3	Beam 4	Sum
0.00	0.00	0.00	0.00	0.00	0.00
5.01	5.18	3.13	0.60	0.40	9.32
10.09	11.33	5.47	0.77	0.37	17.95
15.06	17.90	7.88	0.94	0.33	27.05
20.03	23.25	9.90	0.94	0.30	34.39
Ratios of Load Taken By Each Member					
Load	Beam 1	Beam 2	Beam 3	Beam 4	Sum
0.000	\$0.00	\$0.00	\$0.00	\$0.00	\$0.00
5.005	0.556	0.336	0.065	0.043	1.000
10.087	0.632	0.305	0.043	0.021	1.000
15.057	0.662	0.291	0.035	0.012	1.000
20.027	0.676	0.288	0.027	0.009	1.000

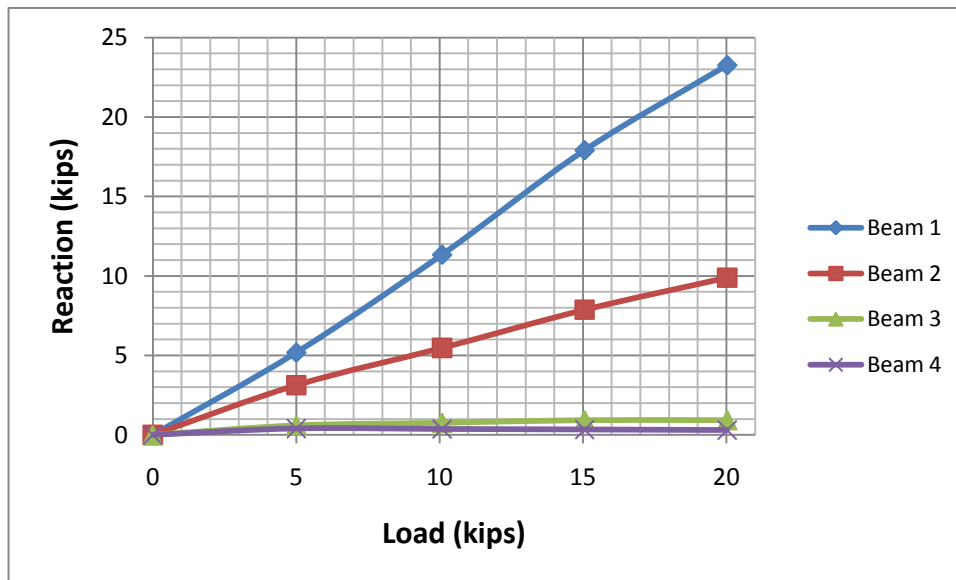


Figure D-2 Reactions - CL BM1

Table D-2 Experimental/ Theoretical Deflections - CL BM 1

Theoretical			Experimental	
Load	Beam 1	Beam 2	Beam 1	Beam 2
5.0	0.071	0.035	0.044	0.028
10.1	0.154	0.062	0.093	0.051
15.1	0.244	0.090	0.143	0.072
20.0	0.346	0.120	0.192	0.092
Load	Beam 3	Beam 4	Beam 3	Beam 4
5.0	0.006	0.004	0.000	-0.005
10.1	0.008	0.004	0.000	-0.009
15.1	0.010	0.003	0.000	-0.012
20.0	0.010	0.003	-0.002	-0.017
% Error				
Load	Beam 1	Beam 2		
5.0	37.19%	20.31%		
10.1	39.71%	17.61%		
15.1	41.43%	20.37%		
20.0	44.63%	23.48%		
Load	Beam 3	Beam 4		
5.0	100.00%	227.92%		
10.1	100.00%	324.65%		
15.1	104.66%	451.97%		
20.0	115.99%	649.15%		

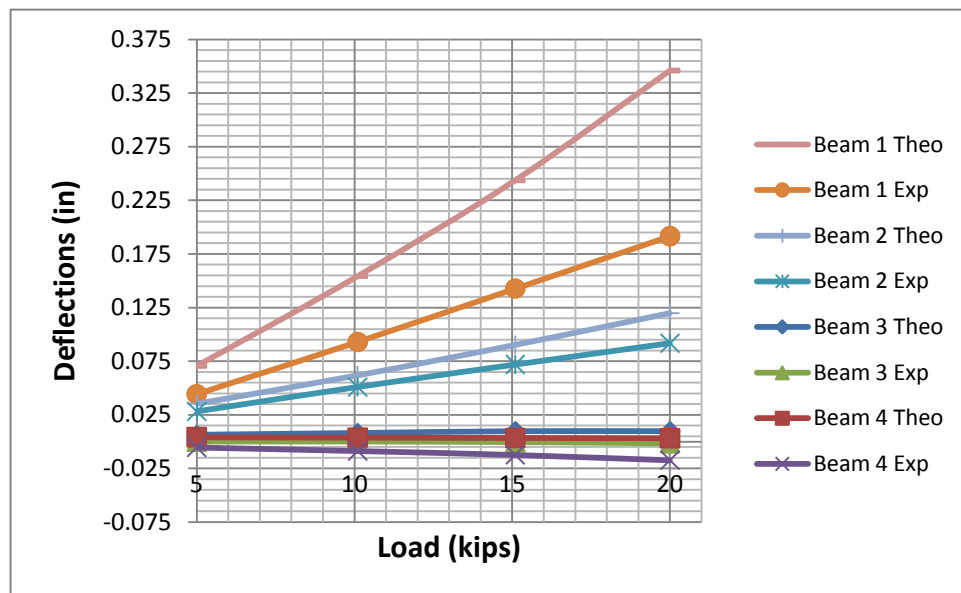


Figure D-3 Deflections - CL BM1

D-2 Loading Scenario: MS 1-2

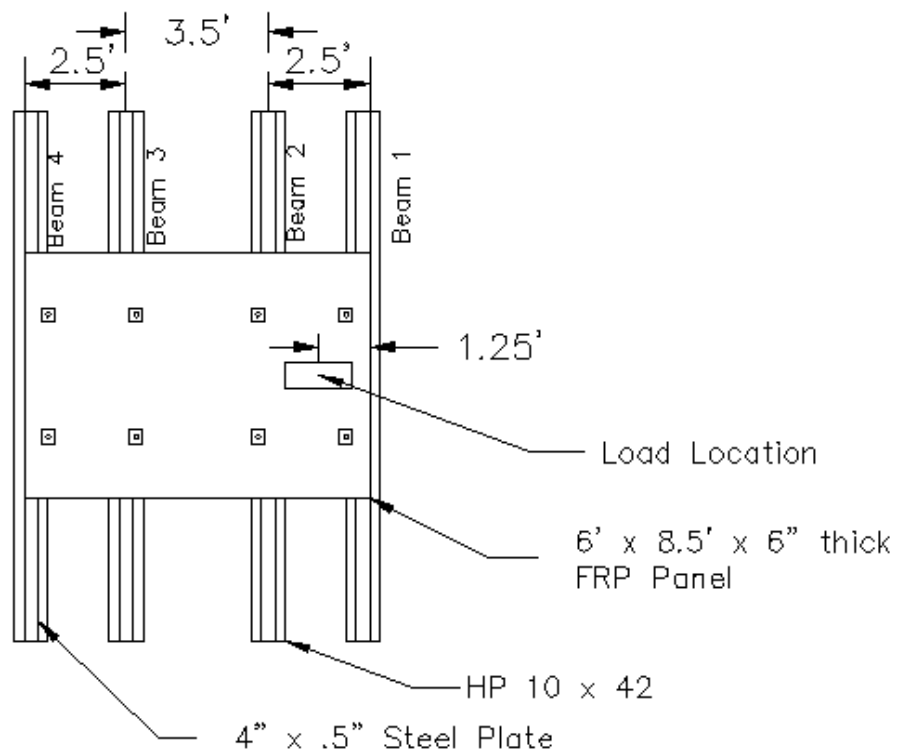


Figure D-4 Load Location – MS 1-2

Table D-3 Reactions – MS 1-2

Reactions (kips)					
Load	Beam 1	Beam 2	Beam 3	Beam 4	Sum
0.0	0.00	0.00	0.00	0.00	0.00
5.1	2.46	2.83	0.60	0.00	5.89
10.1	4.65	5.02	0.72	-0.30	10.09
15.1	7.17	7.43	1.02	-0.49	15.12
20.0	9.46	9.13	1.43	-0.60	19.43
Ratios of Load Taken By Each Member					
Load	Beam 1	Beam 2	Beam 3	Beam 4	Sum
0.0	0.000	0.000	0.000	0.000	0.000
5.1	0.418	0.480	0.102	0.000	1.000
10.1	0.461	0.498	0.071	-0.030	1.000
15.1	0.474	0.491	0.067	-0.032	1.000
20.0	0.487	0.470	0.074	-0.031	1.000

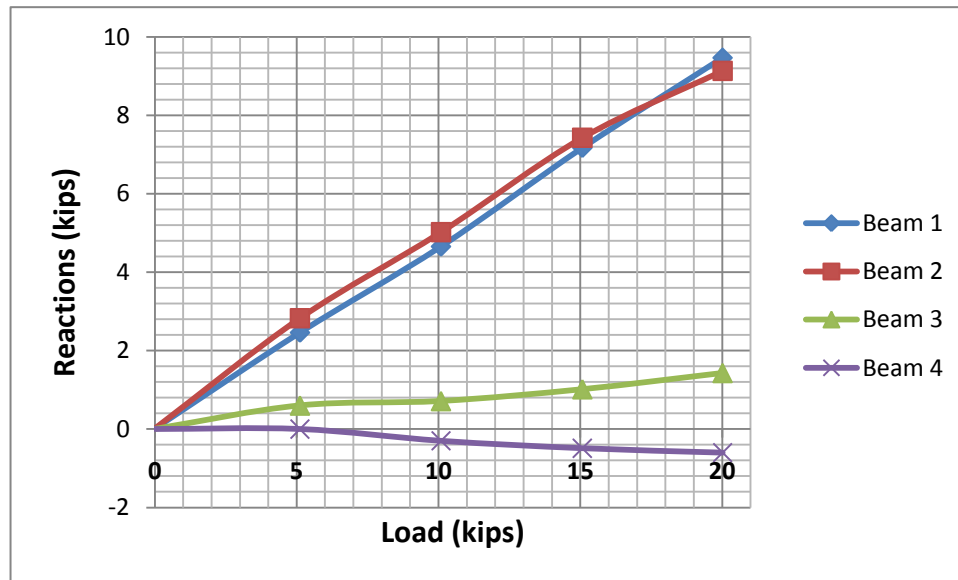


Figure D-5 Beam Reactions - MS 1-2

Table D-4 Experimental/ Theoretical Deflections - MS 1-2

Load	Theoretical		Experimental	
	Beam 1	Beam 2	Beam 1	Beam 2
5.0	0.032	0.037	0.020	0.026
10.1	0.061	0.065	0.042	0.051
15.1	0.098	0.101	0.064	0.072
20.0	0.141	0.136	0.086	0.092
Load	Beam 3	Beam 4	Beam 3	Beam 4
5.0	0.006	0.000	0.003	-0.004
10.1	0.007	-0.003	0.006	-0.006
15.1	0.011	-0.005	0.009	-0.007
20.0	0.015	-0.006	0.012	-0.009
Load	% Error			
	Beam 1	Beam 2		
5.0	37.50%	29.33%		
10.1	31.57%	22.66%		
15.1	34.71%	28.45%		
20.0	38.94%	31.99%		
Load	Beam 3	Beam 4		
5.0	57.52%	380.63%		
10.1	16.24%	-83.06%		
15.1	16.50%	-45.93%		
20.0	21.04%	-42.49%		

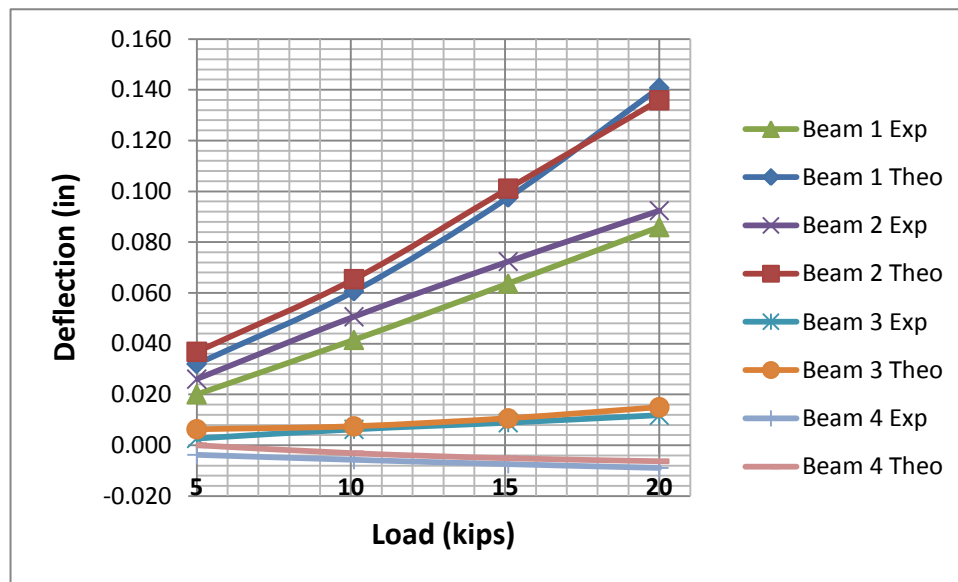


Figure D-6 Deflections - MS 1-2

D-3 Loading Scenario: CL BM2

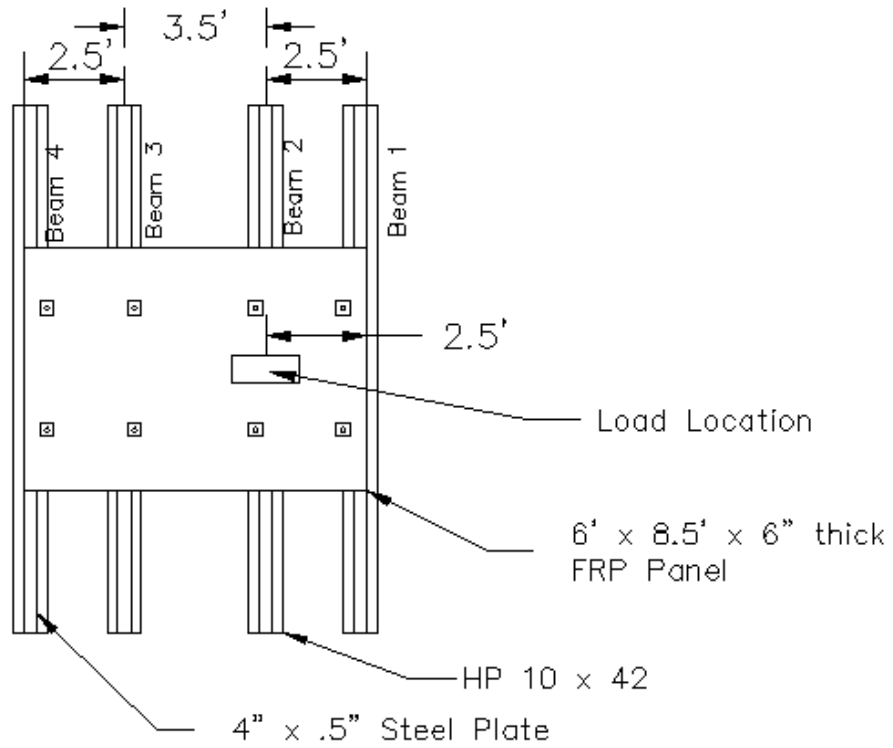


Figure D-7 Load Location - CL BM2 – Cont. Test

Table D-5 Reactions – CL BM2

Reactions (kips)					
Load	Beam 1	Beam 2	Beam 3	Beam 4	Sum
0.0	0.00	0.00	0.00	0.00	0.00
5.1	1.56	2.47	0.87	0.87	5.78
10.1	3.19	5.12	1.84	0.20	10.36
15.1	4.34	7.72	2.44	0.00	14.50
20.1	5.58	9.99	3.28	-0.07	18.79
Ratios of Load Taken By Each Member					
Load	Beam 1	Beam 2	Beam 3	Beam 4	Sum
0.000	\$0.00	\$0.00	\$0.00	\$0.00	\$0.00
5.103	0.271	0.428	0.151	0.151	1.000
10.087	0.308	0.495	0.178	0.019	1.000
15.085	0.299	0.532	0.169	0.000	1.000
20.055	0.297	0.532	0.175	-0.004	1.000

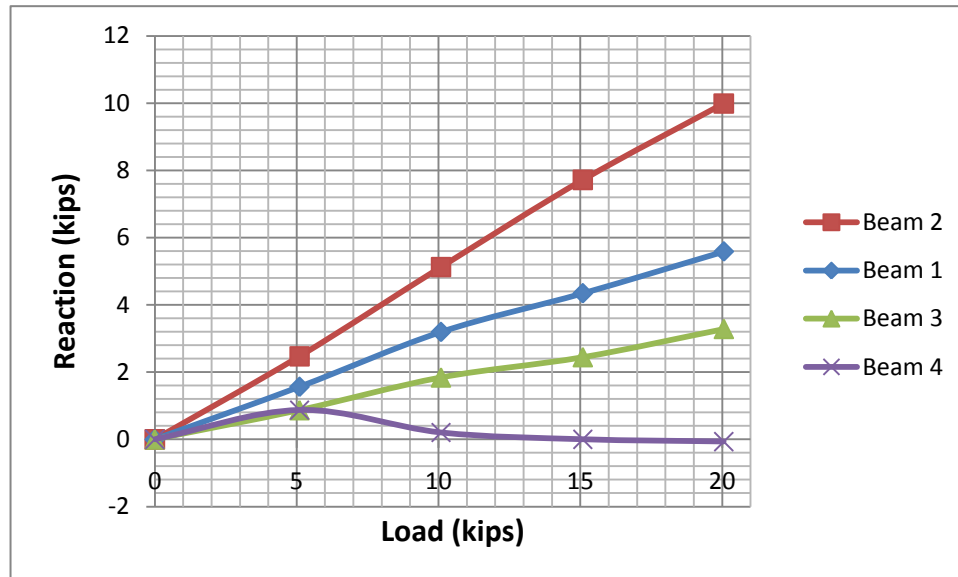


Figure D-8 Beam Reactions CL BM 2

Table D-6 Experimental/Theoretical Deflections - CL BM2

Load	Theoretical		Experimental	
	Beam 1	Beam 2	Beam 1	Beam 2
5.0	0.018	0.034	0.014	0.028
10.1	0.036	0.070	0.027	0.054
15.1	0.050	0.105	0.040	0.079
20.0	0.068	0.149	0.052	0.101
Load	Beam 3	Beam 4	Beam 3	Beam 4
5.0	0.012	0.009	0.008	-0.001
10.1	0.025	0.002	0.015	-0.002
15.1	0.033	0.000	0.023	-0.002
20.0	0.049	-0.001	0.028	-0.002
Load	% Error			
	Beam 1	Beam 2		
5.0	22.27%	18.08%		
10.1	24.76%	22.78%		
15.1	19.46%	25.19%		
20.0	22.54%	32.03%		
Load	Beam 3	Beam 4		
5.0	30.67%	110.80%		
10.1	39.92%	171.77%		
15.1	32.00%	189.82%		
20.0	42.04%	-208.91%		

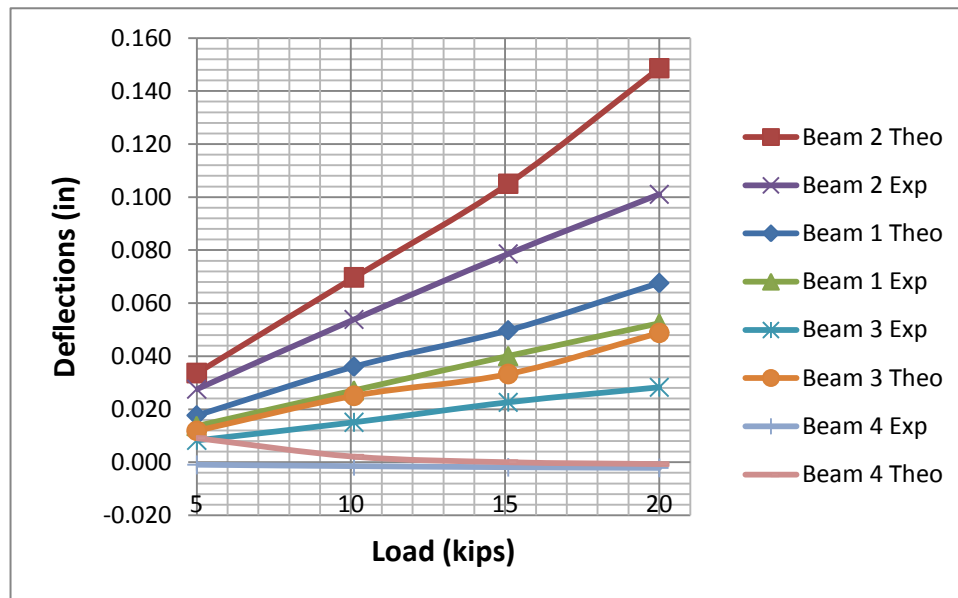


Figure D-9 Deflections - CL BM2

D-4 Loading Scenario: MS 2-3

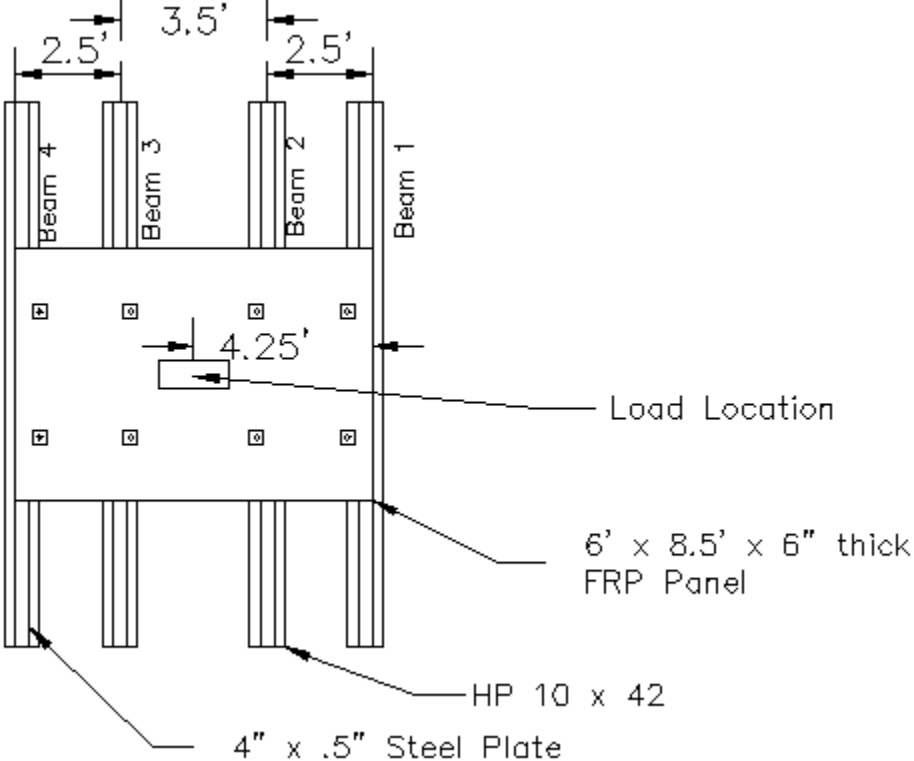


Figure D-10 Load Location - MS 2-3

Table D-7 Reactions – MS 2-3

Reactions (kips)					
Load	Beam 1	Beam 2	Beam 3	Beam 4	Sum
0.0	0.00	0.00	0.00	0.00	0.00
5.2	1.21	1.74	1.86	0.80	5.61
10.3	1.94	3.83	3.62	1.44	10.83
15.1	2.44	6.14	5.52	1.81	15.91
20.0	2.81	7.75	6.81	1.84	19.21
Ratios of Load Taken By Each Member					
Load	Beam 1	Beam 2	Beam 3	Beam 4	Sum
0.000	0.000	0.000	0.000	0.000	0.000
5.2	0.215	0.311	0.331	0.143	1.000
10.3	0.186	0.347	0.332	0.135	1.000
15.1	0.161	0.384	0.346	0.115	1.006
20.0	0.146	0.403	0.354	0.096	1.000

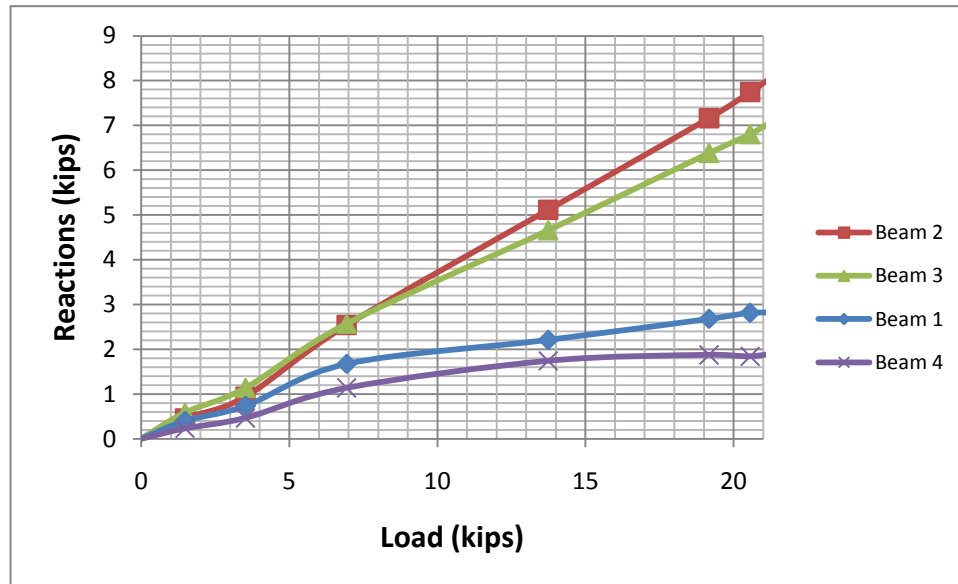


Figure D-11 Beam Reactions - MS 2-3

Table D-8 Experimental/Theoretical Deflections - MS 2-3

Load	Theoretical		Experimental	
	Beam 1	Beam 2	Beam 1	Beam 2
5.0	0.013	0.020	0.006	0.020
10.1	0.020	0.043	0.012	0.040
15.1	0.026	0.070	0.018	0.063
20.0	0.029	0.089	0.022	0.078
Load	Beam 3	Beam 4	Beam 3	Beam 4
5.0	0.021	0.008	0.016	0.008
10.1	0.041	0.015	0.031	0.015
15.1	0.063	0.019	0.050	0.024
20.0	0.078	0.019	0.064	0.030
% Error				
Load	Beam 1	Beam 2		
5.0	49.07%	-0.93%		
10.1	41.59%	7.63%		
15.1	28.74%	10.28%		
20.0	25.33%	12.25%		
Load	Beam 3	Beam 4		
5.0	25.71%	9.13%		
10.1	23.78%	-0.79%		
15.1	20.36%	-26.54%		
20.0	17.58%	-57.60%		

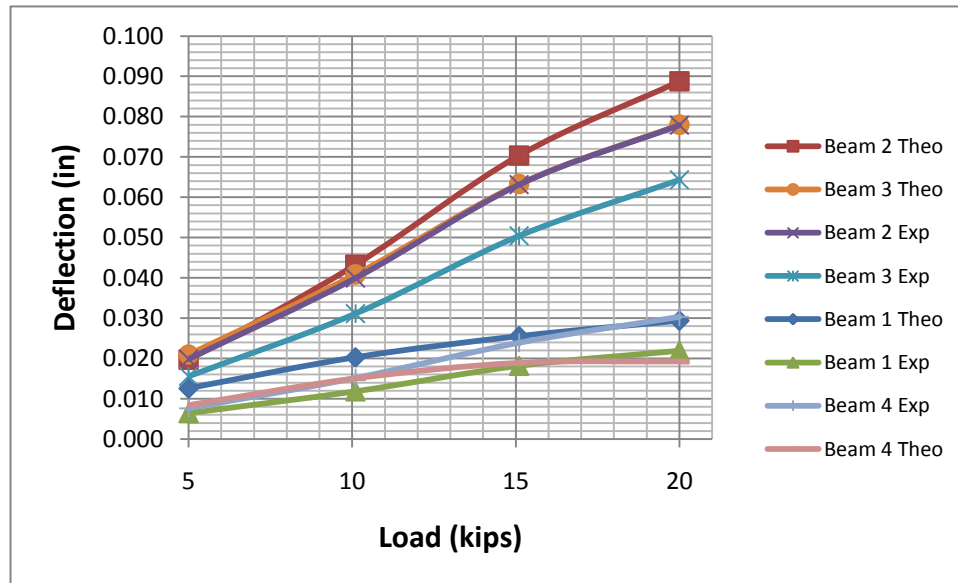


Figure D-12 Deflections - MS 2-3

D-5 Loading Scenario: CL BM 3

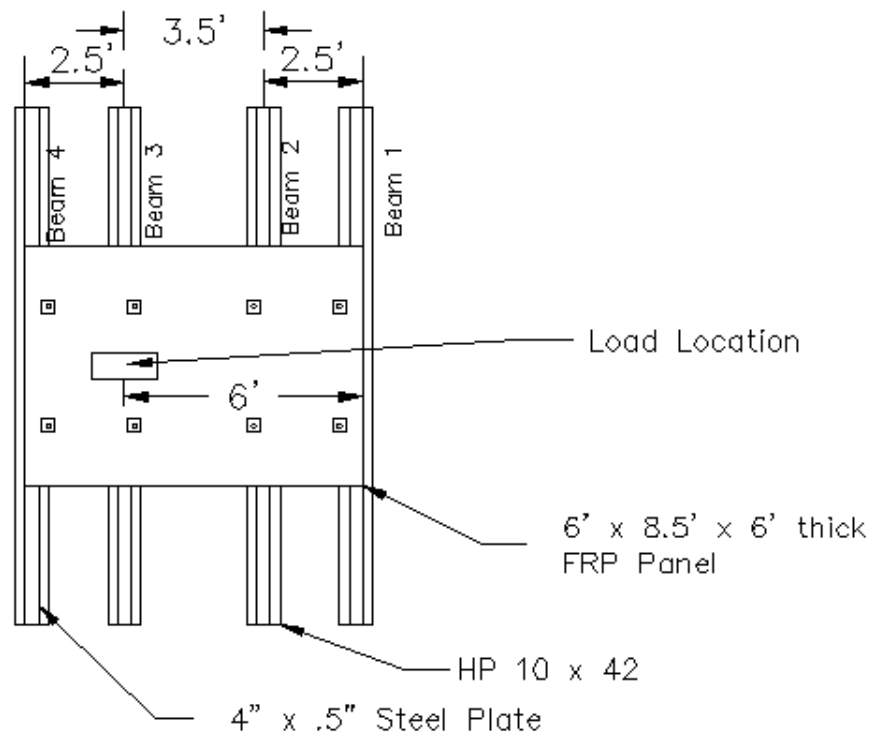


Figure D-13 Load Location - CL BM3

Table D-9 Reactions - CL BM3

Reactions (kips)					
Load	Beam 1	Beam 2	Beam 3	Beam 4	Sum
0.0	0.00	0.00	0.00	0.00	0.00
5.0	0.07	1.11	2.89	1.79	5.86
10.0	-0.27	2.08	5.91	3.75	11.46
15.0	-0.13	3.35	9.49	6.19	18.90
20.0	0.00	4.49	13.15	8.34	25.98
Ratios of Load Taken By Each Member					
Load	Beam 1	Beam 2	Beam 3	Beam 4	Sum
0.0	0.000	0.000	0.000	0.000	0.000
5.0	0.011	0.189	0.494	0.306	1.000
10.0	-0.023	0.181	0.515	0.327	1.000
15.0	-0.007	0.177	0.502	0.328	1.000
20.0	0.000	0.173	0.506	0.321	1.000

Table C-20 Reactions - CL BM3

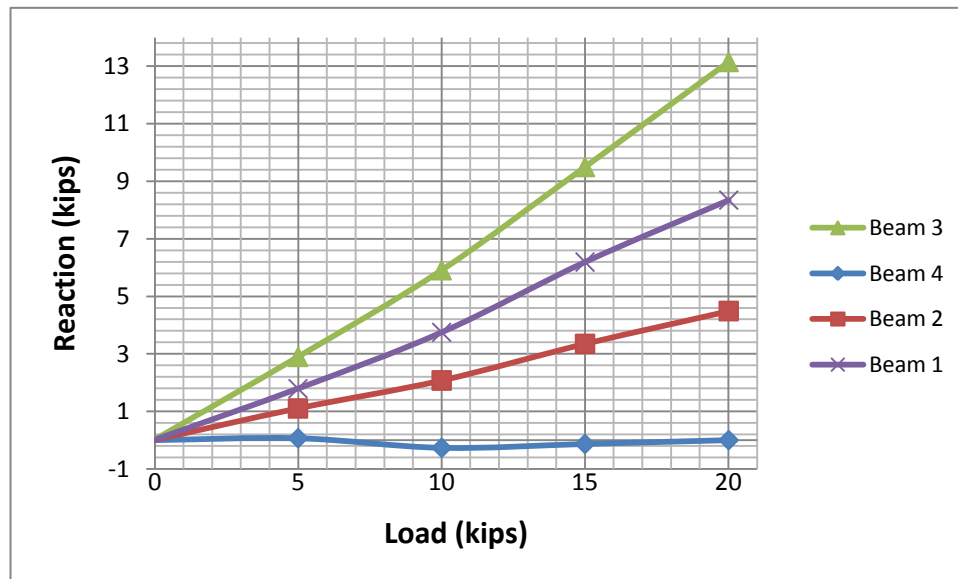


Figure D-14 Beam Reactions - CL BM3

Table D-10 Experimental/Theoretical Deflections - CL BM3

Load	Theoretical		Experimental	
	Beam 1	Beam 2	Beam 1	Beam 2
5.0	0.001	0.012	0.000	0.014
10.1	-0.003	0.022	0.000	0.027
15.1	-0.001	0.035	0.001	0.040
20.0	0.000	0.047	0.003	0.053
Load	Beam 3	Beam 4	Beam 3	Beam 4
5.0	0.039	0.020	0.030	0.036
10.1	0.080	0.042	0.061	0.072
15.1	0.129	0.071	0.092	0.094
20.0	0.196	0.101	0.126	0.113
Load	% Error			
	Beam 1	Beam 2		
5.0	100.00%	-19.99%		
10.1	88.37%	-26.21%		
15.1	188.41%	-15.57%		
20.0	100.00!	-12.55%		
Load	Beam 3	Beam 4		
5.0	23.34%	-80.12%		
10.1	23.69%	-71.05%		
15.1	29.00%	-32.95%		
20.0	35.39%	-12.30%		

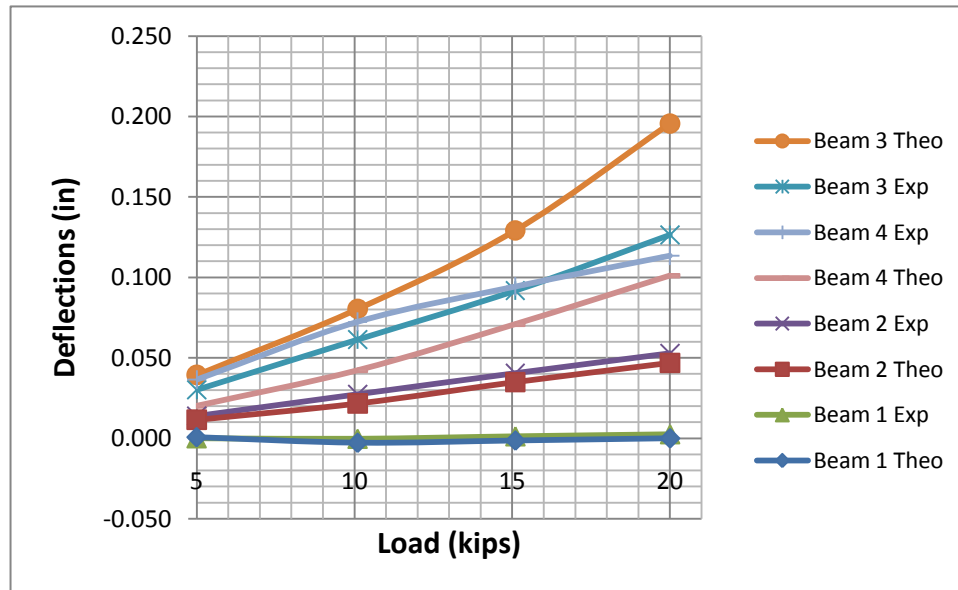
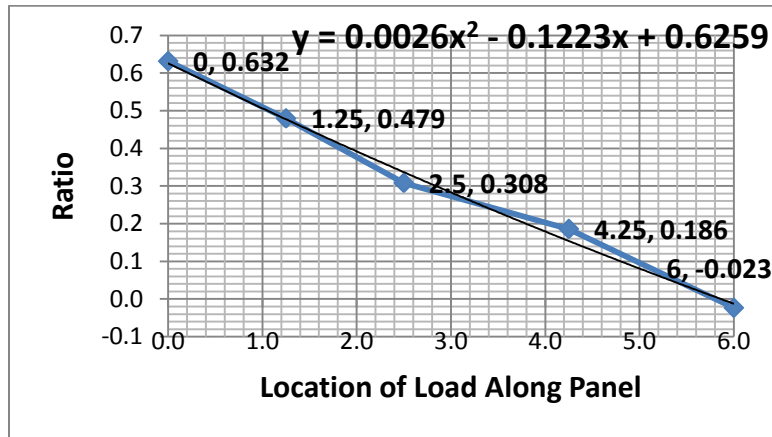
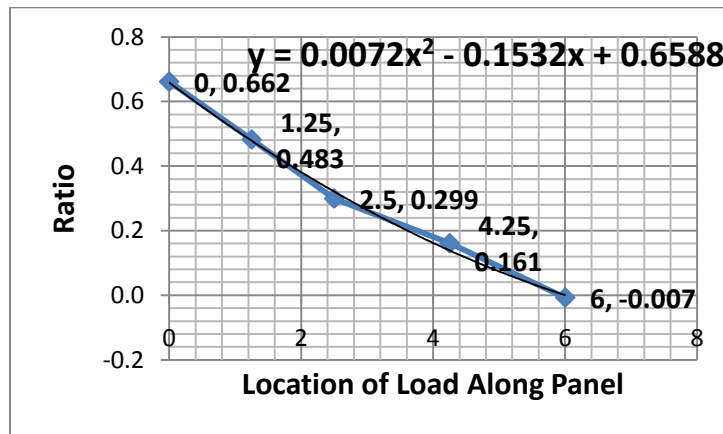


Figure D-15 Deflections - CL BM3

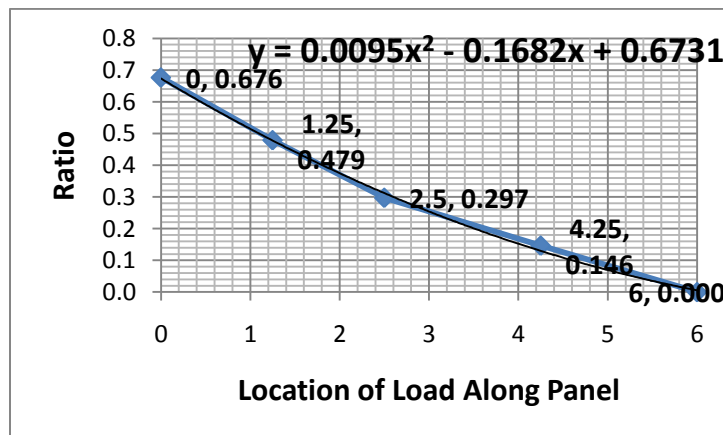
D-6 Load Ratios – Cont. Test



(a)

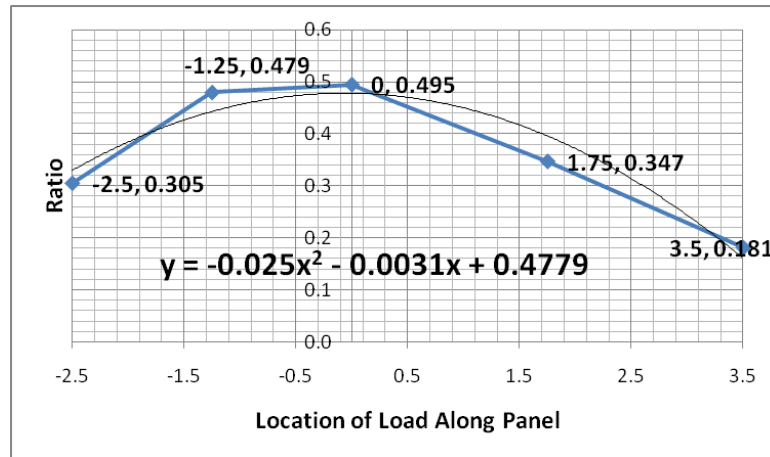


(b)

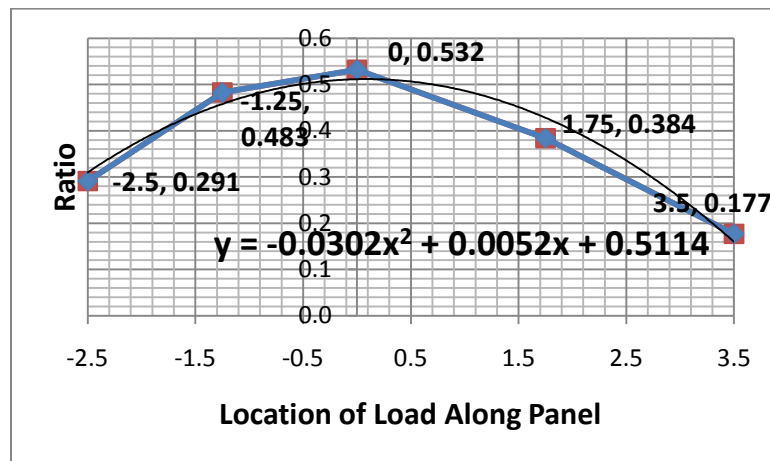


(c)

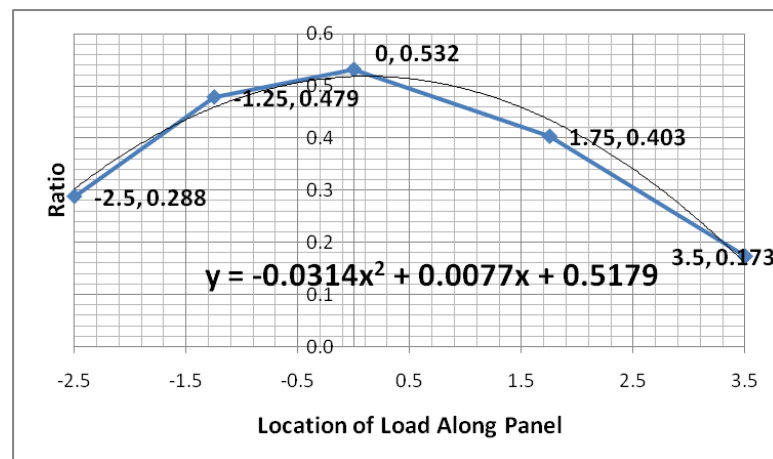
Figure D-16 Load Ratio Chart BM 1 for Load Magnitudes of (a) 10 kips, (b) 15 kips, and (c) 20 kips - Cont. Test



(a)

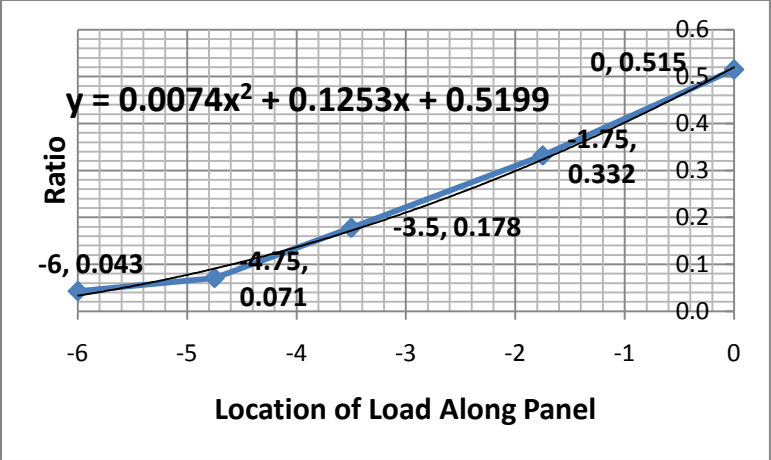


(b)

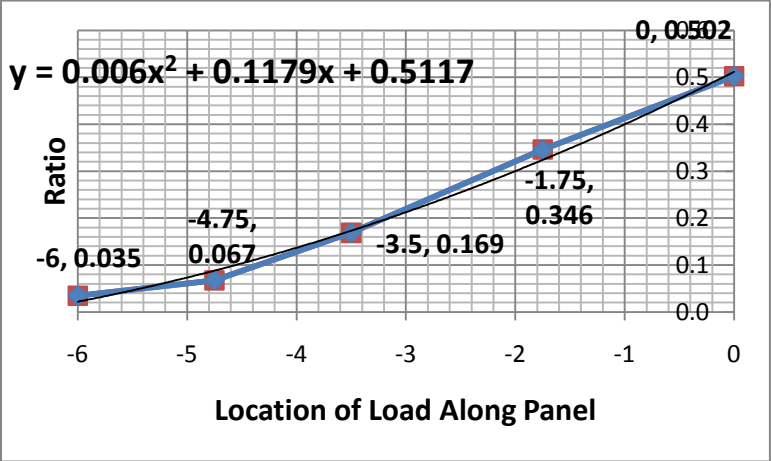


(c)

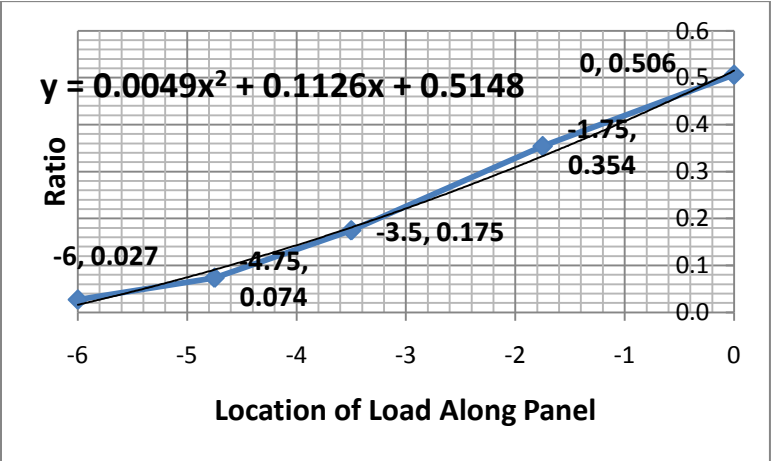
Figure D-17 Load Ratio Chart BM 2 for Load Magnitudes of (a) 10 kips, (b) 15 kips, and (c) 20 kips - Cont. Test



(a)

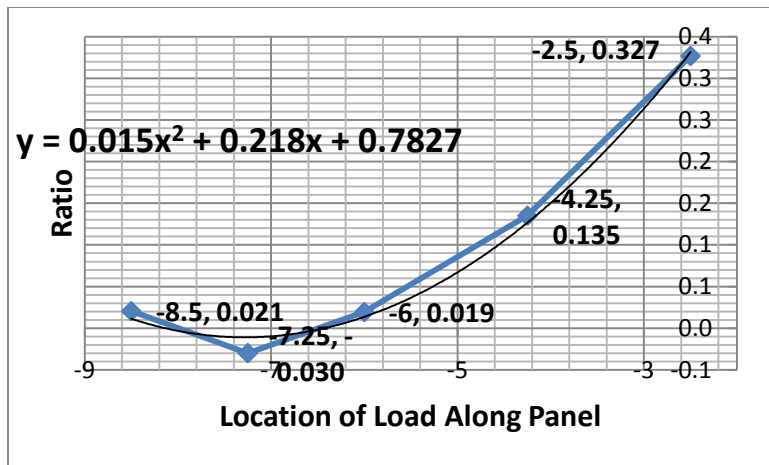


(b)

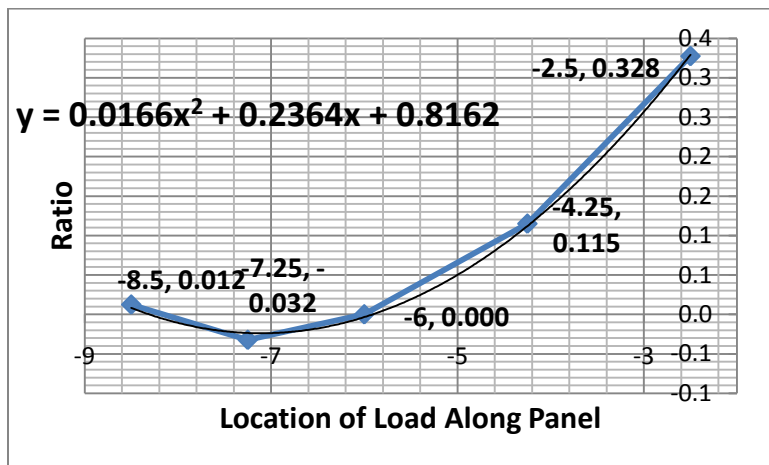


(c)

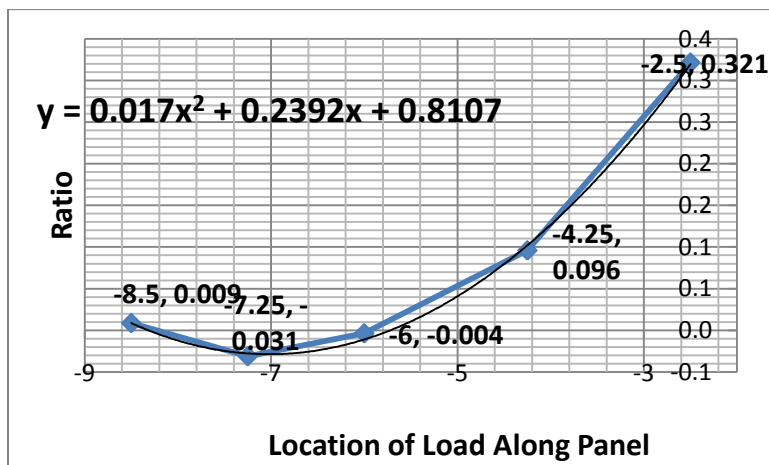
Figure D-18 Load Ratio Chart BM 3 for Load Magnitudes of (a) 10 kips, (b) 15 kips, and (c) 20 kips - Cont. Test



(a)



(b)



(c)

Figure D-19 Load Ratio Chart BM 4 for Load Magnitudes of (a) 10 kips, (b) 15 kips, and (c) 20 kips - Cont. Test

D-7 Load Distribution Summary

Table D-11 Distribution Summary - BM 1 Cont. Test

Simulated Wheel Load	10 kips		15 kips		20 kips	
Location of First Wheel Along Panel (ft)	Load Ratio	S Ratio	Load Ratio	S Ratio	Load Ratio	S Ratio
0	0.63	S/4.7	0.66	S/4.5	0.68	S/4.4
1.25	0.48	S/6.3	0.48	S/6.2	0.48	S/6.3
2.5	0.33	S/9.1	0.31	S/9.6	0.31	S/9.8
4.25	0.19	S/16.1	0.16	S/18.6	0.15	S/20.5
Critical Design Value:	0.63	S/4.7	0.66	S/4.5	0.68	S/4.4
Controlling Critical Design:	S/4.4		Average Critical Design:		S/4.6	

Table D-12 Distribution Summary - BM 2 Cont. Test

Simulated Wheel Load	10 kips		15 kips		20 kips	
Location of First Wheel Along Panel (ft)	Load Ratio	S Ratio	Load Ratio	S Ratio	Load Ratio	S Ratio
-2.5	0.49	S/6.2	0.47	S/6.4	0.46	S/6.5
-1.25	0.55	S/5.5	0.55	S/5.5	0.55	S/5.4
0	0.45	S/6.6	0.56	S/5.4	0.56	S/5.4
1.75	0.35	S/8.6	0.38	S/7.8	0.40	S/7.4
Critical Design Value:	0.55	S/5.5	0.56	S/5.4	0.56	S/5.4
Controlling Critical Design:	S/5.4		Average Critical Design:		S/5.4	

Table D-13 Distribution Summary - BM 3 Cont. Test

Simulated Wheel Load	10 kips		15 kips		20 kips	
Location of First Wheel Along Panel (ft)	Load Ratio	S Ratio	Load Ratio	S Ratio	Load Ratio	S Ratio
-6	0.56	S/5.4	0.54	S/5.6	0.53	S/5.6
-4.75	0.55	S/5.5	0.55	S/5.5	0.55	S/5.4
-3.5	0.22	S/13.6	0.20	S/14.7	0.20	S/14.9
-1.75	0.33	S/9.0	0.35	S/8.7	0.20	S/14.9
Critical Design Value:	0.56	S/5.4	0.55	S/5.5	0.55	S/5.4
Controlling Critical Design:	S/5.4			Average Critical: S/5.4		

Table D-14 Distribution Summary - BM 4 Cont. Test

Simulated Wheel Load	10 kips		15 kips		20 kips	
Location of First Wheel Along Panel (ft)	Load Ratio	S Ratio	Load Ratio	S Ratio	Load Ratio	S Ratio
-8.5	0.35	S/8.6	0.34	S/8.8	0.33	S/9.1
-7.25	0.48	S/6.3	0.48	S/6.2	0.48	S/6.3
-6	0.65	S/4.6	0.66	S/4.5	0.68	S/4.4
-4.25	0.14	S/22.2	0.12	S/26.1	0.10	S/31.3
Critical Design Value:	0.65	S/4.6	0.66	S/4.5	0.68	S/4.4
Controlling Critical Design:	S/4.4			Average Critical Design: S/4.5		